

# **Evaluating a Taxonomy of Seizure Dynamics**

by

Dakota Crisp

A dissertation submitted in partial fulfillment  
of the requirements for the degree of  
Doctor of Philosophy  
(Biomedical Engineering)  
at The University of Michigan  
2019

Doctoral Committee:

Associate Professor William C. Stacey, Chair  
Assistant Professor Omar J. Ahmed  
Associate Professor Timothy M. Bruns  
Professor Geoffrey G. Murphy

Dakota Crisp

[dncrisp@umich.edu](mailto:dncrisp@umich.edu)

ORCID iD: 0000-0001-7921-7824

© Dakota Crisp 2019

## **DEDICATION**

This thesis is dedicated to my mother, Carol A. Crisp, and my late father, Dale N. Crisp. While opposite in most facets, their fundamentals brought them together and laid the foundation for my entire world-view: work hard, live truthfully, and be helpful.

## ACKNOWLEDGEMENTS

Rome was not built in a day, and it surely was not built by a single individual. This has been a tremendous experience, and I could not have done it without all the support. As I write this document, it is so much more to me than just an explanation of my work. The countless hours collecting and analyzing data were not contiguous, but instead interspersed between times of love, failure, and fun. To me, this document is a secret, encoded record of all the experiences behind the work that have shaped my life forever. To that end, I plan to use this section not just to acknowledge those that primarily contributed to my work, but as an acknowledgement to those that contributed to my life.

I would like to thank my family. Specifically, I would like to thank my parents for all their love and encouragement. Mom, thank you for teaching me to be empathetic, to seek the best in others, and to love myself. A PhD takes a lot of creativity and smarts, and it is no secret that I got them all from you. Dad, thank you for the lifetime of wisdom and perspective you shared with me before you passed. You never marched to any drum but your own, and I have benefited from adopting that characteristic. You always told me: “Life is about doing what you should do, not what you want to do”. For the times when it could not be both, your words have always guided me to do the right thing. Despite the arguments and the divorce, I am still amazed at the level of effort and cooperation you both exhibited to make sure I could be my best. You have always been there when I needed it, and I just hope I will continue to make you both proud. In addition, I would like to thank my siblings for extending that net of support. Scottie, we may



not get to game much anymore, but some of the best times in my life were staying up until 5 A.M. playing whatever we could. You definitely helped me take the stresses of a PhD in stride. Rachelle, you were basically a second mom, and that tag-team duo helped me navigate through aspects of life for which school could never prepare me. I would also like to take the time to thank my “second” family: the Kraft's. Alexandra, thank you for keeping me grounded and building my confidence. As I close this chapter of my life and start taking those first steps into the unknown, I'm heartened to know that you'll be with me to make an adventure out of it. To the rest, thank you for all the support and for giving me a home away from home.

I would like to thank my colleagues and mentors. I would like to thank all the members of the Stacey Lab, especially William Stacey and Steve Gliske. Believe it or not, I think I learned the most while we were stuck in conference hotels, trains, and airport terminals. I would like to thank Geoff Murphy and everyone in the Murphy Lab. Who knew a data nerd like me would end up getting his hands dirty and learning a thing or two while doing it? I would like to thank the group at the University of Melbourne, especially Alan Lai. Those 2.5 months went quickly, but I savored our morning chats over tea and our weekly foodie excursions. I would like to thank my collaborators at Aix Marseille Université, Christophe Bernard, Viktor Jirsa, and Marisa Saggio. You all helped provide the theoretical groundwork to make this research possible. I would like to thank the managing partners at The SearchLite, Gautam Rajpal and Steve LaChance. You both showed me a whole new side of the equations. Finally, I would like to thank my committee for guiding me along the right path.

Finally, I would also like to thank my close friends: Steven Peterson and Dylan Klawuhn. I learned from a young age to surround myself with people that inspire me, and you both have

certainly done the trick in your own ways. Wherever life may take us, I look forward to the stories our lives tell.

## Table of Contents

<b>DEDICATION</b> .....	<b>ii</b>
<b>ACKNOWLEDGEMENTS</b> .....	<b>iii</b>
<b>LIST OF TABLES</b> .....	<b>viii</b>
<b>LIST OF TABLES</b> .....	<b>ix</b>
<b>ABSTRACT</b> .....	<b>x</b>
<b>CHAPTER 1. Introduction</b> .....	<b>1</b>
<b>CHAPTER 2. Epidynamics: Navigating the map of seizure dynamics</b> .....	<b>8</b>
2.1 Abstract .....	8
2.2 Introduction.....	9
2.3 Classification of seizure dynamics.....	11
2.4 Taxonomy of human seizures .....	14
2.5 Correlation between clinical data and seizure type.....	18
2.6 Seizure dynamics vary in human epilepsy .....	18
2.7 A theory of seizure generation based on first principles of nonlinear dynamics .....	19
2.8 Ultraslow fluctuations to navigate the map of brain state dynamics .....	22
2.9 Discussion .....	25
2.10 Figures.....	33
<b>CHAPTER 3. Quantifying epileptogenesis with spontaneous and responsive     brain state dynamics</b> .....	<b>41</b>
3.1 Abstract .....	41
3.2 Introduction.....	42
3.3 Materials and methods .....	44
3.3.1 Animal Model .....	44
3.3.2 Stimulation paradigm.....	45
3.3.3 Data collection .....	46
3.3.4 Seizure detection.....	47
3.3.5 Data processing.....	48
3.3.6 Analysis.....	49
3.3.7 Data availability .....	55
3.4 Results.....	56
3.4.1 Seizure onset .....	56

3.4.2 Evoked responses .....	58
3.5 Discussion .....	60
3.5.1 Quantifying seizure dynamics.....	61
3.5.2 Evoked responses.....	62
3.6 Figures.....	64
<b>CHAPTER 4. Carbamazepine and GABA have distinct effects on seizure onset dynamics .....</b>	<b>73</b>
4.1 Abstract.....	73
4.2 Introduction.....	73
4.3 Methods.....	77
4.3.1 Animals .....	77
4.3.2 Experimental Procedure.....	77
4.3.3 Solutions .....	78
4.3.4 Data Analysis .....	79
4.4 Results.....	82
4.5 Discussion.....	84
4.6 Figures.....	87
<b>CHAPTER 5. Discussion .....</b>	<b>89</b>
<b>APPENDIX.....</b>	<b>93</b>
<b>BIBLIOGRAPHY .....</b>	<b>159</b>

## LIST OF TABLES

Table 4.1 Simple rules for visual classification of seizure onset dynamics.....	80
Table 4.2 Reviewer consensus on bifurcation labeling .....	83
Table S1 Visual classification system.....	99
Table S2 Reviewer agreement on simulated data .....	104
Table S3 Accuracy identifying bifurcations in clinical data.....	106
Table S4 Comparison of bifurcations with metadata.....	127
Table S5 Comparison of visual with dynamic classifications .....	129

## LIST OF FIGURES

Figure 2.1 Scaling-laws of bifurcations .....	33
Figure 2.2 Seizure dynamics taxonomy .....	34
Figure 2.3 Manual classification of seizures from long-term intracranial recordings .....	36
Figure 2.4 Modeling seizures.....	37
Figure 2.5 Fluctuations in the ultra-slow modulation of the path causes changes in the dynamics of the seizure .....	39
Figure 3.1 Progression of epileptogenesis .....	64
Figure 3.2 Electrode placement and stimulation pattern .....	65
Figure 3.3 Seizure occurrences and divergence measurements .....	66
Figure 3.4 Progression of seizure dynamics .....	68
Figure 3.5 Evoked response visualization .....	69
Figure 3.6 Probing analysis.....	70
Figure 3.7 Differences between experimental and control evoked responses .....	72
Figure 4.1 Raw waveform examples of the different observed onset bifurcations .....	87
Figure 4.2 Prevalence of seizure dynamics vs experimental condition .....	88
Figure S1A Saddle Node Onset .....	110
Figure S1B Supercritical Hopf Onset .....	112
Figure S1C SNIC Onset.....	114
Figure S1D Saddle Node or Subcritical Hopf Onset .....	116
Figure S1E SN or SubH onset after delta brush .....	117
Figure S1F Saddle Homoclinic of SNIC offset .....	119
Figure S1G Supercritical Hopf offset .....	121
Figure S1H Fold Limit Cycle offset .....	123
Figure S2 Unusual Fold Limit Cycle seizures .....	125
Figure S3 Dynamic classes with baseline shift.....	134
Figure S4 Dynamic classes without baseline shift.....	136
Figure S5 Complexity of classes and data classification results.....	139
Figure S6 Escape from the bistability region into the seizure-only region.....	147
Figure S7 Status Epilepticus patient 1 .....	149
Figure S8 Status Epilepticus patient 2 .....	150
Figure S9 Seizure with acceleration of spike frequency at seizure terminus .....	152
Figure S10 Varied frequency behavior of FLC offsets.....	155
Figure S11 Frequency behavior of SupH offsets .....	157

## **ABSTRACT**

Epilepsy is characterized by spontaneously recurring seizures that severely disrupt quality of life and pose risks of injury and death. Seizures can be seen in a wide range of other diseases (Alzheimer's, autism, Down's syndrome, etc.), indicating that epilepsy is highly heterogeneous and cannot be constrained to a single source. Yet to date, there is no method of categorizing seizures that can help distinguish the link between pathology and seizures. The aim of this work is to validate and explore a method of categorizing seizures based on their fundamental dynamics to provide a framework for future research to better investigate the underlying mechanisms of seizures and therapeutic approaches to stop them.

The first study used predictions from a previously-published computational model to visually classify seizures using dynamical transition features in two large datasets (simulated and real human data). Machine learning was applied to raw signal features to verify the accuracy of the reviewer's labels. It found that visual classification is consistent and supported by the signal feature analysis. We also investigate the model's predictions in real human data, finding that most dynamic classifications were observed and patients can have varying seizure dynamics over time.

The second study used data mining and machine learning in a long-term rat model of epileptogenesis to investigate the viability of these same dynamic principles as a biomarker of epileptic brain state. It also applied the same rigor to an analysis of the response to electrical stimulation. We found that evoked responses can be used to predict if an injured brain would

eventually develop seizures or not. Once seizures began manifesting, both evoked responses and seizure onset dynamics had strong correlation with the progression of epileptogenesis, suggesting they are independent biomarkers.

For the final study, we use the same principles of dynamics and machine learning to characterize differences between a low  $Mg^{2+}$  / high  $K^+$  mouse brain-slice seizure model with and without different anti-seizure drugs. It found that anti-seizure drugs can change the observed seizure dynamics, and each drug has a different effect on brain dynamics.

These three studies provide evidence that seizures can be categorized by their fundamental dynamics. These dynamics can provide mechanistic insights into current brain state, future brain states, and the response to anti-epileptic drugs. The results presented in this dissertation can be used as a framework to further investigate seizure mechanisms and personalize patient treatment and research. Next steps include using this framework to investigate seizure propagation and spatial variability.



## **Chapter 1**

### **Introduction**

Epilepsy is one of the most common neurological disorders, with an estimated prevalence of 50 million afflicted worldwide (World Health Organization 2017). It is characterized by spontaneously recurring seizures, which are “a transient occurrence of signs and or symptoms due to abnormal excessive or synchronous neuronal activity in the brain” (Fisher et al. 2005). As one can expect, these attributes severely disrupt quality of life and pose risks of injury and death.

Despite this considerable burden and risk to patients, it is extremely challenging to both treat and understand epilepsy. Approximately one-third of patients with focal onset seizures (seizures that initiate in only one hemisphere) have intractable epilepsy (Kwan et al. 2010), meaning that during the treatment process at least two different standard anti-epileptic medications failed to suppress seizures. For these patients, further treatment options included experimental drug trials, dietary restrictions, surgical removal of the seizure focus, and therapeutic electrical stimulation. While these options have their own varying degrees of success, a comprehensive and reliable solution is not available. In part, this is because epilepsy is a highly heterogeneous disease, with seizures seen in a wide range of other diseases (Alzheimer’s, autism, Down’s syndrome, etc.). As an effort to combat this heterogeneity, clinicians have tried to develop better seizure classifications, but with little success.

Current clinical methodologies to characterize seizures focus primarily on symptomatic features: focal vs generalized and physical presentations (Fisher et al. 2017). Focal vs

generalized describes the initial location of the seizure onset in the brain, determined electrographically. Specifically, if a seizure originates within one or both hemispheres. For physical presentation, clinicians try to determine if patients are consciously aware during seizures and whether there is motor involvement. While this methodology acts as the current gold standard in clinical applications, it is pure heuristics and far removed from explaining any of the underlying seizure mechanisms, limiting mechanistic reasoning and research. To create a more complete classification method, researchers have further explored electrographic features of seizure onsets in patients' electroencephalograph (EEG) recordings (Piero Perucca, Dubeau, and Gotman 2014; Lagarde et al. 2019a). These studies have classified seizure onset patterns based on basic frequency and amplitude characteristics (low-voltage fast, high amplitude poly-spikes, etc.). However, these studies are purely observational: there is no scientific rationale for the different types of seizure onset patterns, but rather the results of what the researchers found in a dataset. Furthermore, these classification systems are unvalidated beyond ill-defined reviewer consensus. This lack of scientific rationale is what hinders these methodologies from becoming frameworks for future research, which is why the International League Against Epilepsy calls these methodologies "operational (practical)" (Fisher et al. 2017), outlining the need for a seizure classification system based on a scientific rationale.

Jirsa et al. is a recent attempt at a scientifically-reasoned method of seizure classification, based upon first principles of systems dynamics theory (V. Jirsa et al. 2014). This study produced the Epileptor, a canonical model of seizure dynamics, that uses one pair of bifurcations to model the transitions brains make between "normal" and "seizure" states (V. Jirsa et al. 2014). In dynamical systems, a bifurcation relates to a sudden 'qualitative' or topological change in a system's behavior, instigated by changes in a subset of system parameters. Bifurcations are an

ideal modeling tool, as a system with different bifurcation types necessitates different underlying parameters (Seydel 2010). In other words, classifying seizures by their transitions should provide insight into the current state of the neural system. While bifurcations have no direct correlation to the biological properties of the brain, it acts as a new language and framework to study the brain. Jirsa et al. focused on only one bifurcation pair modeling the onset and offset of a single seizure, Saggio et al. created a generalized model, Epidynamics, for all seizure transition dynamics (M. L. Saggio et al. 2017a).

At its core, Epidynamics postulates that the brain can transition from “normal” to “seizure” state using only one of four different kinds of bifurcations (M. Saggio et al. 2017). Similarly, the reverse is also true: transition from “seizure” to “normal” state is made by one of four bifurcations. This means that each seizure can be fully classified by assigning it a pair of onset and offset bifurcations, creating a total of 16 different types of seizures. In theory, each of these bifurcations have three main electrographic signal features that can be used to differentiate them: inter-spike interval (ISI) trend, spike amplitude (SA) trend, and presence of direct current (DC) shift. See Figure 2.1 for reference. For seizure onset transitions, there are four main bifurcation types: Saddle-Node (SN), Saddle-Node on an Invariant Circle (SNIC), Supercritical Hopf (SupH), Subcritical Hopf (SubH). SNIC bifurcations are characterized by non-zero SA scaling and a decreasing ISI trend (scaled to square root function). SubH bifurcations have no specific scaling laws for either ISI or SA. SN also have no specific scaling laws but can be accompanied by a DC shift. Finally, SupH bifurcations have no ISI scaling while the SA scales from zero as a square root function. For seizure offset transitions, there are also four main bifurcation types. The first two are seen in the onset group: SNIC and SupH. These bifurcations are identical to their prior description, except their characteristics are reversed in time. SNIC

bifurcations have increasing ISI trend and SupH have SA that decreases to zero. The remaining two offset bifurcations are Saddle-Homoclinic (SH) and Fold Limit Cycle (FLC). FLC bifurcations are similar to SubH in that they also follow no scaling laws. SH bifurcations have increasing ISI trend that scales following a logarithmic function. While this taxonomy is well-defined, its representation of real seizure dynamics is untested. A model is only as good as its representation of life, and there is a need to bring this classification system from the theoretical to the practical, which is the basis of this thesis.

In Chapter 2, I will first validate the proposed taxonomy as a seizure classification system and then investigate its predictions about seizures. The novelty introduced in this thesis starts with validating the seizure taxonomy, as there is no gold standard procedure to follow. Perucca et al. has two reviewers that independently label their data, and then discuss disagreements until a conclusion is reached. Lagarde et al. also uses two reviewers to independently label their data, but uses a third, senior reviewer to settle any disagreements. A practical taxonomy should not be solely influenced by sentiment, and have devised a novel methodology that cross-validates the classification system on multiple levels. First, similar to previous research, I have multiple reviewers label our dataset. Next, I utilize feature analysis, machine learning, and data mining on the raw signal features to prove that there is a quantitative difference between each classification label. Finally, as a third level of validation, we perform this analysis twice: first on a large dataset of seizures simulated from the Epidynamics model and once more for our large dataset of real patient seizures. Testing our analysis first on the simulated seizures allows us to isolate the efficacy of our visual classification method on the “pure” theoretical dynamical features without the confounding factor of biological variance and real signal noise, producing a ground truth reference. Testing our analysis on the “messy” real seizures allows us to understand how this

taxonomy operates in the real world, providing insight into this taxonomy's translational nature. This level of analytical rigor is not implemented in the current seizure classification literature, and this thesis presents itself as method to standardize future classification validation.

After validating that Epidynamics can truly be used to classify seizures, I explore the predictions of the Epidynamics model, starting with complexity. Complexity is an ideal feature when trying to measure the prevalence of a phenomenon in a system. As an example, I present the case of flipping a coin. After flipping a coin, there can be three possible resting states for the coin: laying heads up, laying tails up, or standing on its edge. Assuming it is a fair coin, the requirements for laying on either side is equally difficult and thus equally likely. However, it is much more difficult for a coin to land and stay standing on its edge. It is possible given the perfect balance of forces on the coin, but such a procedure would be complicated and thus unlikely. Moving back to bifurcations, it turns out that each of the bifurcations presented in Saggio et al. have their own degree of complexity, based on the number of parameters that needs to change to trigger the bifurcation. Because we have bifurcations on a spectrum of complexity, we should have bifurcations that occur more frequently than others. In this study, we classify patients' seizures based on their dynamics, and check their prevalence against their level of complexity. Having this standard by which prevalence can be measured against is novel in the seizure classification literature, as all other research simply reports what is found.

In addition to complexity, Saggio et al. presented a "map" of the different regimes of seizure dynamics. This implies that changes in the brain state do not necessitate seizure freedom, but potentially a dynamically different seizure. In other words, there is potential for a patient's seizure dynamics to change over time. This is contradictory to Perucca et al. and Lagarde et al., as they assume patients each have their own "representative" seizure onset types. We find this

discrepancy important to pursue, as patients with either stereotyped or variable seizure dynamics would surely require different approaches for therapy. Therefore, we investigate seizure dynamics in a subset of patients with long-term, ambulatory data.

Given the knowledge that seizures can be classified by their dynamics, it is hard to truly predict how this might be helpful to patients. However, a good place to start is to look at all the ways we currently try to describe seizures (and fail) and reapply this model. The options for analysis are nearly endless: propagation, initiation, termination, response to therapy, etc. In Chapters 3 and 4, I focus on two specific applications of the Epidynamics taxonomy: progression of disease and response to medication.

In Chapter 3, I quantify changes in epileptogenesis. This is a natural application of the Epidynamics taxonomy, as different bifurcations necessitate different system parameters. Therefore, seizure dynamics can potentially be used as a biomarker for epileptic brain state. To study this, I use these dynamics principles to track seizures in a long-term rat model of epileptogenesis. In addition, the same rigor of analysis was used with electrically induced brain responses as a cross-validation. This study is important as epileptogenesis is a poorly understood process, and further insight could potentially uncover ways to track and control the process before patients develop full-blown epilepsy.

In Chapter 4, I quantify how different medications affect seizure dynamics. This investigation is relevant as the vast majority of epilepsy cases cannot be caught before the disease has fully manifested, producing a real-world need to provide therapy to patients with seizures. Here, I study how these same dynamic principles are influenced in a mouse seizure model with the presence and absence of different anti-seizure drugs. This study is important as it

provides a new language to characterize anti-epileptic medication, which can potentially provide insight into what specific therapies are accomplishing on a system level.

Together, these chapters validate a seizure classification system based on fundamental system dynamics, and use this taxonomy to investigate important aspects of epilepsy research and treatment. This thesis is unique in the way that it utilizes a seizure classification system based upon a scientific rationale and also validates the classification system before exploring various applications.

## Chapter 2

### Epidynamics: Navigating the map of seizure dynamics

#### 2.1 Abstract

Seizures are a disruption of normal brain activity present across a vast range of species, diseases, and conditions. Their underlying mechanisms remain mostly unknown. Here we introduce a mathematical theory– Epidynamics – based upon first principles of dynamic system theory, which provides a conceptual framework to characterize and understand how seizures start, evolve, and terminate. We provide the first objective taxonomy of seizures based on a straightforward analysis of the electrographic data. Analyzing a cohort of over 2000 focal-onset seizures recorded from 7 epilepsy centers on five continents, we find evidence of the predicted 16 Dynamic Classes of seizures. The theory also enables drawing a map of brain dynamics that includes most seizure classes and status epilepticus. We demonstrate that patients navigate the map during their lifetime and verify critical predictions of the theory. Epidynamics not only provides a way to stratify patients in complement to present practical classifications but also guides biophysically based mechanistic approaches and provides a language to describe the most critical features of seizure dynamics. Finally, we discuss how the theory can be practically translated to guide future epilepsy treatment strategies.



## 2.2 Introduction

Epilepsy is one of the most common neurological disorders with an estimated prevalence of 50 million worldwide (World Health Organization 2017). It is characterized by spontaneously recurring seizures, which are “a transient occurrence of signs and or symptoms due to abnormal excessive or synchronous neuronal activity in the brain” (Fisher et al. 2005). However, there are a vast array of signs, symptoms, and underlying causes of seizures. Thus, despite high prevalence and considerable morbidity and mortality, it has been challenging to characterize, treat, and understand seizures, which prevents the development of reasoned, mechanistic approaches to therapy and improved patient care. Seizure classifications to date have been purely descriptive of empirical data: clinical manifestations (e.g. focal vs. generalized) that are based upon the region of brain affected rather than the seizure itself, and visual descriptions of electroencephalogram (EEG) waveforms. These classifications have been subjected to numerous revisions and still have great difficulty reconciling pathology with phenotype. In its latest position paper, the International League Against Epilepsy states: “Because current knowledge is insufficient to form a scientifically based classification, the 2017 Classification is operational (practical)” (Fisher et al. 2017). A theory unifying our understanding of empirical data would constitute a significant step forward. Here we present the first mathematical theory accounting for the essential onset and offset dynamics of electrophysiological seizures based upon first principles. This new “Dynamic Class” allows scientific classification of electrophysiological seizures using practical, objective metrics and provides a conceptual framework to understand why different types of seizures can occur in patients during their lifetime. We then discuss how this theory of a seizure’s canonical dynamic characteristics—which we term the “Epidynamics”—can be used for immediate transfer to clinical practice, to provide a rational

method of characterizing seizures, and to allow a greater understanding of the underlying principles governing seizure generation and termination.

The basis of our theory is the observation that seizures are characterized by abrupt changes in the EEG waveform at seizure onset and offset, which we interpreted as bifurcations known from dynamic system theory (F H Lopes da Silva et al. 2003). As a seizure evolves, the brain moves from a normal state into a seizure and back again. Recent work has focused on describing these transitions with empirically-chosen visual patterns and has found interesting relationships with underlying pathology (P. Perucca, Dubeau, and Gotman 2014), surgical outcome (Jiménez-Jiménez et al. 2015; Lagarde et al. 2016), and Sudden Unexpected Death in Epilepsy (Rajakulendran and Nashef 2015). However, these transitions can also be described more rigorously and mathematically as bifurcations. Bifurcations represent qualitative changes that both define and constrain the system dynamics (Strogatz 2015). The concept has been used to understand neuronal firing: when a neuron goes through a bifurcation, the emergent dynamics often comprise a new set of behaviors such as multiple stable fixed points (rest activity) or limit cycles (oscillatory activity) (Izhikevich 2000). When a neuron oscillates quickly about a limit cycle, it produces fast repetitive activity known generically as bursting. These dynamics can be described by a set of differential equations and accompanying parameters. Concepts about bursting neurons can be extended to seizures, where bursting is used in a mathematical sense, and here refers to the alternation between healthy and ictal (oscillatory) states. Two variables are the minimum necessary to generate oscillations, and in systems with two variables there are only six types of bifurcations involved in bursting (Fig. 2.1). Four can be used to enter the bursting regime, and another four to exit, giving a total of sixteen possible combinations (Izhikevich 2000), which we call Dynamic Classes. A key benefit of this bifurcation-based theory is that it

unambiguously identifies the invariant properties of individual events, which may provide mechanistic insight into the underlying causes and response to specific interventions. It also provides a model that not only accounts for the effects of noise on the system (Suffczynski et al. 2005) and multistability (F. Lopes da Silva et al. 2003; Milton 2012), but also generates a time series. Generalizing this to epilepsy, Jirsa et al. (V. K. Jirsa et al. 2014) proposed the existence of 16 theoretically possible Dynamic Classes (i.e. seizure types), and found one seizure offset bifurcation that was present across multiple species, brain regions, and pathologies, including a small cohort of humans. Based on that initial work, we now expand and build a theory of the full taxonomy of human focal onset seizures. In the following, we begin with the definition of the different types of seizures based on dynamics at their onset and offset. Then, we show that seizures recorded from different centers in the world can be rigorously classified, and how classification can be performed in daily clinical practice. Next, we introduce Epidynamics, a general theory of seizure dynamics, which provides a map where all seizure types can be located. The map allows us to understand complex and unusual seizure patterns from the human dataset, and we demonstrate that patients navigate the map to express different types of seizures. Finally, we discuss how the theory can be used to improve patient care.

### **2.3 Classification of seizure dynamics**

The goal of this work is to characterize seizures by their underlying onset and offset dynamics, which depends upon identifying reliable, canonical dynamic features. While the dynamics of a single neuron have already been described (Izhikevich 2000), linking that behavior to a seizure generated by millions of neurons is complex. We chose to analyze the EEG signal from standard intracranial electrodes, as it is the most clinically-relevant and widely-

studied method to measure brain dynamics. The key to this analysis is to demonstrate that human seizures have the same classes of onset/offset patterns as individual neurons. These patterns, which are visible within the EEG waveform, identify the bifurcations that define the invariant properties, and thus the first rigorous classification, of seizure dynamics. Fig. 2.1 demonstrates these different bifurcations, showing how the signal changes in terms of amplitude and frequency of successive spikes and may contain a shift in the baseline as the seizure starts or stops. Of note, in dynamical terms, a “spike” is defined as any prominent sharp transient associated with the dynamical process. For human EEG, we assume this includes all fast transients  $< 200$  ms with amplitude that is distinguishable from the background. Of note this dynamical definition also includes the fast, low amplitude spiking seen at the beginning of some seizures.

In this work we present algorithms to measure the invariant properties, which can then be used to classify the seizure types. While the theory behind this classification has been proven mathematically (Kuznetsov 2004), measurement of these values under real conditions is challenging. This is because 1) EEG recordings of the brain are much more complex than single bursting cells, 2) EEG is notoriously noisy, and 3) there is limited understanding of the underlying physiology that produces the EEG waveforms (Reimann et al. 2013; Einevoll et al. 2013). Despite these limitations, we found strong evidence that at least one Dynamic Class exists (V. Jirsa et al. 2014). Herein, we present both an automated algorithm and a visual method to analyze these noisy data. We find that visual analysis is quite reliable and often preferable under clinical conditions, as demonstrated by recent work in other noisy neural signals (Haddad and Marder 2018). Therefore, while we do present the algorithm results as validation, the final clinical analysis is based upon the visual classifications.

Onset Types: As described in Fig. 2.1, there are four onset bifurcations. Two of these progress gradually from resting state into seizure via specific scaling laws for the amplitude or frequency (Strogatz 2015): in the supercritical Hopf bifurcation (SupH), the amplitude of the oscillations starts at zero and increases proportionally to the square root of the distance from the bifurcation point; the Saddle-Node on an Invariant Circle (SNIC) bifurcation has oscillations that increase in frequency as the square-root of the same distance. The other two, Saddle-Node (SN) and subcritical Hopf (SubH) bifurcations, have abrupt amplitude and frequency changes that do not follow scaling laws. The SN can contain a jump in the signal baseline (i.e. direct current (DC) shift), but in the absence of a detectable DC shift these two classes can be difficult to distinguish even theoretically. SN without DC shift and SubH are thus grouped together in this work. Further demonstration of the generation of these time series can be found in (V. Jirsa et al. 2014; M. Saggio et al. 2017).

Offset Types: Two of the bifurcations are characterized by decreasing frequency, following square-root scaling for the SNIC and logarithmic scaling for the Saddle-Homoclinic (SH) bifurcation. Both of these dynamics manifest as slowing of the seizure down to zero near its end, which is the well-known clinical hallmark of a seizure (St. Louis and Frey 2016). This “slowing” at seizure termination has been identified as an inherent characteristic of seizures across all spatial scales (M. a. Kramer et al. 2012), and in multiple species and brain regions (V. Jirsa et al. 2014). Due to the small number of spikes near the end of seizures, it is difficult to distinguish between these two scaling laws when using only frequency of spikes (V. Jirsa et al. 2014); throughout this work, when we refer to “slowing-down” it refers to logarithmic or square root scaling, implying scaling down to zero. The other two bifurcations do not require slowing at

termination: the SupH bifurcation with square-root-scaled decreasing amplitude and no scaling law for the frequency, and the Fold Limit Cycle (FLC) that has no specific scaling law. Note that these two offset types would appear somewhat atypical to a clinician, as “slowing down” is expected at the end of most seizures. The only dependence on a DC shift is that only the SH can have a shift, but the absence of a shift can be SH or SNIC.

## **2.4 Taxonomy of human seizures**

We analyzed seizures from 120 patients recorded on intracranial EEG in 7 centers worldwide (Appendix I.1) (Wagenaar et al. 2015; Ihle et al. 2010; Cook et al. 2013; Kanazawa et al. 2015) to identify the bifurcations at onset and offset. All patients had focal onset seizures. Results are shown in Fig. 2.2.

Accurate identification of bifurcations: The canonical features necessary to distinguish the bifurcations are the dynamics of the amplitude and interspike intervals (ISI) and the presence/absence of a DC shift. We identified the spike timing and amplitude to allow for both visual and mathematical analysis (Appendix I.2). In order to validate the analysis, we first compared the results of three human reviewers (Appendix I.3) and an automated algorithm (Appendix I.4) in a gold-standard computational model that generated 60 seizures of each type (M. Saggio et al. 2017). These methods were very successful in distinguishing the different bifurcations in the model data, although we had to consider SN without DC shift and SubH as a single group for seizure onset, and SH without DC shift and SNIC as a single group for offsets because there is no method to distinguish them in EEG data. We then compared these same methods on 120 human seizures. We found that concordance was also reliable in human data

(Appendix I.5). These results show that the chosen features are capable of distinguishing the different bifurcations reliably for both human visualization and algorithms, that human seizure dynamics are consistent with the modeled bifurcations, and that human reviewers can use the methods described in the next paragraphs to classify onset and offset bifurcations reliably. In addition, we found that human reviewers were more reliable than the automated algorithm in noisy clinical data. We then used the human markings on the clinical data for the taxonomy in Fig. 2.2. All code and data for this analysis are freely available for download (Crisp et al. 2019).

Onset dynamics - To analyze onset dynamics, we first investigated all 51 patients that had been recorded using equipment capable of visualizing DC shifts. Of note, DC shift alone has previously been shown to be highly correlated to the seizure onset zone (Kanazawa et al. 2015; Ikeda et al. 1999, 1996). Many seizures (41%) started with constant amplitude spikes and a DC shift, signifying SN bifurcation (Fig. 2.2E). The second most frequent was similar amplitude/frequency dynamics without a DC shift (either SubH or SN, 37%), followed by SupH (14%) and SNIC (6%). Ambiguities in the classification were treated systematically as detailed in the Appendix (I.6), and only 1/51 seizures could not be agreed upon by the reviewers. Despite the inability to distinguish SN (-DC) and SubH, we demonstrate that at least three of the predicted bifurcation types are present at onset in human seizures. Importantly, some seizures display complex dynamics because they go through more than one bifurcation as the seizure begins. For example, nearly half of the seizures labeled as SN onset progressed into square-root amplitude scaling (likely due to spread of the seizure to neighboring tissue) after 2-5 seconds, consistent with a switch to SupH dynamics; we only labeled the initial bifurcation herein. For this reason, we have slightly modified the definition of onset bifurcation as compared to the

literature. Here the onset bifurcation is the one causing a departure from the resting state, even if it is not directly causing the onset of oscillations as there can be intermediate states (Appendix II.1).

We next looked at the onset bifurcations in the other 69 seizures that were recorded with non-DC coupled hardware. Of the four onset bifurcations, SN and SubH become indistinguishable without a DC shift available. Combining these two into a single group, we found that 67% were SN-SubH, 26% were SupH, 6% were SNIC, and only one seizure did not have reviewer consensus.

Offset dynamics – We first examined offsets in those patients with DC recordings for the most robust classification. The analysis of the interspike intervals (ISI) and spike amplitudes revealed a logarithmic/square-root slowing-down with constant amplitude in 20/51 patients, and of those 10 had DC shifts at offset. Thus, 10/51 (20%) were SH, while the remaining 10 (20%) were potentially SH or SNIC (Fig. 2.2F). The remaining 31 patients did not have slowing at the end of their seizure (53% FLC, 6% SupH, 2% no reviewer consensus).

For non-DC coupled data, we grouped SH and SNIC in the remaining 69 patients. The majority of seizures had arbitrary ISI and/or amplitude (54% FLC), while 41% had slowing down characteristic of SH-SNIC. The remaining seizures either had constant ISI with amplitude that decreased as a square root (SupH, 3%) or had no consensus among reviewers (3%).

Examples of the different clinical bifurcations are shown in Appendix I.7.

Analyzing arbitrary dynamics. One significant challenge in the above analyses was the presence of noise. Within the theoretical model, “arbitrary” dynamics refer to abrupt changes without



clear scaling laws to or from zero. However, in human data analysis “arbitrary” includes a wide range of other behaviors, especially noise. It is important to note that the taxonomy above includes the first seizure that could be analyzed from every patient—we did not restrict the analysis to “clean” seizures. Some of the seizures were noisy, either from technical concerns or physiological effects of the seizure. We chose this method in order to provide a robust, real-world demonstration of this analysis. Because noise can be classified as “arbitrary,” this analysis may overestimate the numbers of SubH-SN onsets (no DC shift) and FLC offsets. However, it was clear that this limitation was not merely technical: several patients had complex physiological dynamics. Four of the FLC seizures were highly unusual from a clinical perspective: one had increasing amplitude for the last 10 seconds, one consisted of low-voltage fast activity that ended abruptly without any other change, one ended with irregular spike waves, and one had accelerating frequency at the end (Appendix I.8 and Appendix V).

16 Dynamic Classes of seizures – The preceding data validate that at least three types of onset and offset are systematically present in human focal epilepsy. As detailed above, real clinical data are challenging: the lack of DC shift makes it difficult to distinguish some bifurcations, and the noisiness of EEG is hard to distinguish from arbitrary dynamics. Nevertheless, these results show robust evidence that human seizures conform to both the onset and offset bifurcations predicted by our model. These combinations lead to a taxonomy containing sixteen Dynamic Classes of electrographic seizures (V. Jirsa et al. 2014). We identified the Dynamic Classes in patients with DC recordings. Two patients did not achieve reviewer consensus (one onset, one offset), leaving 49 patients (Fig. 2.2F). We identified 12 different Classes, with the limitation that several of the Classes cannot be fully distinguished in the absence of a DC shift (e.g. SH(-

DC) – SNIC offsets). The taxonomy was dominated by seizures with either SN or SubH onsets and slowing (SH-SNIC) or arbitrary dynamics (FLC) at the end. In this cohort of focal onset seizures, the SupH and SNIC onsets were less common, accounting for all 4 Classes that were absent.

## **2.5 Correlation between clinical data and seizure type**

We compared all available clinical metadata from patients with their Dynamic Class and found no correlation between seizure class and patient gender, pathology, or localization. There was a correlation with age, as older patients tended to have more SupH onsets (Appendix I.9). We also compared these results with a prior visual classification that identifies 7 basic seizure onset patterns (P. Perucca, Dubeau, and Gotman 2014), and found 6/7 patterns without any apparent relationship to clinical data or pathology (Appendix I.10). There were no significant similarities between the Dynamic Class and the visual classification.

## **2.6 Seizure dynamics vary in human epilepsy**

While analyzing this dataset, we noted that one patient had two consecutive seizures belonging to different classes: one supH/supH and one supH/SH, raising the possibility that an individual may express different types of seizures. This finding was surprising, as many clinicians assume that a person’s seizure should be “stereotyped”, i.e. consistent over time. In fact, multiple medical devices have been designed under the presumption that a patient’s seizures would have similar appearance over time (Cook et al. 2013; Morrell 2011). To test whether individuals display different types of seizures over time, we used a unique dataset from Melbourne in which patients had intracranial EEG recorded continuously for many months

(Cook et al. 2013). We analyzed over 2000 seizures from 13 patients. Given the size of the sample, we limited the analysis to the most straightforward metric: the ISI at seizure offset to determine whether there was slowing at seizure termination. This allowed us to differentiate the SH/SNIC from the supH/FLC bifurcations (i.e. slowing-down or constant ISI). There were 658 seizures of sufficient length ( $> 25$  seconds) to measure the offset ISI. To be conservative, we only classified seizures as slowing-down or constant if such a determination was unequivocal and labeled the rest as “not assessed,” meaning that the determination was not readily evident on brief visual inspection. As seen in Fig. 2.3, all 13 patients expressed at least two offset patterns. Note that this is likely an underestimation of the heterogeneity in seizure classes: these recordings did not contain DC coupling so onset bifurcations were not assessed, and we did not distinguish the offsets into all four types. Nevertheless, we can unambiguously conclude that individuals have seizures from different classes over time.

## **2.7 A theory of seizure generation based on first principles of nonlinear dynamics**

The clinical data above show that seizures can be categorized based on their onset/offset bifurcations, that seizures can include several bifurcations and that patients have multiple types of seizures. We thus decided to formalize these findings within a unifying mathematical theory, which can account for all these behaviors (Appendix II). During seizures, the firing activity of neurons becomes organized, enabling the emergence of oscillatory activity that can be observed in electrographic recordings. This greatly reduces the degrees of freedom necessary to describe the observed activity, i.e. a small number of differential equations are sufficient to describe the collective behavior (Fig. 2.4A). We here consider a system with the minimum number of variables necessary to produce oscillatory activity, two. Based on the parameter values, two

states can be distinguished: resting (fixed point) or oscillatory (limit cycle). When these two states coexist for the same range of parameter values (bistability), transitions between them can be promoted by noise if the system is sufficiently close to a bifurcation (F H Lopes da Silva et al. 2003; Kalitzin, Velis, and Lopes 2010). However, the statistics of ictal durations (Suffczynski et al. 2006) points to the existence of a deterministic process governing this transition for seizure offset and possibly for the onset. This can be achieved with the addition of a third variable acting on the timescale of ictal duration. We previously validated this approach with the “Epileptor,” a set of five differential equations able to account for the most dominant seizure class (V. Jirsa et al. 2014) (SN/SH, also known as ‘square-wave’ bursting (Rinzel 1987)). In the Epileptor, the transition from “normal” to seizure state and back again, as well as the seizure dynamics, are controlled by a collective permittivity variable that evolves on a slow time scale. However, the Epileptor only accounted for a single Dynamic Class and is not sufficient to explain the data presented above. The fact that individuals can express different classes of seizures over time leads to two predictions that must be included within a model of human seizure dynamics: different classes of seizures must coexist in the same model, and there must be an endogenous mechanism by which the brain can transition slowly between the different classes.

Addressing these predictions within the framework of bifurcation analysis provides the entry point to propose a general theory of seizures. Previous mathematical work demonstrated that the procedure to build a minimal model for the SN/SH class (Golubitsky, Josic, and Kaper 2001) provides a two-dimensional map for the parameter space of the fast variables on which all the six bifurcations can be placed (Dumortier et al. 1991). In effect, the map is a representation of the range of states in which a brain region can exist, oscillatory (ictal) and non-oscillatory (interictal), and the transitions between them. The oscillatory state produces spiking activity that

is described by the fast variables (millisecond scale activity). However, on a much slower time scale of the order of seizure length, the brain can move towards a transition to an interictal state, as described by a slow variable. Migrations to different locations on the map can occur on a usually even slower timescale (10's-1000's of seconds), which we call here "ultraslow". The use of an ultraslow variable allows full exploration of the map (M. Saggio et al. 2017). Applying these general mathematical principles to epilepsy implies that any brain region able to generate SN/SH seizures can potentially generate other classes by navigating to different dynamical regimes (i.e. changing the parameters of differential equations) (M. Saggio et al. 2017). The map related to the organization of seizure classes is shown in Figure 2.4B-C. The state of a brain region at any moment can be represented as a location on the map, which will define its dynamical properties. Regions in the map that correspond to different regimes, including resting and ictal states, are separated by bifurcation curves. Seizures are represented as black arrows, each arrow corresponding to one specific seizure class. To produce a seizure, the system, which is initially in the resting state within the bistability region, heads towards the onset bifurcation curve. When this curve is reached, the resting state disappears and the system is forced to go into the oscillatory seizure regime within the bistability region. This transition in state causes an inversion in the trajectory of brain state, with the system now heading towards the offset bifurcation curve. When the offset is reached, the system goes back to rest and inverts direction again. Movement along the black arrow is produced by slow (of the order of the ictal length) mechanisms leading to seizure offset. Note that the movement towards the onset and offset bifurcations occurs in both cases from within the bistability region. Ultraslow movements on the map are responsible for changing the location of the brain state while at rest and enable the expression of different classes of seizures as observed clinically. This theory thus provides a

potential explanation for the clinical observation of multiple classes of seizures in a single patient, and the map provides a hypothesis to describe how a patient's current state (i.e. location on the map) can affect seizure dynamics (whether a seizure is likely to occur, and what type is most likely). Figure 2.4C depicts paths (black arrows) for seven of the 16 Dynamic Classes placed on a two-parameter map. Adding one additional parameter allows this map to be extended and create seven other Classes in three dimensions, while the final two Classes require even higher dimensions to create (M. Saggio et al. 2017). These higher-dimensional Classes require very fine parameter tuning, and thus are less likely to occur (M. Saggio et al. 2017; Golubitsky, Josic, and Kaper 2001). It is noteworthy that our clinical data show that the Classes that occurred the most (e.g. SN/FLC and SN/SH) were predicted to be among the most likely to occur (Appendix II.3).

## **2.8 Ultraslow fluctuations to navigate the map of brain states**

It is important to note that the topology of the map in Fig. 2.4 was initially proven mathematically to be generic and rigorously valid for bursting (Dumortier et al. 1991; Baer et al. 2006). This invariance establishes the ground truth to define the relationships between the different bifurcations in the proximity of the SN/SH class, which leads to a key prediction: transitions between certain classes may be more common due to their proximity on the map. For example, considering the bistability region in the upper part of the map, we note that the offset curves of SH and SupH approach until they meet. When the curves are very close, even small fluctuations in the parameters can cause a transition between classes. If fluctuating internal conditions allow individuals to move around these regions of convergence, patients may have seizures belonging to different classes over time, as observed in our longitudinal analysis. The

model predicts that transitions between specific classes are more likely to occur if these classes are close in the map, in the sense just shown of bifurcation curves approaching each other within the same bistability region. On the contrary, transitions between classes belonging to distant bistability regions require stronger changes in the ultraslow variable(s) and are thus less likely to occur.

The map also predicts that movements towards different bifurcations can occur while a seizure is ongoing. As proof of concept, we found several examples of such fluctuations in our cohort. In Fig. 2.5A, one patient's seizure had constant ISI and square-root amplitude scaling for approximately 70 seconds, properties exhibited when approaching the SupH bifurcation. The seizure appeared to be terminating, but then it abruptly restarted to terminate with slowing-down ISI and constant amplitude (SH/SNIC bifurcation). We found five examples of this behavior in our data (out of >2000 seizures) and reproduced it with our model. By definition, the Dynamic Class includes only the onset and final offset bifurcation, but the behavior during this seizure is intriguing and can be explained by the model. We considered a path for the SN/SupH class with an ultraslow drift of the offset point that changed the path to SN/SH and added noise to all variables to simulate fluctuations. With these settings, we ran 100 simulations, which generated several different Dynamic Classes, predominantly SN/SH, SupH/SH, and SN/SupH (Appendix III). Several had transitions during the seizure from one bifurcation to another, 10 of which in the same manner as the data in Fig. 2.5A, switching from SupH to SH offset. Thus, the clinical example is one of the most favorable combinations within the model, as the SupH and SH bifurcations are so close that small fluctuations can cause the switch.

*Status epilepticus*: Explorations of the map also demonstrated another effect sometimes seen clinically: status epilepticus. Simulations with the previous settings in some cases produced continuous seizures that did not resolve by the end of the simulation, equivalent to status epilepticus (El Houssaini et al. 2015). We analyzed the corresponding trajectories on the map to determine how this had occurred. Prolonged seizures occurred when the brain state crossed the SN onset curve but was unable to return to rest through the offset bifurcation and remained mainly in the violet “seizure only” region in Fig. 2.5G. The slow variable naturally drives the state towards offset, but in these cases was continually overridden by noise, causing the state to ‘escape’ from the bistability region. We then analyzed this effect by simulating various levels of noise and showed that there was a clear correlation between the noise variance and the likelihood of entering status epilepticus (Appendix IV). We compared these results with our clinical data, which had two examples of non-convulsive status epilepticus. In both cases, the seizures began in typical fashion, but instead of terminating began having long periods of constant ISI with varying periods of amplitude fluctuations. There were many abrupt transition periods during which the ISI and amplitudes became arbitrary. After these brief periods of disorganization, the dynamics returned to constant ISI. We compared the dynamics of our model results with these human seizures and found that the transition between different dynamics is quite similar. In Fig. 2.5D, we show a portion of two human seizures and one example of the simulation (Fig. 2.5E-F) and movement on the map (Fig. 2.5H-I). Further demonstration of the patients’ status epilepticus is provided in Appendix IV. The patterns of organized- alternating with disorganized- firing, often known clinically as “waxing and waning seizures,” are entirely consistent with the model: the seizure undergoes periods in which it progresses towards termination, then because of noise



it reverts to a point farther away from the offset bifurcation, as described previously (M. A. Kramer et al. 2012).

*Accelerating seizure:* We then analyzed the seizure offset that increased in frequency described in Appendix I.8. In this case, we explored conditions on the map that could produce “speeding up” at the end of the seizure. We identified multiple trajectories in the map of brain states capable of producing these unusual seizure dynamics. As in the case of status epilepticus, these unusual patterns are dependent upon the relative position within the brain map, in this case occurring when brain states along a trajectory are affected by multiple bifurcations that are in close proximity (Appendix V). These results further validate our theory of Dynamic Class and show how it provides a rational explanation for a wide range of physiological dynamics.

## **2.9 Discussion**

Seizures have been recognized clinically for millennia, but after nearly a century of electrographic recordings we still do not have a scientifically-based method of characterizing them. We here address this issue and provide the first general mathematical theory that explains the basic features of seizure onset and offset dynamics, which we term collectively the ‘Epidynamics’ of seizures. In canonical terms, there are 16 Dynamic Classes of seizures, and our theory provides a general dynamical map that describes how a brain region can move between these conditions. Our classification aims at precisely identifying the seizure type in terms of dynamics, without any dependence upon specific symptoms, pathology, or localization. Thus, it is highly complementary to the classical operational classifications used by clinicians to diagnose and treat patients, which are based upon those factors and are continually being updated (Fisher

et al. 2017). The Dynamic Class describes the behavior of the seizure itself, while the clinical classification describes the patient's symptoms: together, both classifications are synergistic and can be used to improve patient stratification and potentially provide more targeted treatments. The classification we propose is based on a simple, invariant, objective metrics that have compelling scientific rationale. With DC-coupled recordings, it is possible to distinguish the Classes with high fidelity, even with visual inspection. This method is thus readily available to clinicians, as many standard EEG acquisition devices now have excellent resolution near DC ( $<0.1$  Hz).

Our interpretation of the results relies on some key assumptions. First, we are assuming that the onset and offset of seizures are brought about by bifurcations. Another common mechanism in the literature is noise-induced transitions (Fernando H. Lopes da Silva et al. 2003), which our model can reproduce (see Appendix II.4 for a discussion of how this affects the classification). Second, we rely on the assumption of timescale separation between the dynamics of the spikes within seizures and the slower dynamics controlling seizure threshold and termination (both in theory and in the simulated sample of data, see Appendix II.5). If this assumption does not hold, different phenomena could occur and the scaling laws could be impossible to identify. Third, we only considered planar bifurcations for simplification (Appendix II.6). These assumptions were the axioms for developing the theory and data analysis. Future work will address the validity and consequences of these simplifying assumptions.

Similar to sleep, seizures are universal from insects to humans, leading to the proposal that seizures are an inherent property of a brain, i.e. they are endogenous activities that perhaps barely changed during evolution (V. Jirsa et al. 2014). This may explain why, despite the vast range of genetic, structural, chemical, and developmental conditions that cause epilepsy, seizures

have a remarkably limited set of dynamical behaviors. It is therefore not surprising that elementary mathematical laws can describe their electrophysiological signature. However, clinical interpretation of seizure dynamics has been almost universally based on simple observation, in which clinicians report the frequency and morphology of spikes. This method is helpful to identify primary generalized epilepsies, but within focal seizures has limited clinical use. Two notable exceptions are the presence of low voltage fast activity (Wetjen et al. 2009) and focal DC shifts (Ikeda et al. 1999), both of which are highly predictive of the true seizure focus. In this work, we now show that both of these patterns are hallmarks of the SN onset bifurcation, showing that identification of the Dynamic Class can have clinical utility. In effect, what those past studies demonstrated was that clinicians had discovered empirically one of the predictions of Epidynamics: the outcome is improved if clinicians can resect the region of brain that showed the clearest SN onset bifurcation.

One limitation of previous clinical descriptions of seizures is that it has been unclear which dynamical features are relevant. There is high variability in the frequency and morphology of spikes due to individual fluctuations and noise. Our analysis identifies the invariant dynamics that impose important constraints on the system. A crucial aspect of our approach is that it allows us to disentangle characteristics that are necessary to describe the dynamics from other seizure related phenomena that are not fundamental to our simplified model (e.g. spike and wave complexes, preictal spikes, etc.). For instance, while spike frequency or amplitude of individual spikes can vary significantly (V. Jirsa et al. 2014) and are not incorporated into our model, the presence of slowing down (SH or SNIC offset) is a fundamental aspect of that seizure's dynamics. It is important to note that we only analyzed the particular case of drug-resistant epilepsies investigated with invasive intracranial recordings; however, it is

unlikely that this theory is specific to such epilepsies as seizures forced in non-epileptic networks follow the same universal rules (V. Jirsa et al. 2014). We note that prior work focusing on individual bifurcations are all also entirely consistent with our comprehensive model of Dynamic Class, which encompasses all these onset and offset possibilities and further shows how they interact (Appendix VI).

This work does not include data from generalized onset epilepsies, as these are not typically recorded with intracranial EEG. Our taxonomy is, however, fully consistent with past work on generalized epilepsy dynamics (Wendling et al. 2015). Absence seizures, for instance, begin with sudden onset and offset of  $\sim 3$  Hz large amplitude oscillations without a DC shift (Slaght et al. 2004) and terminate abruptly without slowing down to zero, which would point to a SubH/FLC class (which is the most likely Dynamic Class (Golubitsky, Josic, and Kaper 2001), see Appendix II.3). In this work with focal epilepsies, the most common Classes were the SN (with DC shift)/FLC and SN/SH (which are also likely Classes).

When comparing our results with a past visual classification system of spike frequency (P. Perucca, Dubeau, and Gotman 2014), we found no correlation with pathology in our cohort of 120 patients. However, our cohort did not have any patients with tuberous sclerosis, which was the only pathology associated with burst suppression in that prior work. Combining the data from both studies, the different patterns appear to be either evenly distributed or too rare to find robust correlations with pathology. Similarly, Epidynamics is not strongly correlated with pathology. In terms of the map of brain activity, we hypothesize that what determines the seizure dynamics is not the pathology per se, but the location of the brain on the map. Specific pathologies may predispose to certain regions, but there are many complex dynamics affecting

brain state and many conditions that can produce similar dynamics. This coincides with the idea of this brain map showing the full range of potential seizure onset and offset activity.

There is great potential in characterizing a seizure's Epidynamics, as it provides a unique perspective on brain networks. We have previously demonstrated that very different biophysical mechanisms can produce the same class of seizures (V. Jirsa et al. 2014). Here we show that seizures from 120 patients with a wide array of focal pathologies can be grouped into similar seizure classes. Our data show that different seizure classes imply different locations within the dynamic map, but cannot be used to infer biophysical mechanisms in the absence of other constraints. Note that operational classifications are not predictive of mechanism either, but Epidynamics provides insight and predictions that can guide future research and clinical decisions. Understanding the underlying dynamics can help in the design of strategies to control seizures, such as with electrical stimulation (Kalitzin, Velis, and Lopes 2010). Studies on neuronal bursters (Izhikevich 2000), which are organized in similar dynamic classes, demonstrate that classes have different sensitivity to stimulation. For example, SubH onset act as resonators, which require a resonant frequency in the stimulus to trigger oscillations, while SN onset behaves as an integrator in which the nature of the stimulus (excitatory or inhibitory) rather than the frequency plays a key role (Izhikevich 2000). There is a long history of using perturbation to probe the proximity of a nearby bifurcation in disciplines such as electrical power (Chow et al. 1990) and reservoirs (Heppell, Caswell, and Crowder 2000). Past work on stimulation to assess epileptogenicity (Alarcon 2005; David et al. 2010; Kalitzin et al. 2005) is similar to such work and would be greatly enhanced with the insight gained from this model to understand the nearby bifurcations. Further theoretical and clinical work is necessary to assess whether knowledge of the Dynamic Class could also improve the ability to abort seizures with

tailored stimulation. The second important prediction is that the synchronization properties of coupled bursters are bifurcation-dependent (Belykh, Reimbayev, and Zhao 2015; Reimbayev and Belykh 2014; H. X. Wang, Wang, and Lu 2011). This is a key issue for seizure propagation, as it predicts that the ability of a seizure to spread is dependent upon its class. Since the spatiotemporal organization of the seizure is part of the data features used to personalize brain network models (Virtual Epileptic Patient (V. K. Jirsa et al. 2017; Proix et al. 2017)) and functional connectivity based approaches (Hutchings et al. 2015; Taylor, Wang, and Kaiser 2017; Sinha et al. 2017), the choice of the right dynamic class is critical for successful patient modeling and clinical translation.

Another significant contribution of this work concerns the dynamics of the slow permittivity variable to explain how slow changes in the behavior/state of a brain region can bring it closer or farther away from different bifurcations, i.e. seizure threshold. The fact that all 13 patients had seizures belonging to at least two classes implies that the permittivity variable moves on a dynamical map in which different types of bifurcations can occur. Each parameter of the map should be considered as a representation of a manifold of physiological variables that cooperate to produce a particular change in the system. Given the slow timescale at which these changes occur, neurochemical substances (e.g. hormones, neuromodulators etc.) are the best candidates. Within the permittivity variable we can here distinguish two timescales: a slow timescale of the order of the ictal length, and an ultra-slow timescale of the order of the interictal length (hours, days, months, years). Typical examples include the circadian regulation of seizures (P J Karoly et al. 2017) and catamenial epilepsy. Interestingly, both males and females display ultraslow (weeks) modulation of seizure probability both in rats (Baud et al. 2019) and humans (P J Karoly et al. 2017; Baud et al. 2018), further suggesting that these results are

species- and sex-independent. Those results and ours strongly support the proposal that patients move closer and farther away from seizure threshold (i.e. “travel the map”) during their lifetime. This theory may also be helpful in assessing a brain’s current proximity to seizure bifurcations, i.e. predict the risk of seizures occurring. Several features are altered when nearing the onset bifurcations, such as preictal spikes (V. Jirsa et al. 2014), variance of the signal (Meisel et al. 2015), and reaction to electrical probing of cortical excitability (Freestone et al. 2011). Recent work has shown that interictal discharges act like system perturbations that behave like the slow approach to bifurcations, just as predicted by our model (Chang et al. 2018). Seizure forecasting, based on electrographic recordings, is already enhanced when circadian rhythms are used to inform the model (P J Karoly et al. 2017). If the ultraslow physiological correlates of the map’s parameter could be identified, measured, and manipulated, this would open new possibilities to assess when the patient is moving towards unsafe regions of the map and to alter their trajectory, i.e. control seizures before they occur.

Our theory describes a map of brain states that accounts for the potential Dynamic Classes of seizures, and how the resting brain can navigate between them. This is not a unifying theory to describe seizures completely, as we defend a complementary approach, combining it with traditional operational classifications. However, it provides a unique avenue to classify seizures based upon their key dynamical features, while providing insight into how seizures become more or less likely to occur at a given time. A necessary corollary is that, although our theory has been developed in the context of seizure dynamics, it likely extends to physiological function of the healthy brain (e.g. alterations between REM and slow wave sleep, and the appearance of gamma frequencies or ripples during slow wave sleep) and stipulates the existence of at least two time scales in any theory of the brain. Slow time scales are present in many

theories of brain function, but typically have been limited to the domain of learning and adaptation, thus functionally separated from fast processes. Here the functional integration and co-evolution of the fast neuroelectric and slow permissive time scales suggests emergent and inherent properties of brain processes.



## 2.10 Figures

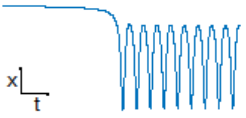
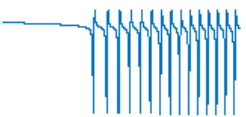
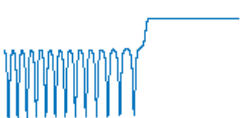
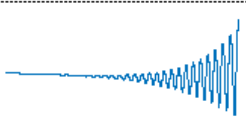
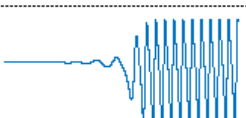
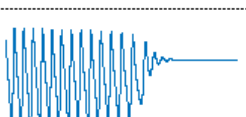
<i>Bifurcation</i>	<i>Timeseries</i>	<i>Amplitude</i>	<i>Frequency</i>	<i>Baseline jump</i>	<i>Rest - Seizure</i>
Saddle-Node (SN)		<i>non zero</i>	<i>non zero</i>	can be present	→
Saddle-Node Invariant Circle (SNIC)		<i>non zero</i>	<i>zero (<math>\sqrt{\lambda}</math>)</i>	no	↔
Saddle Homoclinic (SH)		<i>non zero</i>	<i>zero (<math>\ln \lambda</math>)</i>	can be present	←
Supercritical Hopf (SupH)		<i>zero (<math>\sqrt{\lambda}</math>)</i>	<i>non zero</i>	no	↔
Subcritical Hopf (SubH)		<i>non zero</i>	<i>non zero</i>	no	→
Fold Limit Cycle (FLC)		<i>non zero</i>	<i>non zero</i>	no	←

Figure 2.1 – Scaling-laws of bifurcations. Six bifurcations are responsible for the transition from rest to seizure and vice-versa. For each bifurcation we report: name and abbreviation; an example of timeseries; whether the amplitude or frequency of the oscillations goes to zero at the bifurcation point, and if they do how they change as a function of the distance to the bifurcation point ( $\lambda$ ); whether the baseline of the signal shows a baseline shift; and if the bifurcation can be used to start (→) or stop (←) a seizure or both (↔).

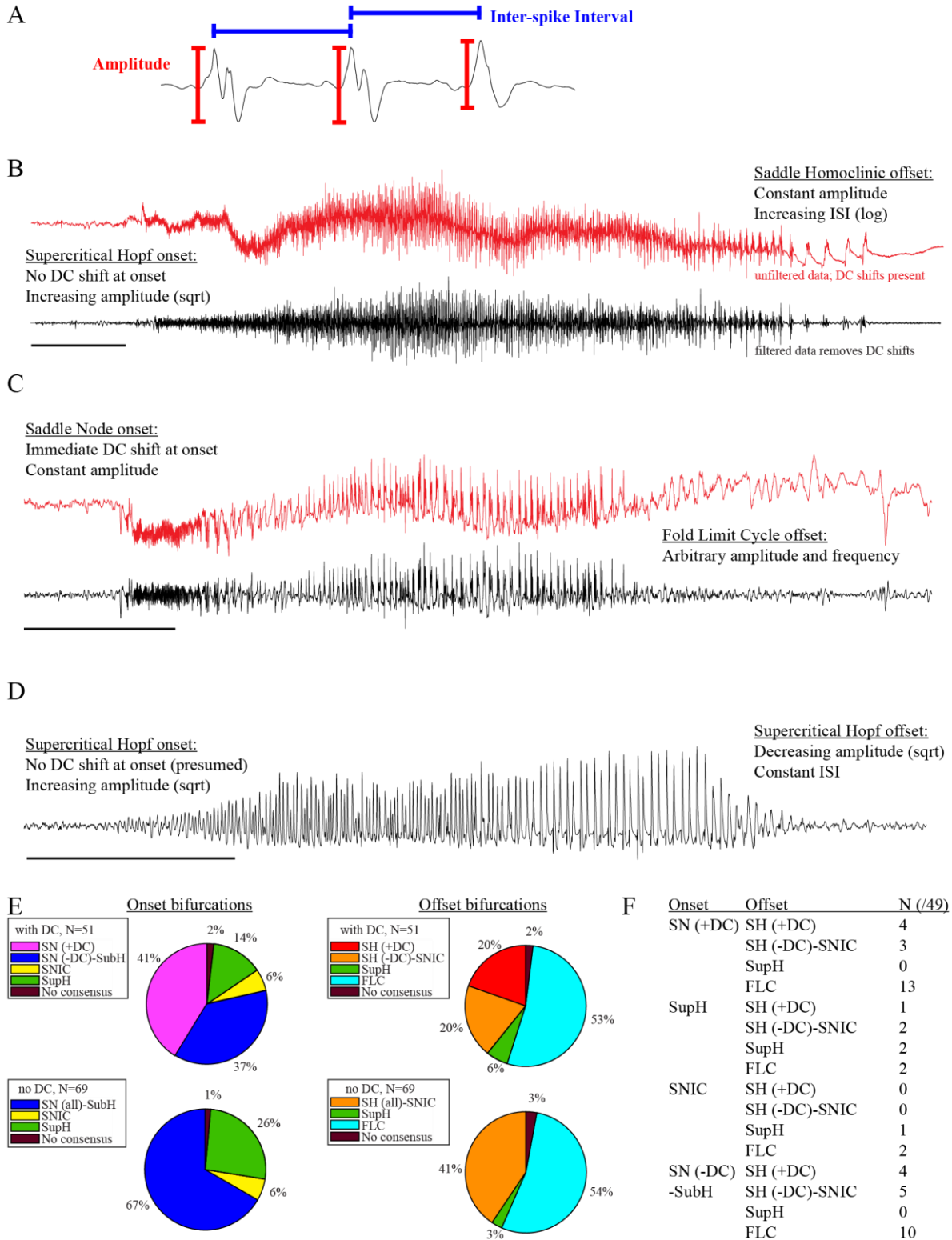


Figure 2.2 – Seizure dynamics taxonomy. (A) interspike intervals (ISI) and peak-to-peak amplitude were measured for every spike during seizures. (B) DC-coupled (red) and high-pass

filtered (black) data of a seizure shows SupH onset and SH offset. (C) SN onset characterized by DC shift at onset. Ambiguous seizure offsets were included in the analysis as FLC. (D) SupH onset and offset. Although this patient did not have DC-coupled recordings, the amplitude scaling is clearly most consistent with SupH. Scale bars: 10 sec. (E) Final results for all onset and offset bifurcations tested. All four bifurcation types were present. (F) Final taxonomy of the 49 patients with onset+offset classifications.

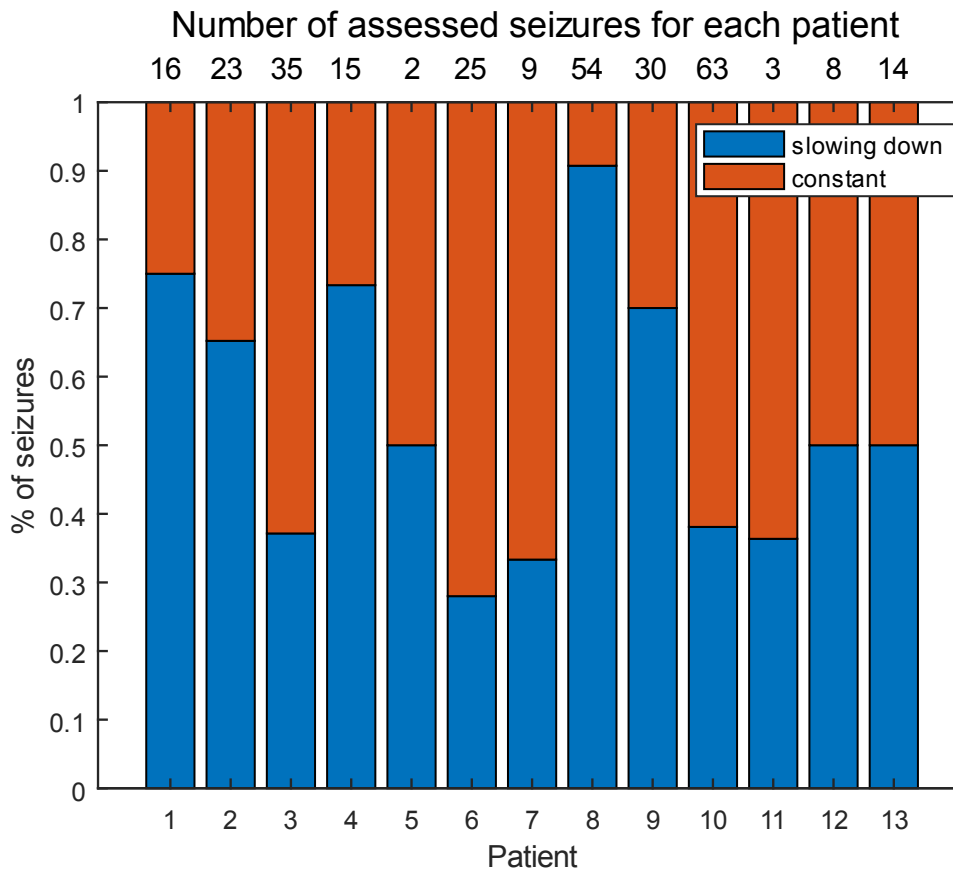


Figure 2.3 – Manual classification of seizures from long-term intracranial recordings. Only seizures with obvious slowing-down (blue) or constant (grey) scaling were labeled; any seizure that could not immediately be characterized was not assessed. Top: the number of seizures analyzed in each patient.

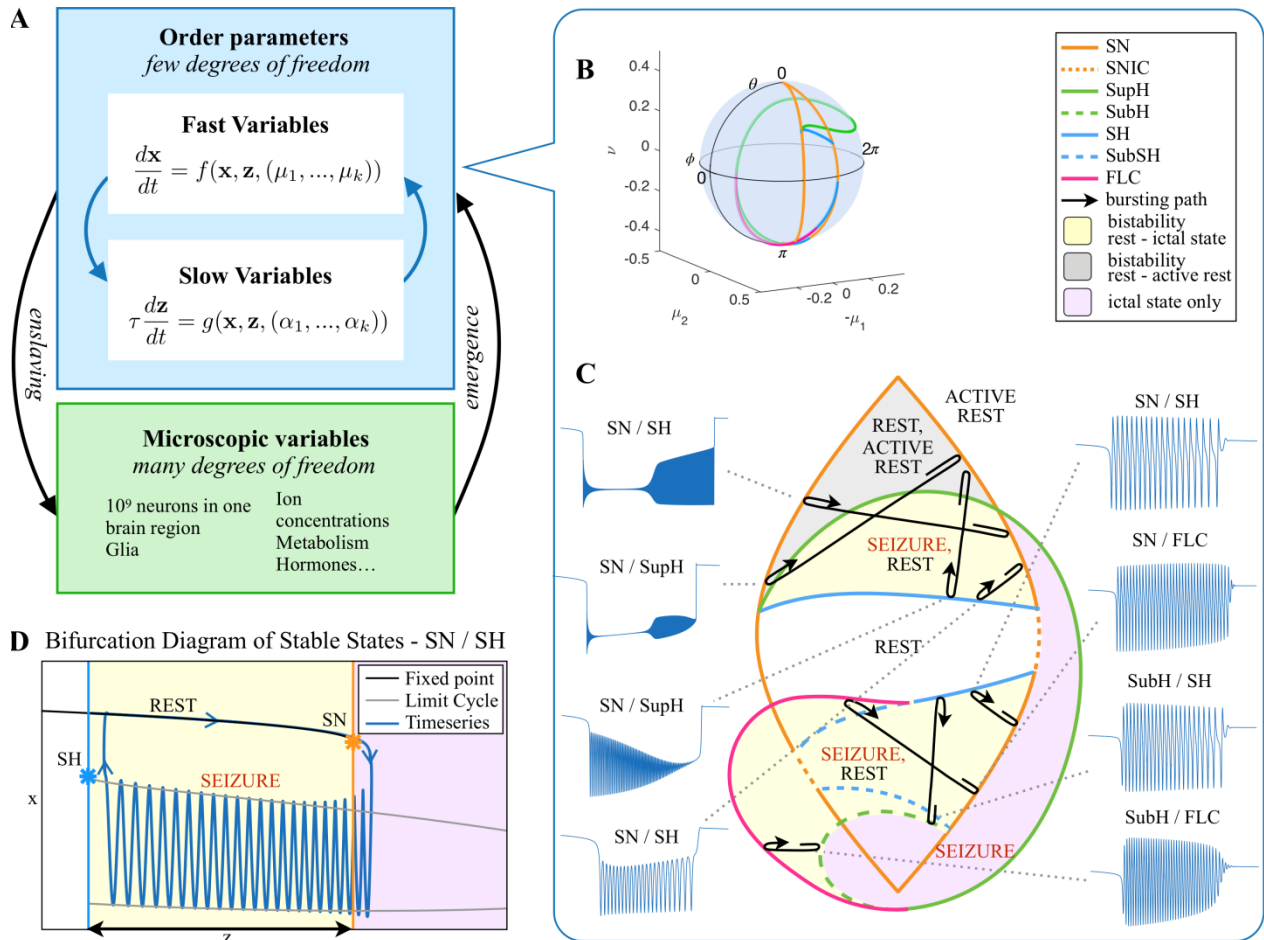


Figure 2.4 – Modeling seizures. A: During a seizure the microscopic physiological variables in a given brain region organize so that the emergent global activity can be described by a few collective variables. These collective variables, on the other hand, act on the microscopic variables, ‘enslaving’ them. B: The fast variables can be in different states depending on the values of the parameters. In our model we have three parameters  $(\mu_2, -\mu_1, \nu)$ , however the

relevant dynamics occur on a sphere with fixed radius. We thus consider the two-parameter spherical surface  $(\theta, \phi)$  that can be sketched with a flat map as shown in C. C: Bifurcation curves divide the map in regions where different states are possible: healthy state (white), ictal state (violet), coexistence between healthy and ictal states (yellow), coexistence between healthy and 'active' rest (a non-oscillatory state with a different baseline than the healthy state (gray)). When a seizure starts because the system crosses an onset bifurcation, the slow variable enables movement along the black arrow (a path in the map) to bring the system back to rest. Note that in this model, the system alternates between the resting and seizing states within the bistability regions. The shape of the arrow is meant to better show the trajectory followed by the system, however movement in the model occurs back and forth along the same curve. Insets show example of time series for different paths. SubSH: Subcritical Saddle Homoclinic, an unstable limit cycle that occupies a small portion of the map but is incapable of starting/stopping seizures, and thus is not included in Fig. 2.1 nor the rest of the analysis. D: An expanded view of one trajectory followed in C. The 'z' path (double arrow) represents movement from resting to seizure state and back by crossing the bifurcations, which in this case are SN and SH. This activity forms a seizure in the time series. The resting state is represented by a black line (fixed point), the minimum and maximum of the amplitude of the seizure (limit cycle) by gray lines.

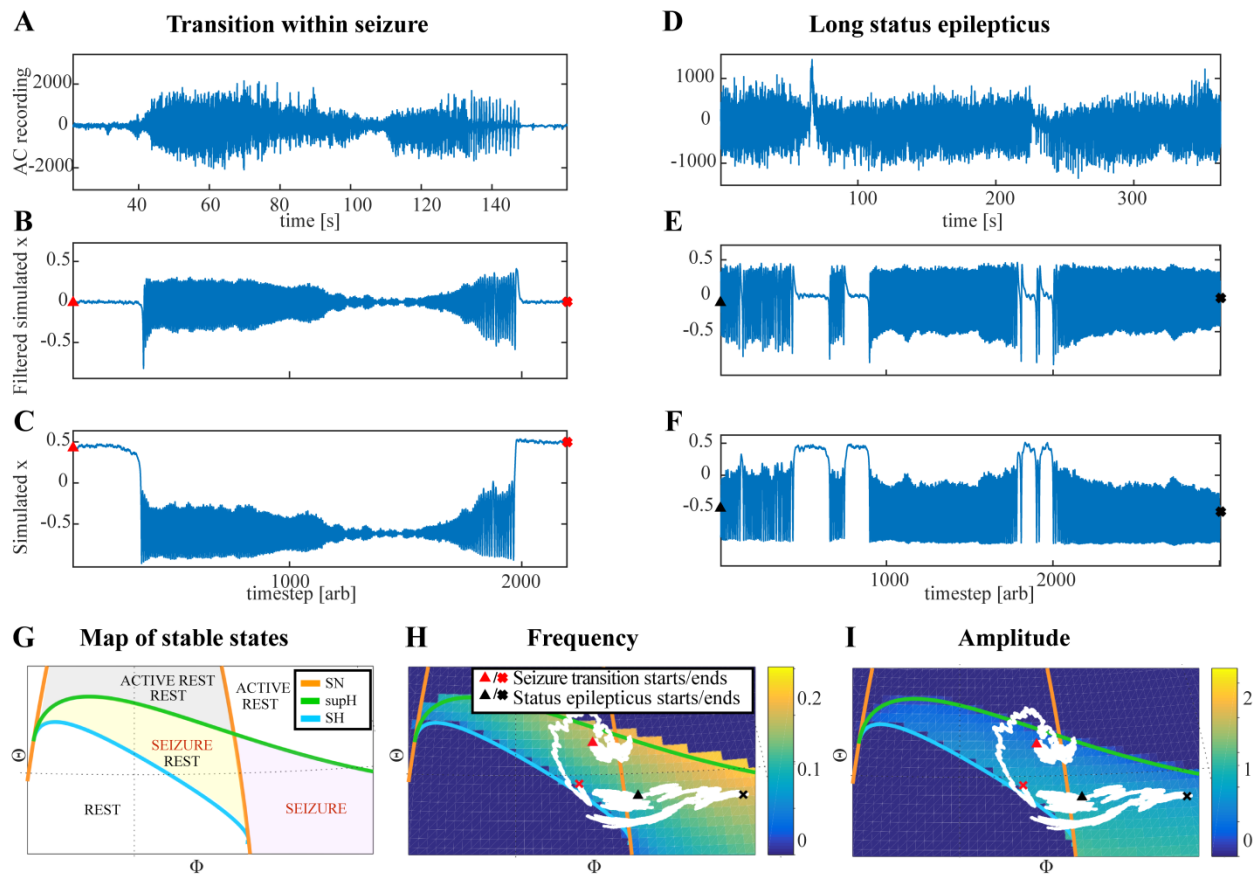


Figure 2.5 – Fluctuations in the ultra-slow modulation of the path causes changes in the dynamics of the seizure. (A) Human recording in which the seizure begins to go towards a SupH offset (square-root decreasing amplitude), but the amplitude increases again and the final offset is SH. (B) A portion of the simulation of the model in (M. Saggio et al. 2017) done to reproduce the dynamics observed in the recording. This time series is high pass filtered to simulate the effect of non-DC recordings. The unfiltered (DC-coupled) simulation is shown in (C). (D) A portion of a long status epilepticus recorded in one patient. The status epilepticus was characterized by transitions in the dynamics (such as at 70s and 220s). (E) High-pass filtered, and (F) unfiltered portion of model data simulating the behavior in D. (G) A zoomed, flattened projection of the map in Fig. 2.4C for reference in H-I. (H, I) Amplitude and frequency maps showing trajectories (white) of the modelled seizures in C,F. The seizure from C begins (red

triangle) and naturally moves upwards towards the supH bifurcation, but a change in the ultraslow drift prior to termination pushes the system downward, changing the offset from SupH to SH. Conversely, the seizure from F begins (black triangle) and repeatedly moves towards the SH termination due to the ultraslow drift, but is pushed back into the seizure regime repeatedly by high levels of noise, which overrides the role of the slow variable in terminating the seizure.



## Chapter 3

### Quantifying epileptogenesis with spontaneous and responsive brain state dynamics

#### 3.1 Abstract

There is a crucial need to identify biomarkers of epileptogenesis that will help predict later development of seizures. This work identifies two novel electrophysiological biomarkers that quantify epilepsy progression in a rat model of epileptogenesis. The long-term tetanus toxin rat model was used to show the development and remission of epilepsy over several weeks. We measured the response to periodic electrical stimulation and features of spontaneous seizure dynamics over several weeks. Both biomarkers showed dramatic changes during epileptogenesis. Electrically-induced responses began to change several days before seizures began and continued to change until seizures resolved. These changes were consistent across animals and allowed development of an algorithm that could predict which animals would later develop epilepsy. Once seizures began, there was a progression of seizure dynamics that closely follows recent theoretical predictions, suggesting that the underlying brain state was changing over time. This research demonstrates that induced electrical responses and seizure onset dynamics are useful biomarkers to quantify dynamical changes in epileptogenesis. These tools hold promise for robust quantification of the underlying epileptogenicity and prediction of later development of seizure

### 3.2 Introduction

Epileptogenesis is defined as the process by which a normally-functioning brain network develops recurrent, spontaneous seizures. This process is incompletely understood, but likely involves a progression of biochemical, anatomical, and physiological changes (Pitkanen et al. 2015). Understanding epileptogenesis and identifying biomarkers associated with it are two of the ‘Benchmarks for Epilepsy Research’ (Long, Fureman, and Dingledine 2016). Current treatment for patients with epilepsy is to administer antiepileptic drugs after seizures begin, which may control the seizures but does not address the underlying pathology (Herman 2006). This strategy is problematic in patients who have a discrete brain insult (e.g. injury or infection), as there is often a latent period before developing seizures in which it is unclear how to prevent epilepsy. It is hypothesized that medical interventions applied during the latent period could prevent epilepsy; however, the selection, timing, and duration of antiepileptogenic agents is difficult because the mechanisms and timing of epileptogenesis after brain insult are not well understood (Herman 2002). Reliable biomarkers of epileptogenesis may help address this problem.

One of the foremost challenges in assessing epileptogenesis is that the primary outcome (seizures) is not present during the latent period. Even after seizures begin, it is hard to quantify epileptogenesis because seizures are infrequent. Molecular biomarkers have shown promise, but are still very difficult to acquire and analyze (Lukasiuk and Becker 2014; Luna-Munguia et al. 2019). Others have used long term electrophysiological recordings, showing that epileptic spikes often appear much earlier than the first seizure (Kadam et al. 2010; White et al. 2010) and that epileptogenesis is not a stepwise process; it progresses even after the first seizure (Dudek and

Staley 2011). These studies suggest that the presence of seizures alone is insufficient to characterize epileptogenesis, and that better biomarkers are necessary to characterize its effects. In this work, we utilize two electrophysiological methods to quantify epileptogenesis. The first is to use electrical stimulation, or “probing,” to quantify neural excitability. Outside of epilepsy, previous research has shown that induced brain responses are good prognostic predictors of overall health condition after brain injury (Narayan et al. 1981; Carter and Butt 2005). Within epilepsy, a range of probing methods (photic, electrical, and transcranial magnetic stimulation) were found to be correlated with impending seizure onset, sleep-wake cycle, rate of interictal discharges, and seizure onset location (Kalitzin et al. 2002, 2005; R. Badawy et al. 2009; Freestone et al. 2011; Luttjohann et al. 2011; R. A. Badawy, Jackson, et al. 2013; R. A. Badawy, Vogrin, et al. 2013; Medeiros et al. 2014; Wendling et al. 2016), but have not been tested through the full development of epilepsy. Thus, the response to probing stimulation has significant potential as a biomarker of epileptogenesis.

The second method is to measure the dynamical features of the seizures themselves to characterize changes in the underlying seizure networks over time. This method uses a scientifically-based classification of seizure dynamics derived from first principles of dynamics theory (V. Jirsa et al. 2014; M. Saggio et al. 2017). The classification is founded upon invariant dynamical properties rather than clinical characteristics, which are the current standard (Fisher et al. 2017). A benefit of the dynamical approach is that there is a broad literature from other fields characterizing the different types of transitions, known as bifurcations, that can lead to seizures. Dynamical theory predicts that different bifurcations can be distinguished by analyzing the spike amplitudes (SA), inter-spike intervals (ISI), and presence of baseline shifts (V. Jirsa et al. 2014). In addition, it also predicts that there will be different responses to perturbing stimuli when the

brain is close to seizure threshold (Ranjan and Abed 2000; Yaghoobi, Hassouneh, and Abed 2001). In other words, the theory predicts that seizure dynamics and the response to probing stimuli are related. We hypothesize that, as the brain goes through the process of epileptogenesis, it will have different behaviors that can be measured by either characterizing the seizure dynamics or analyzing the response to different probing stimulation.

To test this hypothesis, we performed a continuous, long-term study of electrically-induced brain responses during epileptogenesis in an animal model. We measure the response to probing stimuli over the entirety of epileptogenesis, from before seizures began until after they resolved, a period of several weeks. We quantify the changes in both seizure onset dynamics and characteristics of interictal, electrically evoked responses throughout the course of the study. We find that these two measurements are closely linked, suggesting that the underlying brain state is changing during epileptogenesis, which produces alterations in seizure characteristics simultaneously with differences in the response to electrical stimulation. Most importantly, we find that the response to probing stimuli can successfully predict which subjects will later develop epilepsy.

### **3.3 Materials and Methods**

#### **3.3.1 Animal Model**

This study uses the intrahippocampal tetanus toxin rat model because it produces frequent, stereotyped, electro-clinical events that spontaneously remit 6-8 weeks after one stereotaxic toxin injection (0.1 g/L – 30 ng of tetanus toxin dissolved in 300 nL solution) (Jefferys and Walker 2006). For sham control animals, the same procedure was performed with an injection of phosphate-buffered saline. The model can be characterized by three phases (Fig.

3.1). The Pre-seizure phase is the latency period, which is defined as the time between tetanus toxin injection and the first seizure. The Rising-seizure phase is marked by the emergence of seizures, where daily seizure rate (SR) begins small and increases as time progresses. The final, Falling-seizure phase begins when the SR reaches its maximum, known as the inflection point, and lasts until seizures have completely remitted. We postulate these three epochs of differing epileptic behavior are representative of quantifiably different brain states, making the tetanus toxin model an ideal candidate for analysis. The experiments consisted of repeated, longitudinal measurements of the characteristics of spontaneous seizures as well as the response to a probing stimulation. The experiments were approved by the St. Vincent's Hospital (Melbourne) Animal Ethics Committee and were conducted in accordance with the "Australian Code for the Care and Use of Animals for Scientific Purposes, 8th Edition" (2013).

### 3.3.2 Stimulation Paradigm

Five epidural electrodes, which included one reference, were implanted in each animal with a configuration shown in Fig. 3.2A. Electrodes B, W, G, and R were connected to the EEG acquisition system. Electrodes G and R were momentarily switched to the stimulator to be the source and sink, respectively, of electrical current for discharging one biphasic stimulus. These electrodes were chosen for stimulation as they were the closest to the tetanus toxin injection site, which is deemed to be the most representative of epileptic tissue. Stimulation began on Day 2 after tetanus toxin injection and comprised alternating probing-on and probing-off phases. The probing-on phase consisted of 100 biphasic pulses (phase-width 0.5ms, current/phase:  $1.2 \pm 0.024$  mA, interphase gap: 20  $\mu$ s) over a 301 second period, with an inter-pulse interval of 3.01 seconds. The probing-off phase did not employ stimulation and was also set to a 301 second

period (see Fig. 3.2B). Stimulation continued (~5 minutes on, ~5 minutes off) without interruption for the entire experiment except for 1-hour daily check-ups. The same procedure was performed on the sham control animals.

### 3.3.3 Data Collection

Nine male Sprague-Dawley rats, obtained from the Animal Resources Centre (WA, Australia), were used for this experiment. Only male rats were used to avoid any effects that sex and the estrous cycle might have on the probing responses. These rats were split into sham control (3) and experimental (6) groups. For each rat, a single, intrahippocampal injection of tetanus toxin (experimental) or phosphate buffered saline (sham) was administered on Day 0 and subjects were transferred to the EEG recording room on Day 2, upon which recording and electrical probing protocols were immediately conducted. Data were recorded continuously in 23-hour intervals, allowing a 1-hour window for daily maintenance checks and data backup. Animals were under investigation for 9-10 weeks. All recordings were sampled at 2048 Hz with direct current (DC) coupling using an EEG acquisition system. The DC coupling assured that lower frequencies such as DC shifts were observed. Electrical probing was administered via a stimulator (neuroBi, custom built jointly by the University of Melbourne and Bionics Institute of Australia, VIC, Australia (Slater et al. 2015)). The dark/light cycle in the recording room was controlled by a standalone timer with 8-hour dark time and 16-hour light time. The temperature inside the room was controlled within the range 21–26 °C. Each rat was housed individually with ad libitum access to food and water.

### 3.3.4 Seizure Detection

Seizures were marked by a custom-designed seizure detection algorithm, then verified by manual review. The EEG signal processing steps were as follows: (1) Every stimulation artifact was replaced by a line interpolating two end points of that artifact. (2) Signals were filtered by a 3rd-order Butterworth IIR high-pass filter that had -3 dB cutoff frequency at 1 Hz. (3) A spectrogram was generated with the following settings: 4096-point (2 sec) Blackman-Harris window and 50% window length overlap. (4) The 13-48 Hz band power was calculated by integrating the power spectral density between 13 and 48 Hz. Seizure activities contained higher than usual power across the whole available bandwidth. However, the frequency band below 13 Hz was contaminated by residual stimulation artifact and the 50 Hz frequency band was contaminated by power line noise. Therefore, the 13-48 Hz frequency band was chosen for seizure detection. (5) A 5-point median filter was applied on the 13-48 Hz band power. (6) A 5 min (2.5 min before and 2.5 min after the current time point) moving average of 13-48 Hz band power was generated.

We used a sensitive algorithm to screen for potential seizures, then verified each detection manually. A potential seizure event was detected if it fulfilled either of the following criteria: (1) the instantaneous 13-48 Hz band power was at least three times greater than the 5 min moving average for at least 9 sec or (2) the instantaneous 13-48 Hz band power was at least 7 times greater than the 5 min moving average for at least 3 sec. The event was classified as a seizure if it was detected on two or more electrodes simultaneously. The output of the algorithm was then validated by a human reviewer visualizing every detected event. Throughout this study, the term “seizure” refers to either a clinical or subclinical (electrographic) seizure. It should be noted that no seizures were observed in the control group.

### 3.3.5 Data Processing

Only data from Electrode-R (Fig. 3.2A) were used to ensure consistency between both evoked response and seizure onset analyses. This channel was chosen because seizure onsets were nearly identical across electrodes at any given time and this channel was found to be the most reliable across all rats.

Evoked Response. Responses from all 100 pulses were averaged for each pulse train to provide representative system responses at equal time points across the experiment. This analysis utilized the full 2048 Hz sampled data. To extract each individual evoked response within the pulse train, we examined the first 1000 data points (~488 ms) starting at the peak of each pulse. The first 4 data points were redacted to remove the majority of the stimulation artifact. The remaining stimulation artifact in each evoked response data was minimal and did not affect the analysis. Any averaged evoked responses that overlapped with seizures were removed from the analysis (range of 7-14% responses removed per animal with 10% average). The averaged evoked response amplitudes were then scaled between 0 and 1 to minimize the effect of changing electrode quality over the course of the study, thus emphasizing changes in frequency content (see Fig. 3.5B). This analysis did not investigate any features of the probing-off period.

Seizure Onset. Seizure onset data were captured using an 8 sec window centered on the estimated seizure onset time obtained from the custom detector. In other words, each sample waveform included roughly 4 sec of baseline and the first 4 sec of seizure data. Seizure onsets that were uninterpretable due to stimulation artifacts were removed from the analysis (range of 6-12% seizures per animal removed with ~9% average). Because the differences in seizure onset



dynamics that we measured occur at frequencies  $< 100$  Hz (V. Jirsa et al. 2014), all onset samples were decimated to 204.8 Hz to increase processing efficiency.

### 3.3.6 Analysis

**Definition of Brain States.** As mentioned before, the tetanus toxin model consists of three epochs of epilepsy: (1) Pre-seizure, (2) Rising-seizure, and (3) Falling-seizure. We analyzed the evoked response and seizure onset characteristics independently across these epochs and then compared these results.

Recording started on day 2, which was prior to development of seizures in any animals, and continued every day until seizures had appeared and resolved, lasting several weeks. We defined the Pre-seizure epoch as all recordings done on days prior to the day of the first seizure. The Rising-seizure phase begins at the time of the first seizure and ends at the inflection point when the rate of seizures begins an overall decreasing trend. However, the seizure rate was not necessarily unimodal and had considerable variability from day to day; thus, determination of a precise inflection point was ambiguous. Therefore, as an estimation, we determined the total number of seizures ( $N$ ) that occurred in each animal and defined the Rising-seizure phase as the first  $N/2$  seizures, and the Falling-seizure phase as the second  $N/2$ . This scheme assured that the two groups have similar size. We compared this method with results using the manually-determined absolute maximum rate and there were no appreciable differences in any of the results. Analysis of the evoked responses included data from all three epochs. Obviously, seizure onset dynamics were only evaluated during the Rising-seizure and Falling-seizure epochs.

Divergence Measurements & Statistics. A major goal of this work is to characterize the brain states and determine if there are measurable differences between states. We used a data-science approach for this analysis, quantifying features of the data using objective algorithms and comparing the statistical distributions of those features. When feature distributions from different states can be distinguished, we refer to the distributions as “separable,” which in this case suggests that it is possible to identify the different states reliably and that the different states produce fundamentally different brain activity. If they are not separable, then either the brain states are not functionally distinct, or the chosen features are incapable of identifying any difference.

The method for distinguishing different groups is very important, especially for large datasets. With large numbers, simply finding the “statistical significance” (often a p-value of a comparison test such as Student’s t-test) is not necessarily useful, as the populations may be “significantly different” due to the large sample size but essentially indistinguishable in any meaningful way. A more robust method of distinguishing large groups is to use a test of divergence, which not only assesses significance but also separability. In this study, we utilized a measure related to the Henze-Penrose divergence (specifically using the quantity in Eq. 5 in (Berisha et al. 2016), which ranges between 1 (for completely separable distributions) to 0 (for completely indistinguishable distributions). We denote this measure the Henze-Penrose statistic. We first reduced the dimensionality of the features by computing the first three principal components. Outliers whose principle component values exceeded 2 standard deviations were removed from the analysis (removed data percentage ranged from 4.6-13.8%, avg. 9%), creating a more conservative measurement. For the features of seizure onset dynamics there were only two groups to compare: the Rising-seizure and Falling-seizure epochs. We computed the Henze-

Penrose statistic between the two distributions, providing a measure of their separability. To estimate the statistical significance of the separability, we performed a permutation test in which we randomly scrambled the labels of the original data groups and recomputed our divergence measurement. This permutation test was repeated 10,000 times for robustness. In all six subjects, the divergence measurement for the actual labels was higher than all 10,000 permutations ( $P < 0.0001$ ).

For the evoked response data, the same analysis was performed with three exceptions. First, because the evoked response data encompassed all three epochs, we determined the separability between Pre- and Rising-seizure phases in addition to the Rising- and Falling-seizure phases. Second, only the first two principal components were used for the evoked response data, as these were sufficient for full separability. Third, no principal component values were removed by thresholding from the analysis, as the evoked response data were not as noisy.

Feature Analysis. Features from evoked responses and from seizure onset were independently extracted, normalized by subtracting the mean and dividing by standard deviation, and their dimensionalities reduced using standard principal component analysis (PCA).

Evoked Response Features. A frequency analysis was performed on each of the averaged evoked responses acquired for each stimulation period. A separate analysis was performed for every Probing-on epoch, and evaluated the averaged response of all 100 stimuli in that epoch. The analysis consisted of estimating the spectral power distribution over every ~2 Hz increment from 0-1024 Hz. This was computed using the power spectrum density estimate (MATLAB's 'pwelch(x)', window = 996, noverlap = 0, nfft = 996, fs = 2048 Hz). Therefore, each evoked

response had 499 features, where feature #1 is the power of the evoked response from 0-2.0562 Hz, feature #2 is the power of the evoked response from 2.0562-4.1124 Hz, etc.

Seizure Onset Features. A dynamical model based upon the first principles of dynamics (V. Jirsa et al. 2014) predicted that the brain's transition from normal to seizure state (seizure onset) can be described using bifurcation theory and that there are four basic onset bifurcations: Saddle-node (SN), Saddle-node on an invariant cycle (SNIC), Supercritical Hopf (SupH), and Subcritical Hopf (SubH). These different bifurcations each have unique pairs of interspike interval (ISI) and spike amplitude (SA) scaling laws that can be used to distinguish them (V. Jirsa et al. 2014; M. Saggio et al. 2017). SNIC bifurcations are characterized by non-zero SA scaling and a decreasing ISI trend (scaled to square root function). SubH bifurcations have no specific scaling laws for either ISI or SA. SN also have no specific scaling laws but can be accompanied by a DC shift. Finally, SupH bifurcations have no ISI scaling while the SA scales from zero as a square root function. True biological data is noisy and can be difficult to characterize exactly, so the primary goal of our analysis was not to "fit" seizure onsets to any particular type of bifurcation. Instead, the analysis was a data-driven approach using the values of these basic features as a framework to quantify the seizures: analyzing the presence of a DC shift and the scaling behavior of the SA and ISI. Based upon this framework, we developed a set of features that focus on the key dynamical features. Each of the eight features are listed below in detail. As a reminder, the 8 sec waveform of seizure onset data consists of 4 sec of pre-onset baseline and 4 sec of seizure data.

*DC Shift:* We calculated the normalized area under the post-onset signal, as this feature estimates the relative prominence of the DC shift. This was performed by taking the following steps: (1) smooth the data with a 3rd-order median filter ('medfilt1(x)' in MATLAB), (2) subtract the median of the first four seconds of baseline from the entire signal, (3) divide the entire signal by the maximum value of the signal, and (4) sum the result.

*Deviation Sum:* This feature was developed to capture general trends post-onset. (1) smooth the data with a 3rd-order median filter ('medfilt1(x)' in MATLAB), (2) truncate the initial four seconds of baseline, (3) subtract the median of the remaining signal, and (4) sum the absolute value of the result.

*Deviation Variance:* As with 'Deviation Sum', except Step 4 is replaced with taking the variance of the result.

*Signal Power:* We quantified the power spectrum density estimate (MATLAB's 'pwelch(x)', window = 821, noverlap = 0, nfft = 821, fs = 204.8 Hz) of the seizure onset (i.e. the last 4 sec of the data). The resulting power output corresponding to frequencies greater than or equal to 2 Hz were summed.

*Gamma Band Power:* Like 'Signal Power', but only power corresponding to frequencies greater than or equal to 32 Hz were summed.

*Variance:* To account for changes in electrode quality, we scaled the signal to be between 0 and 1. This was accomplished by first subtracting the minimum amplitude of the signal and then dividing by the new maximum amplitude. Finally, the variance of the scaled signal was taken.

*Linear Amplitude Trend:* Two linear models were fit to the data. First, a linear model was fit to the first 3.2 sec of pre-onset baseline. Then, another linear model was fit to the last 3.2 sec of seizure data. The slopes from both models were extracted and the baseline slope was subtracted from the seizure slope. This provided the relative linear amplitude trend of the seizure onset waveform with respect to baseline.

*Burst Count:* This feature was designed to differentiate seizures that consisted of bursts from those that consisted primarily of spikes. We first performed high-degree, non-linear smoothing on the waveform (Savitsky-Golay filter, 11th order, 201 frame length). The resulting data was normalized between 0 and 1 by first subtracting the minimum amplitude then dividing by the new maximum amplitude. Finally, we found the peaks ('findpeaks' in MATLAB, 'MinPeakProminence' of 0.3) and counted them.

#### Classification of Pre-seizure state.

The most important goal of the evoked response experiment was to determine if the Pre-seizure state could be detected, i.e. if it was possible to predict which animals would develop seizures. We developed a classifier to distinguish between Control and Experimental animals. In order to standardize the measurement across all animals, we first normalized by aggregating all Experimental animals, and for each measurement subtracting the group's mean and dividing by

the group's standard deviation. We then found the principal components of the aggregate of all 6 Experimental animals, which projected all 6 into a single "PCA space". We then normalized the Control animals' data using the mean and standard deviation of the Experimental group, and used the matrix that produced the Experimental principal components to project the 3 Control animals' data into the same space. We used the first 3 principal components for the classifier. This process allowed for dimensionality reduction that was dependent upon the differences caused by epileptogenesis but could compare data from all 9 animals. We used a support vector machine ('fitcsvm(X,Y, 'KernelScale', 'auto', 'KernelFunction', 'gaussian')' in MATLAB) with these data to distinguish between the corresponding labels (i.e. Control or Experimental). The model was validated with 10-fold cross validation. Only the first 10 days of evoked response control data were used to mirror the general window of time the Pre-seizure phase occurred in the experimental animals (mean: 6 days, range: 4-9 days). Coincidentally, this first 10 days created a total sample size of 3977 samples across all three control animals, which was comparable to 3915 samples across all experimental animals. The base rate probability (i.e. the minimal success rate using random chance – the sum of the squares of the probability of each label occurrence), was then computed to be 50.00%.

### 3.3.7 Data Availability

All data and associated scripts/tests can be found at the University of Michigan's Deep Blue Library (Crisp et al. 2019).

## 3.4 Results

### 3.4.1 Seizure Onsets

All six experimental animals developed seizures after the tetanus toxin procedure. Seizures began after 6 +/- 2 days and tended to increase in frequency for several days before reaching peak frequency (Fig. 3.3 – column 1). Animals also tended to produce seizures in bursts, having more some days and less others. This is consistent with previous findings in long-term human data that showed seizure frequency is cyclic (Philippa J. Karoly et al. 2018). Each animal also spontaneously remitted from seizures after several weeks. This time course is well-suited for epileptogenesis research as it includes a known trigger, a latent period, then a progressive course of seizures. We observed that there were clear differences in the seizures over this time course. We found that the seizure onset dynamics in a given animal changed over this period (Fig. 3.4). The first seizures to appear tended to have a DC shift with fast spiking (Fig 3.4 – column 1). Over many days, the seizure features changed: the seizures began to have short clonic bursts with DC shifts (Fig 3.4 – column 2), then later they had bursts without DC shifts (Fig 3.4 – column 3). This transition represents a continuum from seizures that have features consistent with a SN onset (Jirsa et al., 2014) during the first seizures (DC shift, constant amplitude and frequency), transitioning to features from a SNIC or SubH onset (M. Saggio et al. 2017) during the last seizures (no DC shift, constant amplitude, and increasing/arbitrary frequency). During the end of the recordings, there were two other patterns intermittently seen in some subjects. One was an onset with no DC shift, rising amplitude, and constant frequency (in 4/6 animals, Fig. 3.4 – column 5), which was similar to a SupH onset. The other was an abrupt onset of discrete spike wave discharges, which is similar to a different type of SNIC/SubH bifurcation (in a different 4/6 animals, Fig. 3.4 – column 4). Note that these



different onset patterns were intermittent and variable: during the course of epileptogenesis a given animal alternated between these different types, but the overall collection of seizure dynamics was clearly altered from the beginning to the end of the experiment as illustrated in Fig. 3.4.

Although assigning specific bifurcations would be possible at the extremes, there were many seizures during the course that would be difficult to assign to a single classification, as there are features from different types mixed together (e.g., some DC shift with increasing frequency). For this reason, we did not attempt to fit each seizure to specific classifications; rather, we used the features that distinguish the bifurcations as the input for the divergence analysis. Using the seizure features described in the Methods, we calculated the first three principal components (Fig. 3.3 – column 2) and used them to calculate the Henze-Penrose statistic between data from the two epochs (Rising-seizure and Falling-seizure). Note that a value of ‘1’ indicates complete separability, and ‘0’ means they are indistinguishable. For each of the six subjects, the Henze-Penrose statistics were  $0.6157 \pm 0.1983$ , all significantly larger than values computed for all 10,000 random permutations of the labels ( $P < 0.0001$ ). This demonstrates that the seizure onset features are not only significantly different, they also easily distinguish the two phases.

To further validate the changes occurring in the seizure onset data, we separated both the Rising- and Falling-seizure phases into halves (early and late), creating a total of four epochs (Fig. 3.1, see dotted vertical lines). We then computed the Henze-Penrose statistic between each neighboring pair of the four smaller epochs. We found that seizure onset features from all six animals changed significantly between all compared phases (all  $P < 0.0001$ ). Thus, every ~10 days the seizure onset patterns had changed significantly in each animal.

### 3.4.2 Evoked Responses

Independent of the noticeable differences in seizure onset dynamics, we also found important differences in the response to provoking stimulation during interictal periods. We used a similar data-driven analysis to characterize these effects, though in this case we were also able to quantify the Pre-seizure phase.

There is a great clinical need for a biomarker that can inform clinicians about the state of the Pre-seizure phase, as there is potential for early treatment to avoid, diminish, or prolong seizure development. However, this success is only available if clinicians can differentiate between a healthy brain and a brain progressing along the track of epileptogenesis without the obvious standard biomarker (seizures). Our analysis seeks to train a classifier to determine if incoming evoked responses come from a normal, healthy brain, or from a brain progressing along the track of epileptogenesis.

We first used spectral features to quantify the dynamical effects as epileptogenesis progresses. We measured the features over the entire time course and found that the evoked responses were distinct during each phase of epileptogenesis (Fig. 3.5). The most visually obvious change was a consistent trend in amplitude (Fig. 3.5A); however, this effect was also noted in the sham control animals, suggesting it was due to the experimental procedure. We found that the frequency response was more specific to the epileptic animals. We therefore normalized the amplitudes to focus the analysis on the frequency response to the stimulus, which primarily occurred in the first few milliseconds of the response (Fig. 3.5B,C). The epileptic animals began to have changes in the evoked responses immediately after the tetanus toxin injection. The changing nature persisted, and in each stage of epileptogenesis it was easy to distinguish the responses. Because there were so many measurements each day, we were able to

quantify these responses and show how the distribution of the features changes over time, i.e. how “separable” the distributions are. To illustrate the strong separability in just one of the features, we highlight the temporal band power changes by normalizing via standard deviation each frequency component over time (Fig. 3.6 – column 1). For 5 out of 6 animals, we see that changes in power bands separate into three distinct bands. Frequency ranges were similar enough for these animals to estimate by visual inspection: 0-169 Hz, 170-769 Hz, and 770 - 1024 Hz. The 0-169 and 770-1024 bands were similar in their power distribution across epochs. These bands started with minimal power in the Pre-seizure phase and gained power over time with increases in power correlating with transitions between each epileptogenic phase. The final frequency band, 170-769 Hz, displayed the opposite trend. Specifically, we see a high proportion of power during the Pre-seizure phase that decreases over time. One noticeable difference in this band compared to the others is that the trends in power distribution are highly subject specific. One subject was distinct from the others (S3) and had a different time course, but also showed clear differences over the course of epileptogenesis.

To quantify these effects similar to our analysis of seizure onset dynamics, we computed the principal components (Fig. 3.6 – column 2) and then investigated how easily the evoked response features can be distinguished between the different phases of epileptogenesis. All phases were clearly distinguishable in all six animals (permutation test,  $P < 0.0001$ ). Of particular interest is that in each of the six subjects, most of the change in principal components occurred within the first 10 days, suggesting that there is significant evolution in frequency response even before seizures begin.

The most important step was to see if the evoked responses could distinguish between healthy (i.e. no seizures forthcoming) and epileptogenic (i.e. Pre-seizure) brains. This analysis

used spectral band power in a support vector machine to distinguish the two groups. We found that the first three principal components of the evoked response features during the first 10 days were very accurate in identifying which animals would later develop epilepsy (Experimental animals vs. Control, 97.19% accuracy compared to 50% accuracy for random chance classification, 10-fold cross validation). Fig. 3.7A compares the first 3 principal components of the Pre-seizure and Control animals (days 2-10), showing a clear separability that was captured by the support vector machine. Also striking is the clear evolution of features from the beginning to the end of epileptogenesis, suggesting a permanent change in underlying dynamics. When all 6 Experimental animals are projected into the same PCA space (Fig. 3.7B), it is clear that this progression is similar in most animals. However, there were no consistent changes in the Control animals, which had evoked responses that were similar at the beginning and end of the recording. These findings illustrate that there are measurable changes in the evoked response that start immediately after the epileptogenic insult and progressing throughout epileptogenesis, which can be generalized across animals.

### **3.5 Discussion**

For the first time, both seizure onset dynamics and electrically-induced brain responses were studied continuously over a long-term period to determine their roles as biomarkers for the epileptogenic brain. There has been some previous work for electrically-induced brain responses in humans, though limited to shorter recordings and always for patients who are long past the epileptogenesis stage (Kalitzin et al. 2005; Freestone et al. 2011; Pigorini et al. 2015; Wendling et al. 2016). This tetanus toxin animal model provides a unique opportunity to study epileptogenesis from insult to epilepsy, and in this case also to remission. This study is unique

because it compares two fundamentally different biomarkers simultaneously, through multiple stages of epileptogenesis.

### 3.5.1 Quantifying Seizure Dynamics

In both clinical and basic research, it is often necessary to describe seizure characteristics and attempt to compare them across different conditions. However, these comparisons have previously been limited to visual descriptions such as morphology and peak spiking frequency (P. Perucca, Dubeau, and Gotman 2014; Lagarde et al. 2019a). These methods of comparison are the basis of clinical epilepsy, but it is unclear when those differences comprise fundamental changes in the seizures themselves, e.g. is a 4 Hz versus a 7 Hz spike train really a different “type” of seizure? The result is that it is very difficult to compare seizures across time and different subjects. In this work, we designed features based upon invariant aspects of seizure dynamics (V. Jirsa et al. 2014). In effect, these are the features that define when one seizure is “different” from another, based upon principles of dynamics. Interestingly, this theory actually predicts that the spiking frequency is not important—only the temporal trend is. This robust method is designed to classify seizure dynamics, applicable to any seizure: computer model, experimental animal, or human.

Our primary result was that there were clear differences in seizure dynamics over the course of epileptogenesis, as evidenced by the Henze-Penrose statistic results. These measures indicate that the epileptic tissue follows a fairly stereotyped dynamical pathway over the course of the tetanus toxin induced epilepsy, tending to form seizures with fast, low amplitude spiking and DC shift at the beginning, versus seizures with repetitive bursts with increasing frequency at the end. While investigating the mechanisms underlying this change was beyond the scope of

the current work, these results provide an intriguing guide for such research in the future. In effect, this type of analysis can quantify differences between seizures, identifying salient differences and providing rigor to future epileptogenesis research.

While not a main focus of the current research, it is also interesting to comment on the types of bifurcations seen over the course of epileptogenesis. In all animals, the initial seizures tended to have features consistent with SN bifurcations, while the final seizures more commonly were consistent with SNIC or SubH bifurcations. However, between these times, there was a range of different dynamics. There were two phenomena noted in all animals. First, each animal had seizures with different dynamics alternating over time, e.g. SN alternating with SNIC or SupH bifurcations. The relative frequency of each type changed over time, with SN being much more common in the Rising phase and SNIC/SubH more common by the end. Second, as shown in Fig. 3.4 (column 2), there were many seizures that did not conform to strict bifurcation types. Viewed collectively, it appears that many seizures between the early and late patterns (which clearly change from SN to SNIC/SubH) have mixed characteristics, as if the seizures make a slow transition from SN to SNIC/SubH over the course of weeks. This transition suggests a “map” of brain states, wherein the progression of epileptogenesis slowly moves the dynamics from one region to another, as proposed by Saggio et al. (M. Saggio et al. 2017).

### 3.5.2 Evoked Responses

Quantifying the response to a perturbing stimulus has been very limited in epilepsy research but has shown intriguing results (Alarcon 2005; David et al. 2010). This procedure has a robust history in other fields such as ecology, power systems, and reservoirs (Chow et al. 1990; Kikani and Pedrosa O. A. 1991; Heppell, Caswell, and Crowder 2000; Martinez, Messina, and

Barocio 2004; Ehrlén and Groenendael 2008; Ma, Wang, and Lan 2012) but is difficult to perform in vivo. The basic theory is that perturbation is a probe of excitability and thus should change if the network is inherently “more epileptic”, i.e. closer to seizure threshold. In addition, perturbation can be used to assess proximity to specific bifurcations because it shows different responses when a SubH or a SupH bifurcation is nearby (Bryant and Wiesenfeld 1986; Vohra, Fabiny, and Wiesenfeld 1994; Yaghoobi, Hassouneh, and Abed 2001).

Our data demonstrate that, like seizure dynamics, evoked responses show clear evolution over the course of epileptogenesis. Perhaps the most important result is that these changes started even during the latency period, and that evoked responses taken during this time can be used to distinguish which animals are going to develop epilepsy. This outcome shows that this method may be a useful tool to assess the progression of epileptogenesis even prior to the first seizure. Additionally, the response after seizure remission was different than at onset, suggesting that the brain had undergone a permanent alteration despite remission of the seizures. This observation was not present in the control data, as responses from the beginning and ending of the experiment had comparatively minimal differences. These results are limited because there were no evoked responses done prior to the tetanus toxin injection to establish the healthy baseline. Future studies will evaluate these potential confounds.

### Summary

Treating epileptogenesis has been challenging due to the inherent heterogeneity of epilepsy as well as the temporal changes in molecular mechanisms. This has motivated research to develop biomarkers to track the disease progression in models of acute brain injury. Electrically-induced evoked responses have been successful in diagnosing neural excitability to

determine many epileptic characteristics. Additionally, a recent framework of seizure dynamics has been produced, creating a foundation and methodology for characterizing seizures based on signature dynamic manifestations. These two independent features hold great promise as biomarkers of epileptogenesis. This study investigates how the different stages of epileptogenesis modulates these features. We provide proof-of-concept evidence that these features change over time and can be used to inform the progression of the disease, in particular that the response to stimulation can predict which subjects will develop epilepsy in the future. These features, in conjunction with other methodologies, can be used to better research progression of epilepsy as well as asses the efficacy of administered drugs post-injury.

### 3.6 Figures

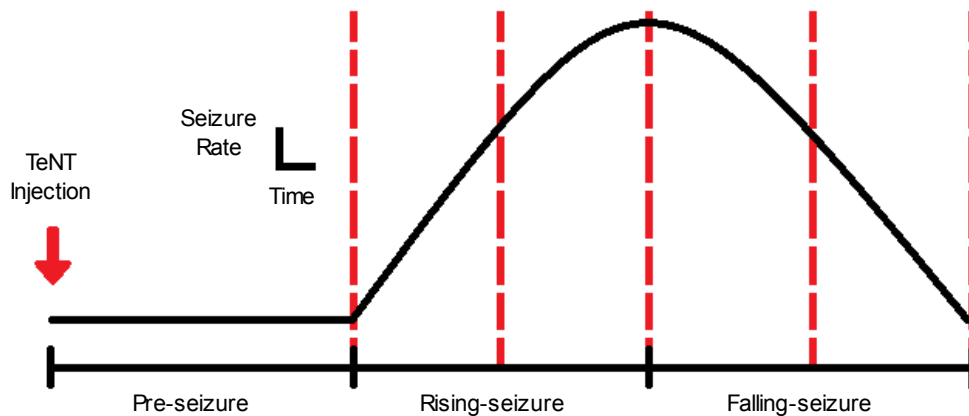


Figure 3.1 – Progression of epileptogenesis – Representation of an animal’s seizure rate over time in the tetanus toxin model. The Pre-seizure period refers to the latency between the injection and the first observed seizure. The Rising-seizure period represents the emergence of seizures coupled with increasing seizure rate before the inflection point. The Falling-seizure period starts



at the inflection point and has a decreasing seizure rate moving toward seizure remission. Dotted vertical lines represent a simple quarterly viewpoint beginning at the emergence of seizures.

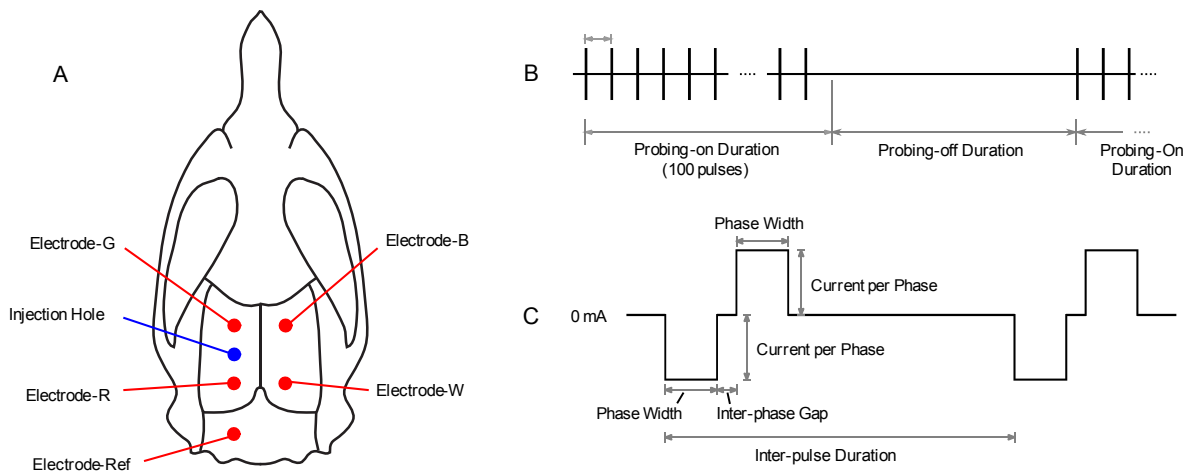


Figure 3.2 – Electrode placement and stimulation pattern – (A) Example rat skull diagram showing the tetanus toxin injection site and electrode placements. Electrodes G and R are also the stimulating electrodes. (B) Example of the pulse trains and timing of stimulation, which occurred every 3.01 seconds for a total Probing-on duration of 301 seconds. Each vertical line represents a single pulse waveform, which are detailed in (C). (C) Waveform used for the stimulation.

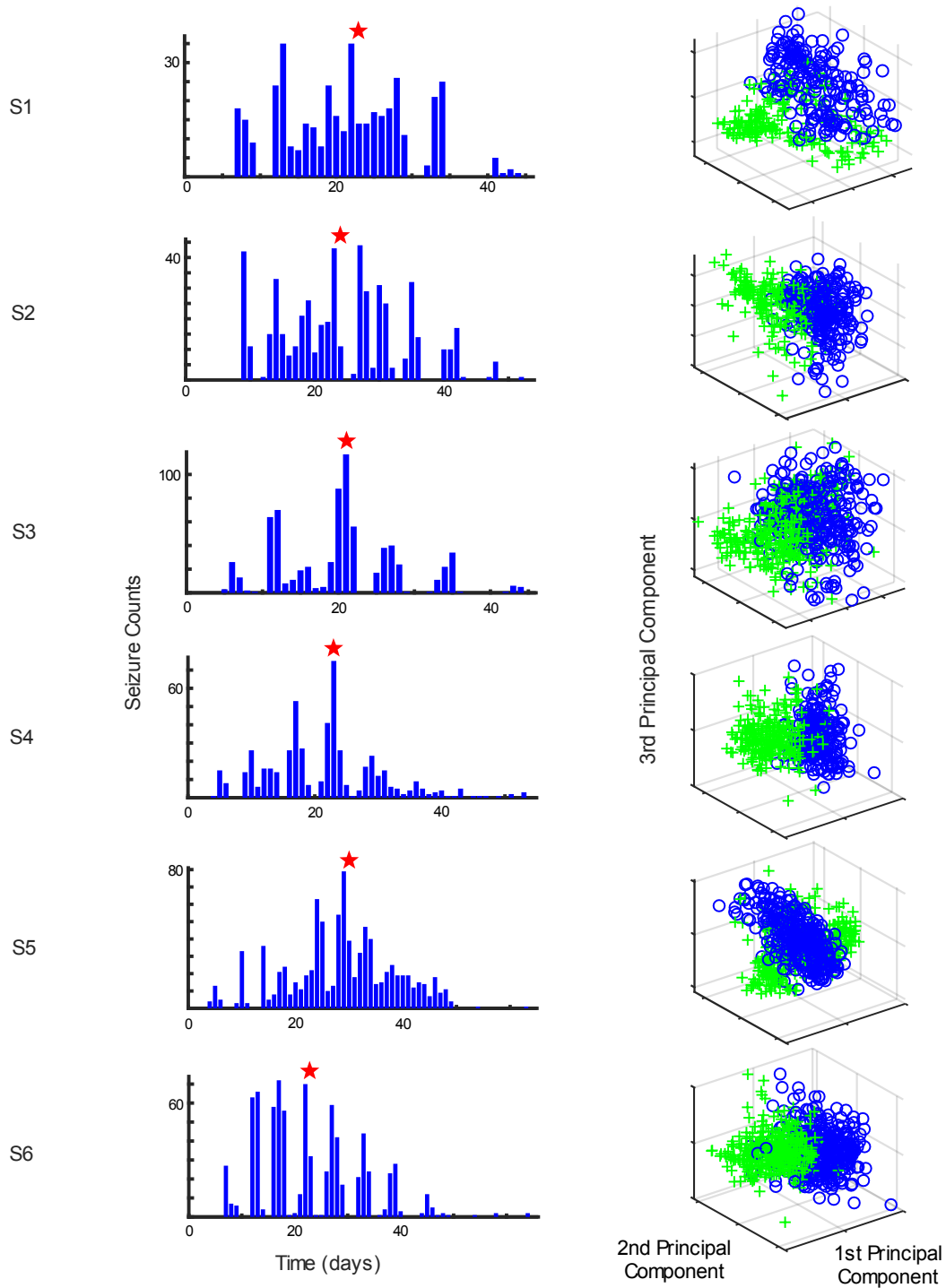


Figure 3.3 – Seizure occurrences and divergence measurements – (Column 1) Seizure occurrence over time for each animal. The star indicates the estimated inflection point, separating the Rising- and Falling-seizure phases. (Column 2) The corresponding principal components of the

seizure onset features used for the divergence measurements between the Rising- and Falling-seizure phases. Green “+” indicates seizure found in the Rising-seizure phase, while blue “o” indicates seizure from the Falling-seizure phase. Purely by visual inspection, it is clear that these distributions are not identical.

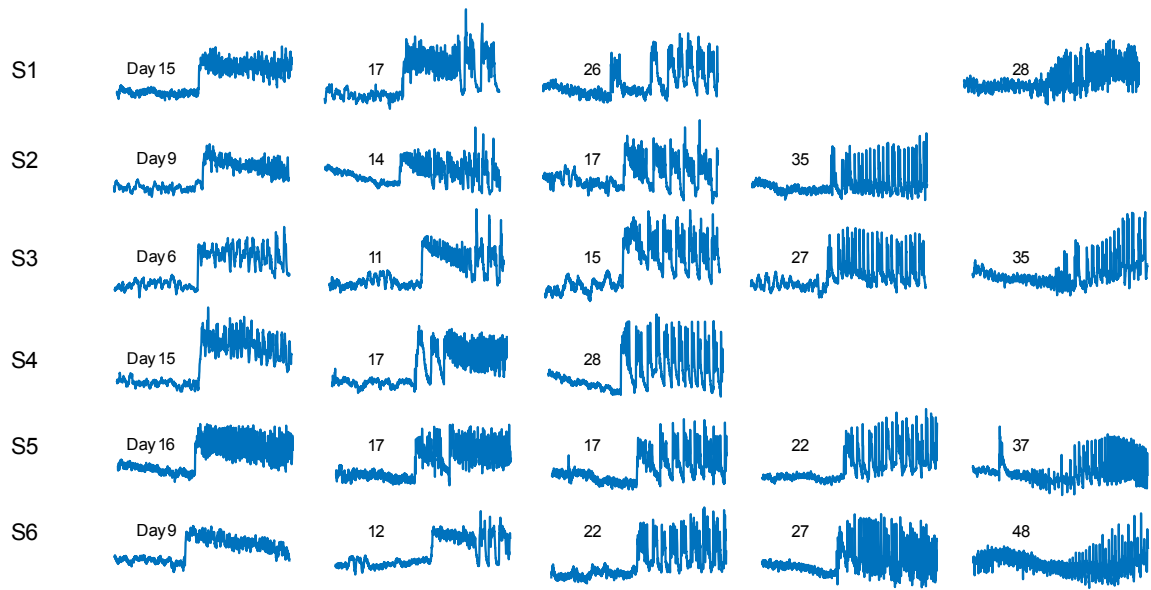


Figure 3.4 – Progression of seizure dynamics – Examples of seizure onset dynamics over time in all six animals. Each row (labeled S1-S6) represents seizures in a specific Experimental subject. The days shown mark the day since tetanus toxin injection on which each seizure occurred. These seizures represent the most common seizure morphology at similar time points. The first column of seizures is representative of SN bifurcations. The third column of seizures is representative of SNIC bifurcations. The second column of seizures represents an evolution between SN and SNIC. The fourth column represents SNIC/SubH bifurcations. The final column is representative of SupH bifurcations.

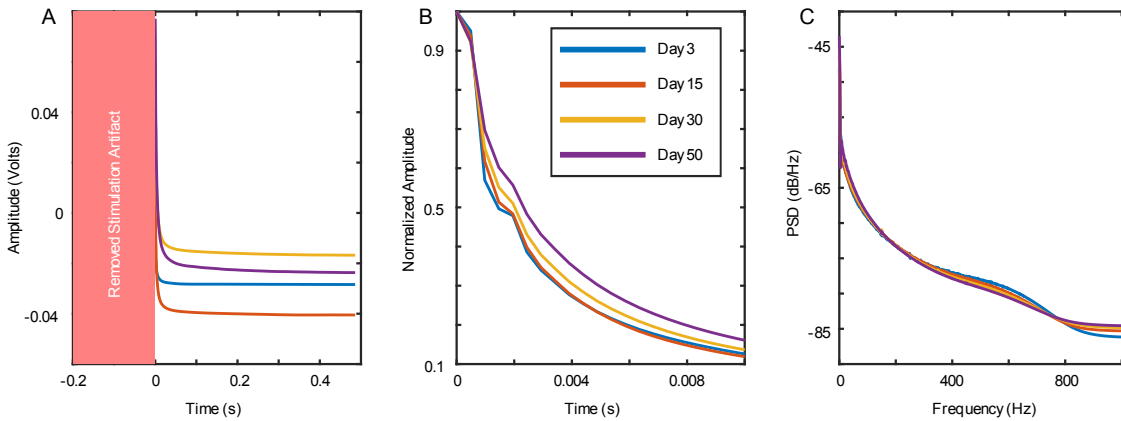


Figure 3.5 – Evoked response visualization – Each figure contains the evoked response from the first stimulation epoch occurring on days 3, 15, 30, and 50 to show the temporal evolution (colors represent the same days in each panel). (A) The average waveform of 100 evoked responses from a single train of pulses. Stimulation artifact is not included in the analysis. Note that on this long time scale the largest difference is the amplitude after stimulation. After normalization, the largest different occurred in the first 0.01 s after stimulation (\*, small bar), which are expanded in “B”. (B) The average waveform normalized between 0 and 1 (subtracting the minimum and dividing by the new maximum for each averaged tracing). This is done to minimize amplitude changes due to electrode variability over time. (C) The power spectrum density was computed for each averaged waveform. These findings were highly consistent across time in the epileptic animals, but not in the control animals.

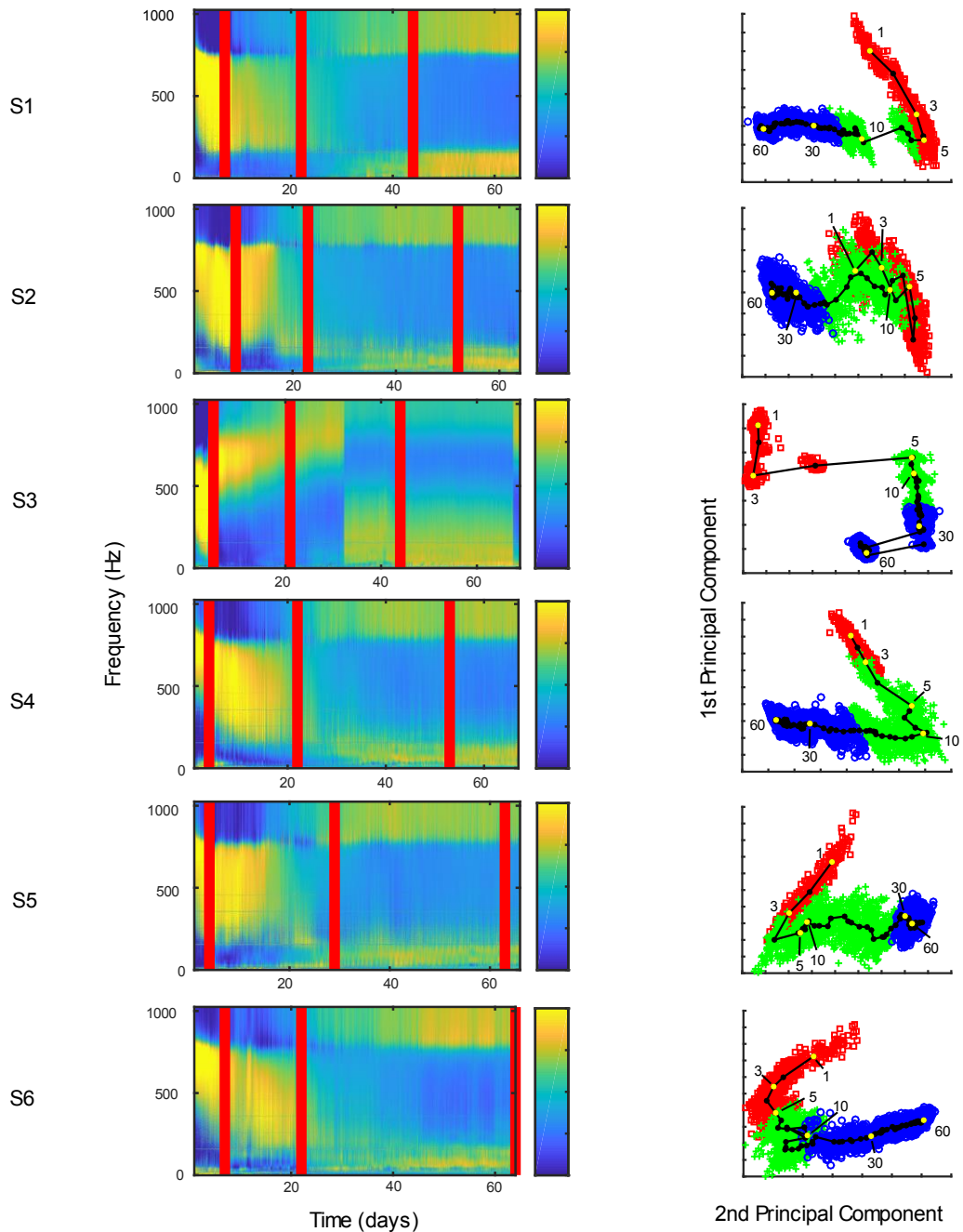
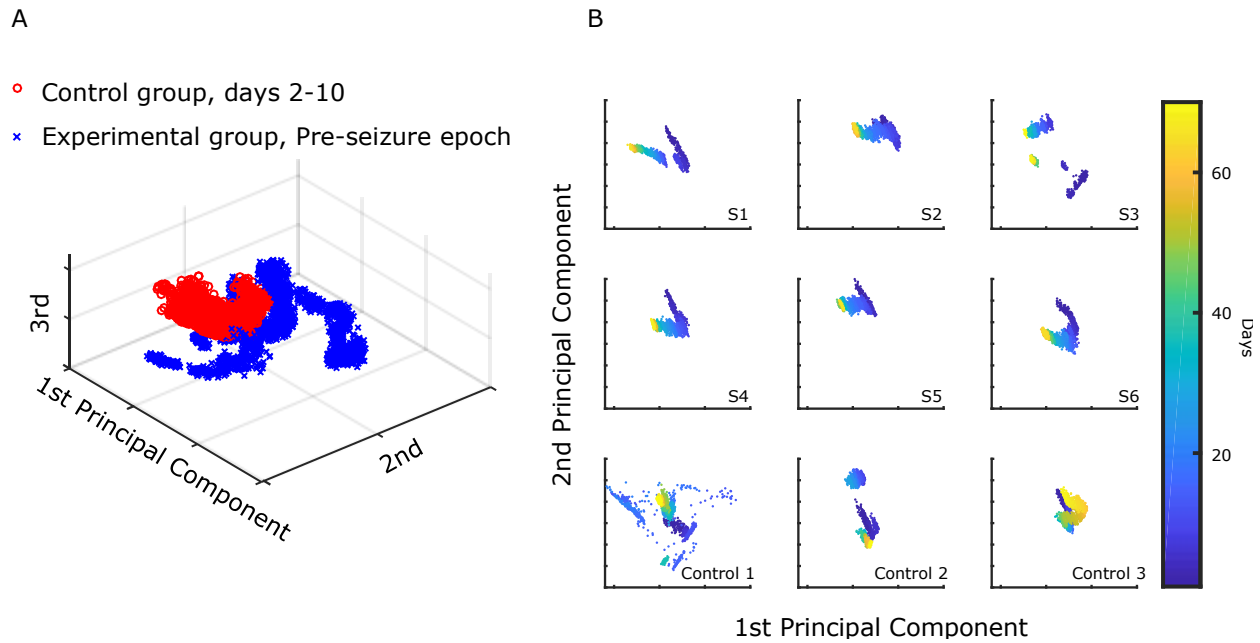


Figure 3.6 – Probing analysis – (Column 1) Power spectral density for each averaged electrically evoked response, plotted for each animal (S1-S6) over the course of the study. The power bands were individually normalized by subtracting the mean and dividing by the standard deviation to highlight changes in a single frequency band over time. In each experiment plot, there are three

vertical lines. The first line corresponds to the day that seizures first commenced. The second indicates the point of inflection separating the Rising- and Falling-seizure phases. The third shows the day of the last recorded seizure. (Column 2) Frequency information from the analyses were investigated by principal component analysis, and the first two principal components are plotted and labeled based on their epileptogenic phase membership (Red “squares” = Pre-seizure phase, green “+” = Rising-seizure phase, blue “o” = Falling-seizure phase). As seen in the figures, all three phases were quite distinct in all animals. The principal component analysis was performed separately for each of the six subjects. In order to demonstrate the temporal evolution of the induced responses, the first and second principal component values were segmented based on day and their centroids were calculated and plotted in the line-dot graph. Centroids referring to days 1, 3, 5, 10, 30, and 60 were colored different and labeled.





## Chapter 4

### Carbamazepine and GABA have distinct effects on seizure onset dynamics

#### 4.1 Abstract

Clinicians need to improve their characterization of seizure medication. This work investigates how anti-seizure medication influences seizure onset dynamics of the Epidynamics taxonomy. The low  $Mg^{2+}$  / high  $K^+$  mouse brain-slice seizure model was used to consistently generate a large quantity ( $N = 80$ ) of epileptiform onsets. We used the Epidynamics taxonomy to label the onset bifurcations of control samples and compared them to the labels of two experimental groups that added GABA or carbamazepine, two anti-convulsant medications. The addition of anti-convulsants changes the types of bifurcations observed, and different kinds of drugs affect the dynamics in different ways. This provides proof-of-concept evidence that brain states exist on a “map” of seizure dynamics, and that perturbations can change the positioning of the brain states on that map.

#### 4.2 Introduction

Epilepsy is a prevalent, heterogeneous disease with a vast array of signs, symptoms, and underlying seizure causes. These highly variable qualities make rationalized treatment difficult and impede therapy. One avenue to combat this heterogeneity is to classify manifested seizures. Labeling seizures can provide insight into the conditions and current state of the diseased brain and its dynamics. Unfortunately, our current classification methodologies ignore the underlying

dynamics, and are designed to describe clinical symptoms but not brain dynamics, which limits reasoned, mechanistic research (Fisher et al. 2017).

Fisher et al. attempts to update and standardize clinical methodologies for seizure classification (Fisher et al. 2017). In summary, this taxonomy characterizes seizures based on a few key components: focal versus generalized electrographic onset, patient awareness during seizure, and the presence of motor function during seizure. While this attempt at standardization is critical to clinical practice, a primary conclusion of the paper is that this taxonomy characterizes seizures by their qualitative behavior and fails to deliver insight to the underlying brain system.

Trying to improve upon the current classification systems, Perucca et al. a recent attempt to utilize electrographic data to provide a seizure taxonomy based specifically on seizure onset (P. Perucca, Dubeau, and Gotman 2014). In their work, Perucca et al. reported differences in frequency and amplitude characteristics of the seizure onset, resulting in 7 different observable seizure onset patterns. Lagarde et al. followed this example, but performed their analysis on a larger patient population and investigated lower frequency components of the seizure signal (DC shift) (Lagarde et al. 2019b).

While these studies strive to supplement current seizure classification systems, both studies are limited in two key areas. First, they produced taxonomies that were purely empirical. Specifically, each study investigated many seizure onsets, grouped the onsets by visual similarity, and gave them a label based on their amplitude and frequency characteristics. These taxonomies lack a scientific rationale and are purely observational, limiting their utility for future research. Second, these classification systems are un-validated. Classifications in Perucca et al. were performed by two independent reviewers. Disagreements on pattern classification were

resolved following a discussion between the reviewers. Lagarde et al. followed a similar protocol, except that a third, senior researcher was used to arbitrate. No other statistical tests were performed to ensure this taxonomy was repeatable or reliably represented the data. These two components, scientific rationale and validation, are important aspects of a impactful classification system, outlining a need for future development.

Epidynamics, is the first scientifically-reasoned seizure classification system, based on the first principles of dynamical systems theory. This taxonomy focuses on how the brain enters and exits seizure states, modeling these transitions using bifurcations. It proposes that the brain can transition from "normal" to "seizure" state via 4 unique bifurcations, and can exit via 4 unique bifurcations. This creates a total of 16 different seizure classifications, based on the onset and offset pairs. For onset, the four bifurcations are Saddle-Node (SN), Saddle-Node on Invariant Circle (SNIC), Supercritical Hopf (SupH), and Subcritical Hopf (SubH). Our previous studies validate a simple method for visual classification, and showed that these dynamical patterns can also be distinguished quantitatively from raw signal features. Epidynamics directly addresses the question of scientific rationale and validation, creating an ideal starting point for future epilepsy research. The next step is to use this taxonomy to re-interpret our current understanding of epilepsy.

In Saggio & Crisp et al. (Chapter 2) patients were found to have dynamically different seizures over time, contrasting from Perucca et al. and Lagarde et al. that assume patients have typical, representative seizures. In Crisp et al. (Chapter 3), seizures dynamics correlated with disease progression in epileptogenesis, providing evidence that disease alters the dynamics of the brain over time. Both of these studies provide evidence that the brain does not have a single pathway into seizure, but several, which may suggest that the underlying brain state is changing.

This concept was predicted by the "map" of brain dynamics, first proposed by Saggio et al. (M. L. Saggio et al. 2017b). When shown as parameters, there are invariant relationships between the different bifurcations, and the location of the brain state can be manipulated within the map. One prediction is that the underlying brain state can be closer or farther from seizures, providing a framework for future epilepsy research.

It is hard to predict how Epidynamics and the map will ultimately be useful to epilepsy research. However, a good place to start is to look at all the ways we try to describe seizures (and fail) and reapply this model. The possibilities are nearly limitless: propagation, initiation, termination, response to therapy, etc. In this study, we investigate response to therapy. Specifically, the effect anti-epileptic drugs have on seizure dynamics.

This research proposes to investigate the relationship between seizure onset bifurcations and underlying mechanisms in a simple model of epileptiform activity. The bifurcations presented in Epidynamics are not dependent upon any physiology. However, for epileptic seizure, the physiological mechanisms hold some intriguing potential connections to the bifurcations. SupH bifurcations start with a very small initial spike that gets larger over time, which fits very well with the idea of a small focus recruiting more and more tissue. This is in contrast to SN, SNIC, and SubH bifurcations in which full amplitude spikes start immediately, suggesting that large networks activate simultaneously. In this study, our specific hypothesis is that anti-convulsant factors can increase the likelihood of SupH bifurcations, based on the fact that anti-convulsant factors may disrupt simultaneous large network activation.

To test this hypothesis, we performed repeated, isolated studies in a mouse brain-slice seizure model. We visually classify onset bifurcations for each experimental condition. We quantify the changes in onset dynamics. We find that making perturbations to the onset pathway

changes the observed dynamics, suggesting that brain states exist on a dynamic “map” and can be moved via pharmaceutical therapy.

### **4.3 Methods**

#### **4.3.1 Animals**

Wildtype 129S6 mice (1.68-9.80 months old, mean at 5.31, std at 2.46) were used, cared for, and ordered in accordance to previous research (Moore, Throesch, and Murphy 2011). A total of 38 mice (16 male) were sacrificed, resulting in 92 slices total. All procedures were approved by and performed in accordance with the University Committee on the Use and Care of Animals at the University of Michigan.

#### **4.3.2 Experimental Procedure**

All animals were deeply anesthetized and rapidly decapitated following the procedures of previous research (Moore, Throesch, and Murphy 2011). This study used modified horizontal slices (330  $\mu\text{m}$ ) to allow for simultaneous recordings in the CA3 of the ventral hippocampus (Hipp), entorhinal cortex (EC), and amygdala (Am) brain regions, each known for having different structure and organization (Stoop and Pralong 2000). Brains were sliced (Leica VT1000; Wetzlar, Germany) in a sucrose slicing solutions and incubated in standard oxygenated artificial cerebrospinal fluid (ACSF) for at least one hour. After incubation, slices were transferred into a recording chamber filled with flowing ACSF. There, three in-house pipette electrodes were each separately placed into the Hipp, EC, and Am brain regions. Baseline activity was recorded for 1 min, immediately followed by a wash of pro-convulsant solution for the next 44 min. Only recordings where washes elicited epileptiform activity after a latency

period were used. All solutions were warmed to 31-32° C before entering the recording chamber to insure consistent temperature (Moore, Throesch, and Murphy 2011). After a total recording of 45 minutes, the slice was discarded and the recording chamber was drained, rinsed with standard ACSF, and reset for the next sample.

The specific contents of pro-convulsant solutions depended on experimental condition. All slices were treated with a standard low Mg<sup>2+</sup> / high K<sup>+</sup> (LMHK) ACSF with concentrations taken from past research that were designed to produce epileptiform activity within a short period of time (Moore et al. 2011). The control group (41/92) received no additional anti-convulsants, while the two experimental groups were treated with LMHK + 10 uM gamma-amino butyric acid GABA (28/92) or LMHK + 50 uM carbamazepine (CBZ) (23/92). The concentration of anti-convulsants were chosen based on previous research that showed anti-convulsant efficacy, but not total seizure blockage. GABA (a chloride channel agonist) and CBZ (a sodium channel blocker) were chosen to effect distinct anti-epileptic mechanisms. It should be noted that in any given slice, only one experimental condition was chosen (i.e. LMHK / LMHK+GABA / LMHK+CBZ). In other words, multiple conditions were never tested on the same slice.

### **4.3.3 Solutions**

Standard ACSF and a sucrose solution, which was used to prevent excitotoxicity during slicing, were created and maintained in accordance with previous research conducted by the Murphy Lab (Moore, Throesch, and Murphy 2011). A solution of 0 mM MgSO<sub>4</sub> and 10.00 mM KCl (Moore, Throesch, and Murphy 2011) was used as a pro-convulsant. Modifications to the

pro-convulsant solutions, used during various experimental conditions, were as follows: 50 uM Carbamazepine (Dreier, Zhang, and Heinemann 1998), 10 uM GABA (Williamson et al. 2015).

#### **4.3.4 Data Analysis**

##### **Bifurcation Labeling**

Our previous work demonstrated that bifurcations can be classified reliably with straightforward visual rules that isolate the features of each bifurcation type. In order to validate our visual classification, bifurcations were independently marked by three separate, trained reviewers. Each waveform was individually plotted and the reviewers selected the bifurcations blinded to results from the other reviewers. Onsets were colored differently than the rest of the waveform to ensure that all reviewers were provided the same reference point. These onsets were manually chosen and reviewed by a trained epileptologist. All samples were de-identified and presented to reviewers in random order. Reviewers had three separate choices for marking bifurcations: SN/Subh, SNIC, or SupH. SN and SubH categories were combined, as the experimental setup was incapable of recording DC components, disallowing a separation of the two.

Once all reviewers had generated markings, a Fleiss' Kappa test was performed to test reliability. The comparison between the markings of all three reviewers was statistically significant ( $P < 1e-324$ , less than MATLAB's smallest number). Finally, markings from all three reviewers were combined, creating a majority-vote label that was henceforth considered ground truth, in line with our previous practices (Crisp et al. 2019). Only 2/92 samples could not be agreed upon by at least two reviewers and were subsequently removed from all further analysis, bring the total samples analyzed to 90 slices.

<b>Visual Condition</b>	<b>Bifurcation Label</b>
If the amplitude of the spiking activity scales up from 0	SupH
If spikes are increase in frequency	SNIC
If the other two conditions are not met	SN/SubH*

Table 4.1 – Simple rules for visual classification of seizure onset dynamics. \* If the dataset allows for DC coupling, then SN and SubH can be differentiated if seizure onset is initiated by a DC shift.

### **Feature Analysis**

In addition to our visual bifurcation labeling, we also performed two types of algorithmic feature analysis. The first analysis focused on a subset of features found in Luna-Munguia et al. 2017 and Chen et al. 2018 (Luna-Munguia et al. 2019; L. Chen et al. 2018), which were used to provide “signal” features that are commonly used to describe seizures. In addition, we also calculated “dynamic” features that focus on the transition dynamics, and are identical to the ones used in Saggio & Crisp et al. (Crisp et al. 2019) These dynamical features are used to validate that the majority-vote labels mark different dynamic features. Feature definition and computation for each type of analysis is listed here:

#### Signal features:

Feature 1 – Spikes-per-second: Number of spikes divided by the length of the seizure.

Feature 2 – Median spike amplitude: The median value of all spike amplitudes.

Feature 3 – Median interspike interval: The median value of all interspike intervals.

Feature 4 – Mean Teager-Kaiser Energy: The Teager Energy Operator is computed on the raw signal. The mean of the output is taken.



Feature 5 – Standard deviation Teager-Kaiser Energy: As with Feature #4, but the standard deviation is measured instead of the mean.

Feature 6 – Burstiness: (1) compute the standard deviation of the interspike interval (called Bsd). (2) compute the mean of the interspike interval (called Bu). Burstiness =  $(Bsd - Bu)/(Bsd + Bu)$ .

Feature 7 – Memory: The Spearman rank auto-correlation of the interspike interval at a lag of 1.

#### Dynamical features:

Feature 1 – ISI Trend: The ISI of all spikes were computed and plotted consecutively. A simple line was fit to the data with a least squares algorithm and the slope of the line fit was extracted as the overall ISI trend.

Feature 2 – Amplitude Trend: The feature was computed exactly as in ISI Trend, except the peak-to-peak spike amplitudes were used in place of ISI.

#### **Comparisons & Statistics**

This study utilizes three types of analyses for statistical testing. The first analysis is used to verify if the algorithmic features accurately capture the differences between the experimental scenarios. This distinction is important as we are not trying to determine which features are best, but rather do these features successfully characterize the differences. To do this, we start with preparing the data. Our features undergo normalization (subtract the mean, then divide by the standard deviation) and then dimensionality reduction via principle component analysis. The first two principle components are paired with their experimental condition label and fit to a

multinomial logistic regression model (MATLAB's "mnrfit"). This model fitting procedure produces a measurement called “deviance”, which indicates the model’s goodness-of-fit. Based on the model’s deviance, we can then assess how well the features capture the differences of the condition labels. To compare this deviance with random chance, we also compute the baseline deviance for this model to provide a reference on how separable the data is on its own. This is performed by randomly scrambling the labels of the data and re-computing the deviance measurement. This is done 10,000 times, allowing us to compare our true deviance measurement against a random distribution of deviance scores, bootstrapping a P-value. This method was used on both the signal features and dynamical features.

The second analysis is used to compare the inter-rater variability with our bifurcation labels. This analysis is performed using a Fleiss Kappa test, and performed on our human markings.

The final analysis is to test the hypothesis that different experimental conditions change the bifurcations. We do this by creating a contingency table using the number of different bifurcations found in each experimental condition. A Chi-square test then assesses the differences between each condition.

## **4.4 Results**

### **Bifurcation vs Experimental Condition**

Epileptiform activity was found across all three experimental conditions. Only slices that developed sustained epileptiform bursting after being exposed to a pro-convulsant solution were included in the analysis. All three possible onset dynamics (SN/SubH, SNIC, and SupH) were present in all three experimental conditions (Fig. 4.1). Labels from all three reviewers were

found to be consistent (Fleiss Kappa test,  $P < 1e-324$ ), with a clear majority of cases being unambiguous (Table 4.1). Only 2/92 samples were ambiguous and were removed from further analysis. Dynamical features associated with the bifurcation labels were also found to be significant compared to baseline ( $P < 1e-324$ ), again reinforcing the findings in Saggio & Crisp et al. that visual classification can differentiate dynamically difference seizures. Signal features associated with experimental condition were also found to be significant compared to baseline ( $P < 1e-324$ ), validating the efficacy of the experimental drugs.

	Unanimous	2/3 agree	No consensus
Onset Bifurcation (N = 92)	57	33	2

Table 4.2 – Reviewer consensus on bifurcation labeling. Reviewers agreed unanimously on the clear majority of seizure onsets (62%). Less than 2.5% of seizure onsets could not be agreed upon by reviewers.

In the control group (brain slices exposed to only LMHK), the majority (~65%) of onsets had spikes that started slowly and sped up over time (SNIC bifurcation). The next most common (~26%) was onsets without any clear trend in ISI or amplitude (SN/SubH), aside from the fact that spikes were immediately large and distinguishable from baseline. SupH was the least prominent (~10%). In the group exposed to GABA (LMHK + GABA), there was a stark shift in dynamics: SN/SubH was most common (~54%), followed by SupH (~38%), and finally SNIC (~13%). With Carbamazepine, (LMHK + CBZ), the most prominent bifurcation was split between SNIC (~43%) and SupH (~43%). The remaining ~14% were SN/SubH. See. Figure 4.2.

In summary, onset bifurcations were found to significantly change between the different experimental conditions ( $P = 9.1e-5$ , Chi-squared)

## 4.5 Discussion

This work provides evidence that scientifically-based seizure onset dynamics can be modulated by application of different anti-convulsant medications. While no prior work has shown a direct correlation between onset bifurcations and medications, these results are in high agreement with previous work classifying two different visually-identified, empirical onset patterns that can be affected by different pathophysiology (Salami, Levesque, et al. 2015).

### Onset Bifurcations

In this brain slice model of seizure activity, we have discovered that the addition of anti-convulsant medication can influence how the slice traverses from “normal” to “seizure” state. We see that adding either anti-convulsant increases the chance the brain will enter an epileptiform state via a SupH bifurcation. In addition, we found strong differences between the effects of the two medications. What is most prominent in each experimental case was that one bifurcation group was LESS likely. In other words, brain slices with no anti-epileptic drugs (LMHK) rarely produced SupH bifurcations. Blocking sodium channels (LMHK + CBZ) restricted the production of SN/SubH bifurcations. Finally, the introduction of GABA (LMHK + GABA) restricted SNIC bifurcations. This study provides evidence that anti-convulsant medication influences seizure dynamics, and that specific drugs influence the dynamics in specific ways. These findings could be used to help inform clinical decisions with respect to patient drug selection. Furthermore, these findings act as further evidence that the epileptic brain exists on a "map" of seizure dynamics, i.e. that there are certain pathophysiological conditions

that tend to place the brain closer or farther away from specific types of seizures, and that this “location on the map” can be manipulated.

Obviously, mouse brain slices are not a perfect model for clinical human epilepsy. Despite this discrepancy, the same Epidynamics taxonomy was found in the brain slices as well as clinical human data (Chapter 2). This finding is evidence that seizure dynamics are a fundamental characteristic of brain networks, regardless of physiology or pathology. Future research should investigate the differences of seizure dynamics between clinical human data and brain slices.

Our initial hypothesis was that CBZ and GABA would increase the probability of seizure onsets occurring as SupH bifurcations. This hypothesis was based on the understanding that the overall excitability of the neurons would be diminished, and thus more cells would be less prone to initiating the seizure. We hypothesized that, given the inexorable progression to seizure-like activity with the low  $Mg^{2+}$ /high  $K^+$  solution, the medications would not stop the seizure altogether but would manifest as a small number of the most excitable cells starting to burst, then slowly recruiting the rest of the slice—which would appear physiologically as a SupH bifurcation. In contrast, without the anticonvulsants most of the cells would be recruited to the bursting very quickly, which would appear as one of the other bifurcations because the initial bursts would involve so many cells and have high amplitude. Note that this effect may not have occurred in this brain slice model, which typically is considered to produce generalized, rather than focal, seizure onsets. In addition, the mechanisms of action of CBZ and GABA are completely different, so it was not certain that both would produce a similar effect on onset dynamics. Despite these limitations, we found that SupH bifurcations increased under both conditions. However, the prevalence of onset dynamics was quite different in each case for

reasons that are not currently understood. Future research can investigate the underlying mechanisms of these differences.

Overall, our hypothesis is that any drug with anti-convulsant properties could potentially increase the prevalence of SupH seizures. However, we note that the Epidynamics taxonomy is based purely on the first principles of dynamics, independent of any physical property of the brain. Thus, any physiological mechanism that predispose to specific bifurcations may be sufficient, but will not be necessary nor unique, for such an effect. This study serves as a proof of principle that such mechanisms are capable of influencing these onset dynamics, opening the way for future research into how these high-level dynamics can be explained and manipulated by physical properties and interventions.

### Summary

Despite innovation in pharmaceutical therapies, treating epilepsy continues to challenge researchers and clinicians alike, due to the inherent heterogeneity of the disease. This has motivated research to find a better way to characterize seizures to facilitate better treatment approaches. Jirsa et al. and Saggio et al. have provided a novel way to characterize seizures in a way that can provide mechanistic insights into the brain system. This study investigates the relationship between these Dynamic Classes and the application of different anti-convulsants. We provide proof-of-concept evidence that these Dynamic Classes are linked to underlying seizure mechanisms, and that changes in anti-convulsant therapies can also change the Dynamic Class. This provides a new language for researchers and clinicians alike to characterize both seizures and pharmaceutical therapies.

## 4.6 Figures

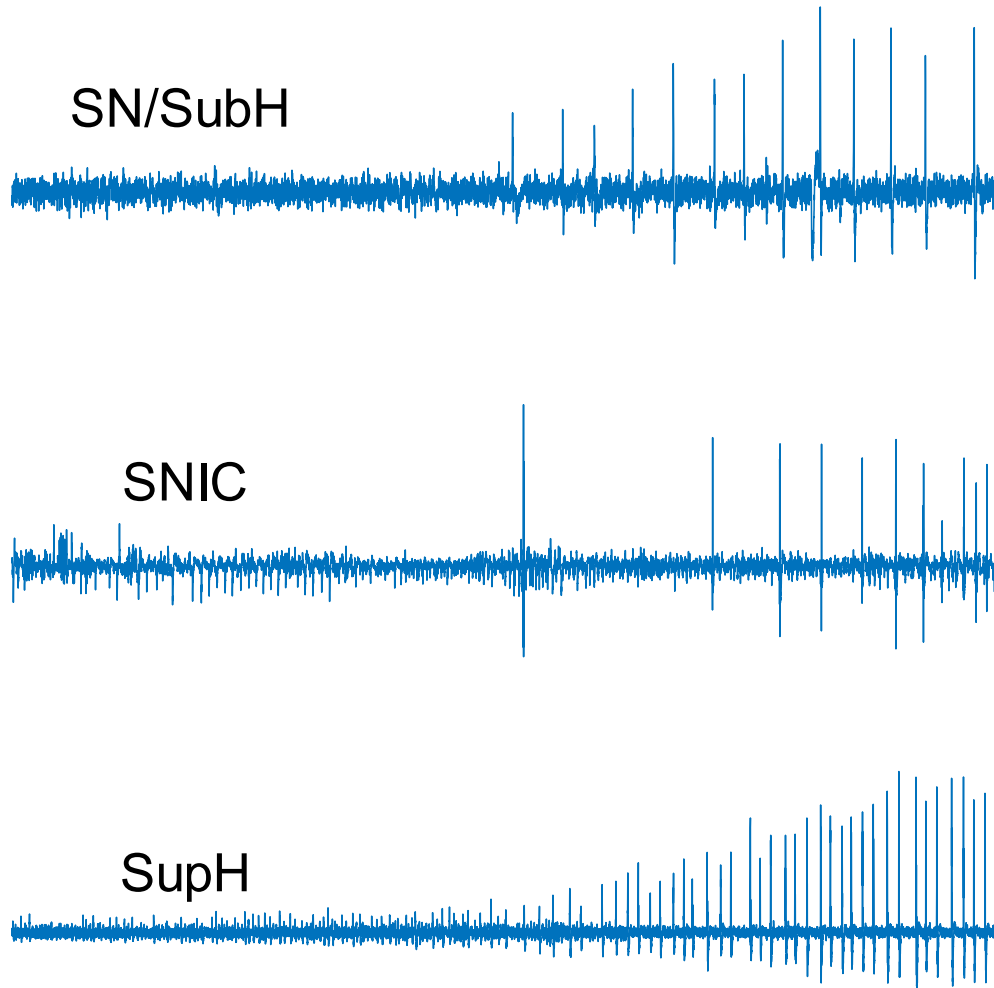


Figure 4.1 – Raw waveform examples of the different observed onset bifurcations.

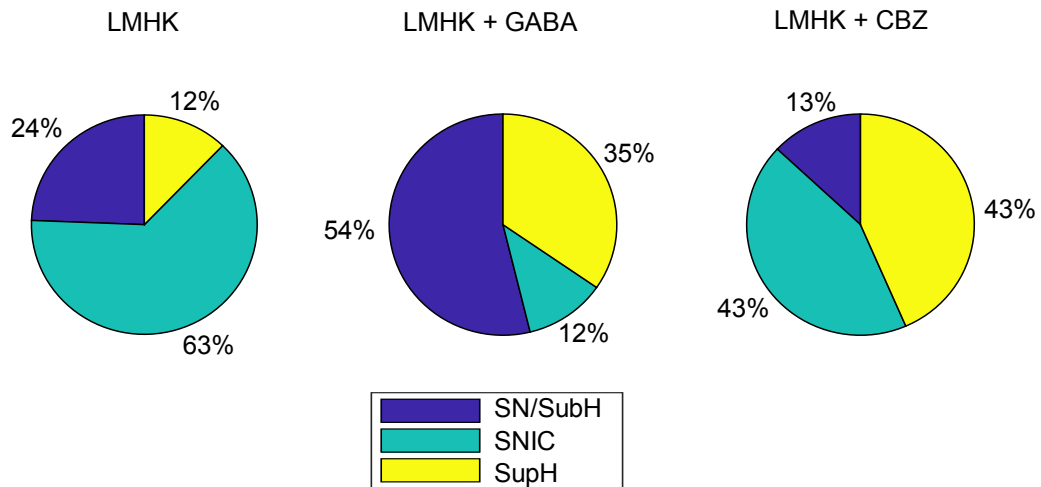


Fig 4.2 – Prevalence of seizure dynamics vs experimental condition. (LMHK) SNIC bifurcations were dominant in slices using only low  $Mg^{2+}$  / high  $K^+$ . (LMHK + GABA) Introducing GABA decreased the prevalence of SNIC bifurcations, instead increasing the prevalence of both SupH and SN/SubH. (LMHK + CBZ) Introducing CBZ made slices produce equal numbers of SNIC and SupH bifurcations and minimal SN/SubH.



## **Chapter 5**

### **Discussion**

The current clinical standards for seizure classification are simply too observational for effective epilepsy research, producing the need for a seizure taxonomy based on scientific rationale. This thesis provides several studies that show categorizing seizures based on their fundamental dynamics is a viable option, and shows promise in tracking epileptic brain state over a variety of conditions.

In Chapter 2, I developed a robust validation method for a seizure classification taxonomy and found that seizures can be categorized based on their fundamental dynamics. In this chapter, I also discovered that some seizure dynamics occur more frequently than others and that seizure dynamics can change over time in patients. These findings suggest that the brain moves around a dynamical map, and that certain seizure types are more likely due to the relative complexity of the different bifurcations on that map.

Chapter 3 investigated brain state dynamics in both active (electrically-induced brain responses) and passive (seizure onset dynamics) modalities with reference to epileptogenesis. This is the first study to pair seizure onset dynamics and induced brain responses to track epileptogenesis in long-term data. Evoked brain responses show robust ability to predict which animals will develop epilepsy. Both evoked brain responses and seizure onset dynamics show that epilepsy continues to develop throughout the time course of this model of epileptogenesis, and that both these measurements can independently quantify these changes. These findings

suggest that this disease alters the brain over time, moving the brain state around a dynamical map.

Chapter 3 does come with a few caveats, starting with the assumption of the independent relationship between seizure dynamics and evoked responses measurements. While we assume that both measurements are independent, repeated stimulation has been found to have therapeutic effects on the brain (Yamamoto et al. 2002; R. Chen et al. 1997). Therefore, it could be the case that the time-varying seizure dynamics are an outcome of therapy rather than disease progression. However, the ultimate outcome is still the same: seizure dynamics can be a biomarker of epileptic brain state.

Another caveat concerns the results of our classifier. While we are able to use evoked responses to differentiate rat brains by whether or not they will develop epilepsy at a future state, our choice of model limits the generalizability of the claim. For this research, we implemented the tetanus toxin rat model, and in all six experimental animals, spontaneous seizures were created. This setup limits what can be interpreted from this, as we essentially classified whether a brain was traumatically injured or not. Currently, it is unknown what magnitude of injury is necessary to start the process of epileptogenesis. Future research could use a similar model of epileptogenesis that had a specific probability of developing epilepsy. With this hypothetical setup, researchers could efficiently test when an injury is sufficient to cause epileptogenesis, increasing the translatability to clinical cases.

Chapter 4 investigated how seizure dynamics respond to anti-seizure drugs. While previous studies have explored seizure onset patterns with various anti-seizure drugs (Salami, Lévesque, et al. 2015), their patterns are again observational and not based on any scientific rationale. Seizure dynamics can change with the addition of anti-epileptic drugs, and different

drugs produce different dynamical changes. These findings suggest that drugs can be used to move the brain state to different parts of the dynamical map, and that different drugs affect the brain state in different ways.

One caveat from Chapter 4 concerns the characterization of epileptic brain slices. In Chapters 2 and 3, we focus our research primarily on focal onset epilepsy. Chapter 4 presents a disconnect, as brain slices are categorized as producing generalized epileptiform activity. Future research should investigate seizure dynamics in a focal brain slice model, perhaps by implementing microinjection dispensal systems. In addition, future studies performed in brain slices should be done with recording equipment that can appropriately record DC shifts.

A common trend uncovered in this thesis is that seizure dynamics are both highly variable and highly manipulable. These studies suggest that time, disease, and drugs can influence the brain's current state and move it to different dynamical regimes. This is further evidence for a map of seizure dynamics that the brain state can navigate, which was first introduced by Saggio et al.

Future work entails continuing to reapply this taxonomy to various aspects of epilepsy research. Specifically, our next steps include investigating seizure propagation and the brain's response to therapeutic stimulation. Seizure propagation has a direct application to focal resection surgery. Having a supplementary tool that can further guide clinical action may help surgical outcomes. Electrical stimulation as an epilepsy therapy has gained traction in recent years, with examples such as NeuroVista and the Vagal Nerve Stimulator. Similar to our investigation of the effects of anti-seizure drugs, uncovering the effect electrical stimulation has on seizure dynamics may help researchers better characterize and test these therapies.

The work described in this thesis has provided a new language, Epidynamics, for researchers and clinicians alike to characterize epilepsy, epileptogenesis, and associated therapies. It has also produced a methodology for validating modifications to the Epidynamics taxonomy or for validating completely new ones. Finally, this thesis serves as a gateway for future research to investigate epilepsy with a mechanistic and reasoned approach, which should encourage fast and effective translation.

## Appendix

### Supplementary information for Chapter 2

#### I. Methods

##### *I.1 Data collection*

###### *Human EEG data*

Data were collected from seven international epilepsy centers: University of Michigan, Mayo Clinic, Hospital of the University of Pennsylvania, Children's Hospital of Philadelphia, University of Melbourne, University of Freiburg, and Kyoto University Hospital (Cook et al. 2013; Ihle et al. 2010; Kanazawa et al. 2015; Wagenaar et al. 2015). All patients consented to share their data according to the local institution's review board policy. Data were de-identified EEG collected with each institution's clinical EEG equipment. All EEG data used in this work were from either grid or depth intracranial electrodes. All sampling rates were  $> 200$  Hz and antialiasing filters  $> 100$  Hz, but there was variability between centers (XLTek, Nicolet, Natus, Nihon Kohden, NeuroVista). The Melbourne patients had ambulatory devices that recorded data for several months (Kanazawa et al. 2015), while all the others were acquired during acute inpatient recording sessions. As the analysis was limited to amplitude and interspike intervals that should not be affected by the different techniques used, we did not stratify by center, but we did verify that the results did not depend upon center for offset dynamics. For onset dynamics, there were only two centers (Kyoto, Michigan) that had amplifiers that recorded low enough frequency content (high pass filter 0.016 Hz) (Kanazawa et al. 2015) to allow analysis of direct

current (DC, i.e. very low frequency) shifts, and so only those centers were included in the analyses that involved DC coupling.

In every patient, EEG from a single electrode was used for analysis. The electrode was chosen in each case by reading the official clinical report to identify the seizure onset zone and choosing the electrode with the highest amplitude within the seizure.

### *Simulated seizures*

Validation of the classification scheme required a gold standard dataset, which we generated by simulating 60 random iterations of each type of onset and offset bifurcation. The simulation used the model and methods to begin/end at specific bifurcations described in Saggio et al (M. Saggio et al. 2017) and a function to generate a trajectory across each bifurcation. The trajectory was an arc of great circle as described in section II for the model, but the crossing point on the bifurcation curve and the inclination of the path with regards to the bifurcation curve changed randomly at each iteration to produce adequate variability within each bifurcation type. These conditions were implemented to create a robust data set that would mimic biologic variability. We simulated an equal number of seizures per bifurcation. The final result was 240 seizure onset and 240 seizure offsets, each with random characteristics and spanning a wide range of physiologically-relevant parameters. The 480 seizures were used to assess the accuracy of both the human and algorithm classification schemes.

For each bifurcation, we created an algorithm able to choose a random point on the bifurcation curve (see section V) and a random point on a curve we designed to run parallel to the bifurcation curve. A trajectory linking the two points would cross the bifurcation curve with different inclinations at each iteration. The combination of a random point on the bifurcation

curve and different inclination gives different amplitude/frequency behaviors, as shown in Figures S10 and S11. Given that variability in the non-prescribed trends is due to the presence of other bifurcations nearby, we ignored portions of the bifurcation curves far from others, such as the portion of SupH behind the sphere as compared to the bistability regions. Two of the onsets (SubH and SupH) required a small amount of noise to be added to the simulations in order for the system to be able to leave the unstable equilibrium. The velocity of the slow variable,  $c$ , was chosen for each class to be small enough to ensure time scale separation so that the prescribed scaling law would be visible.

As these simulations had arbitrary timescale and different levels of background noise, we then post-processed the data to blind the reviewers. We first added normal random noise (MATLAB's 'normrnd',  $\mu = 0$ ,  $\sigma = 0.01$ ) to all samples of every signal based upon the existing noise. We then rescaled all seizures so that the final interspike intervals would be  $\sim 0.2$  s, then downsampled ('decimate' function in Matlab) so the sampling rate would be  $\leq 200$  Hz. All code is available for download at <https://doi.org/10.7302/ejhy-5h41> (Crisp et al. 2019).

## ***1.2 Spike analysis***

As stated in the main body, we define a “spike” in dynamical terms: any prominent sharp transient associated with the dynamical process, which for these human EEGs means any fast transient  $< 200$  ms long and amplitude discernable from the background. Inter-spike interval (ISI) is defined as the time between sequential spikes. Amplitude for a given spike is defined as the absolute maximum peak-to-peak difference in a window of time ranging from the halfway point of the first spike and the halfway point of the latter spike (see Fig. 2A in main body). Beginning/ending spikes utilize only the halfway point of the nearest spike. All analyzed data

were decimated to ~200 Hz for efficient analysis. In order to remove slow transients and identify the local spike amplitudes, raw EEG data were first high-pass filtered (MATLAB's 'highpass', 1 Hz). Peaks were found in Matlab using the 'findpeaks' function, after manually optimizing amplitude, time, and prominence for each patient. This process required iterating the features until visually confirming that spikes were correctly detected, using plots in Matlab with the spike detections superimposed upon the EEG signal (see Fig. S1). Due to the wide variability between patients, we were unable to develop a reliable automated method to determine the spike locations in every patient.

Sentinel spikes. Some seizures began with a single high amplitude 'sentinel spike,' which typically was present in many electrodes and was not directly related to the seizure dynamics thereafter. Additionally, it was sometimes difficult to know whether these events were actually true sentinel spikes versus a transient caused by a filtered DC shift (e.g. the first spikes seen in Fig. 2B&C, Fig. S1A&C). This spike was used as the initial seizure onset time but was not included as a detected spike for seizure dynamics, as this phenomenon is not a canonical feature of any of the onset bifurcations.

Spike-wave complexes. Some seizures had spike-wave complexes in which the aftergoing slow wave was very prominent, similar to the waveforms seen in absence epilepsy. In these cases, the highest amplitude of the whole complex was used, even if it was the slow wave, and only a single event was counted from each complex (see Fig. S1C).

Clonic spiking. As described previously 7, when there was clonic spiking at the end seizures, the interclonic interval was used to evaluate the presence of slowing down, and the ISI between successive fast spikes within each clonic burst were ignored (see Figs. 2B & S1F).



It is important to note that this analysis does not address every feature of the seizures. There are many phenomena, such as the three listed above, the shape and frequency of the spikes, and other complex patterns, that are not invariant features of the bifurcations. While these are important to the clinical description and can be relevant to understand the underlying dynamics, in the framework here proposed they do not contribute to defining the Epidynamics of seizure onset and/or offset.

### *1.3 Visual classification of seizure dynamics*

The key to differentiating the bifurcation type is to identify the invariant dynamical features, which can be summarized as the presence of a DC shift and the behavior of the ISI and amplitude (see Fig. 1). These features are typically quite easy to distinguish. The only prominent ambiguity is that it is not feasible under clinical conditions to distinguish between the logarithmic and square root functions at offset, as previously described (V. Jirsa et al. 2014). Thus, our first test was to determine if human reviewers can classify the different bifurcations visually using simple rules.

The presence of a DC shift and the general trends of ISI and amplitude can readily be determined upon visual analysis. The basis for this analysis is to determine whether the amplitude and ISI scale to zero. For ISI, this appears as a decreasing frequency as  $T$  approaches 0, i.e. slowing down at seizure offset, or speeding up after seizure onset. For amplitude, it appears as a gradual change in the spike amplitudes, with the spike at  $T=0$  being very small compared to the baseline, then increasing further away from  $T=0$ . This description is qualitative but is readily applied to typical EEG data. Since the onset/offset dynamics are typically defined by only 5-10 spikes and there is considerable noise and variability in real EEG signals, rigorous

curve fitting is rarely possible (though we included it in the examples in Fig. S1). Just as with clinical EEG reading, we found that a much simpler and more reliable classification system was to visualize the ISI and amplitude plots of the first and last 10 spikes and determine whether the trends were scaling to zero, constant, or arbitrary, and if there was a DC shift. For amplitude, we defined ‘scaling to zero’ as steadily diminishing to less than 3 times the background level near  $T=0$ . For ISI, we define it as steadily larger ISI near  $T=0$ , with the last two ISI  $> 50\%$  larger than the mean ISI 10 seconds prior. All analysis for onset and offset concentrated on the first/last 5 seconds of data, but occasionally used up to 15 seconds to observe the full patterns. Using these definitions, we developed a visual classification system (Table S1).

<b>Onset</b>	
<b>DC Shift</b>	SN
<b>Amplitude increasing</b>	SupH
<b>ISI decreasing (frequency increasing)</b>	SNIC
<b>ISI and Amplitude constant/arbitrary (no DC shift)</b>	SN or SubH
<b>Offset</b>	
<b>DC Shift</b>	SH
<b>Amplitude decreasing</b>	SupH
<b>ISI increasing (frequency decreasing) (no DC shift)</b>	SH or SNIC
<b>ISI and amplitude constant/arbitrary (no DC shift)</b>	FLC

Table S1 – Visual classification system. Classification relies upon visualization of the given features. In case of multiple features present, the bifurcation listed on top takes priority. DC shift: a sharp deflection  $> 5$  times the background that occurs in  $< 0.5$  s, then lasts  $> 1$  s. Constant: the value is consistent and does not trend upward or downward for 10 spikes. Arbitrary: no consistent unimodal trend over 10 spikes.

#### ***1.4 Features for automated classification of seizure dynamics***

We also developed an analytical tool to use quantitative features and machine learning to identify the Dynamic Class. The goal of this analysis was to determine if the features used in the qualitative study were robust. We designed features based upon the visual classification system

in Table S1, focused on quantifying DC shift, amplitude trends, and interspike interval trends. Definitions, feature computation, and feature descriptions are as follows:

Baseline Definition: Several features require definition of the baseline, i.e. seizure activity vs. non-seizure activity. All analyzed waveforms include a period of baseline, followed by seizure activity, followed by more baseline. Computationally, the term ‘baseline’ below is defined here as the segment of the waveform that started before/after a seizure. For an onset baseline, this segment was taken as the start of the waveform up until seizure onset. For an offset baseline, this segment was taken as the point after seizure offset to the end of the waveform.

DC vs. Non-DC: Data acquired at Kyoto (Nihon Kohden EEG 1100 amplifier) or Michigan (Natus Quantum amplifier), both of which record down to 0.016 Hz, were included in the DC cohort, and all other data was considered “non-DC”. Non-DC data were first filtered with 1 Hz highpass filter (Matlab ‘highpass’), then all features extracted. On the DC data, features were computed on the raw, unprocessed EEG.

Preprocessing steps: 1) Onset/offset times, as well as the relative bifurcation window lengths, were determined by a trained epilepsy specialist. 2) Spikes were identified using findpeaks.m (Matlab) to locate upper (maxima) and lower (minima) spikes. 3) Seizure polarity was determined by determining whether the median of the upper or lower spikes had a greater absolute difference from the baseline median. The value with larger difference was chosen as the true “spikes” and were used for all further analysis. All amplitudes were taken as absolute values. This step accounts for the fact that spikes can be either positive or negative in intracranial electrodes.

Feature 1 – ISI trend: The ISI of all spikes were computed and plotted consecutively. A simple line was fit to the data with a least squares algorithm and the slope of the line fit was extracted as the overall ISI trend. For onset (offset), the first (last) 5-15 spikes were used, using as many as possible until a clear inflection point in the line. The order was reversed for offset.

Feature 2 – Amplitude trend: This feature was computed exactly as in ISI trend, except the peak-to-peak spike amplitudes were used in place of the ISI.

Features 3&4 – normalized upper and lower peak median: The signed distance between the median of the upper peaks and the baseline median was computed (upm). That same was done for the lower peaks (lpm). If  $|upm| > |lpm|$ , then normalized values were  $nupm = 1$ ,  $nlpm = upm/lpm$ . If  $|lpm| > |upm|$ , then  $nlpm = -1$ , and  $nupm = -lpm / upm$  (note that lpm is negative in all cases). These features identified DC shifts.

### ***1.5 Validation of classification methods***

In our prior work with the Epileptor model (the SN/SH Class), we proved the goodness-of-fit to the logarithmic equation for terminal ISI (V. Jirsa et al. 2014). However, in the current work we found that GoF methods were not robust when discerning between multiple seizure types in noisy data. This is because the number of samples (spikes) is small, while the combined uncertainty in the noise as well as the classification of the different Classes can be significant. The result was that the variability due to noise was often more prominent than the differences between bifurcation types. This difficulty is not surprising, as seizures are notoriously difficult for automated algorithms to identify under clinical (noisy) conditions, and classification will be even more difficult. More importantly, even under ideal conditions any such analysis would be

limited due to the lack of a gold standard. We therefore decided on an alternate and more rigorous approach, appropriate for the data quality of clinical seizures.

In order to validate our classification system, we used a multi-step approach. The key to this validation was the generation of a gold-standard with simulated data, in which we know which bifurcation is present. Using the gold standard, we first used machine learning tools to assess how accurately our chosen features are capable of identifying the differences between the bifurcations. We then tested how accurately human reviewers could identify each bifurcation using visual review. After proving that the human reviewers were accurate and reliable in the gold standard, we tested their reliability in the true clinical dataset. These steps are detailed below.

#### Step 1: Feature validation and bootstrapping:

**OBJECTIVE:** Determine whether the chosen features capable of discerning between the four bifurcations in the gold standard.

**METHODS:** Using the simulated seizures (240 onsets, 240 offsets), supervised learning was chosen to quantify how well the simple features in I.4 captured the differences between the different Dynamic Classes. This was performed by fitting labeled features to a statistical model to generate a goodness-of-fit measurement. Specifically, we used a multinomial logistic regression model ('mnrfit', Matlab), which outputs a model parameter 'deviance' that estimates the Goodness-of-Fit. The GoF was compared with the gold standard in the simulation data. Note that this method is not used for classification nor to determine the "best" potential fits. Rather, we used the GoF statistic to assess whether our chosen features were capable of discerning between the four bifurcations. While there certainly could be better features, we chose these

because they recapitulate what experts use for visual analysis, which is what this test is trying to validate.

To provide reference for the GoF computation, we performed a permutation test by randomly scrambling the bifurcation labels and re-fitted the data to the model. This was repeated 10,000 times to provide the distribution of random GoF, which can then be compared with the index case and provide a p-value, a process known as bootstrapping.

**RESULTS:** For both onset and offset bifurcations, the GoF with true labels was better than all 10,000 permutations ( $p < 1e-4$ ). This result indicates that the 4 features are very effective in capturing the differences between the 4 onset and offset bifurcations and extremely unlikely to be due to chance.

**CONCLUSION:** The chosen features are capable of discerning between the bifurcations.

## Step 2: Human visual analysis of simulated data:

**OBJECTIVE:** Validate whether visual analysis by human reviewers accurately identifies the different bifurcations in the gold standard.

**METHODS:** Using the simulated seizures (240 onsets, 240 offsets), three independent reviewers labeled all bifurcations using an in-house Matlab viewing program that kept labels blinded while also randomizing the order in which the seizures were viewed. DC-coupled data were shown with two waveforms: raw data and 1 Hz highpass filtered data ('highpass', Matlab), in order to highlight DC components while also allowing viewing of spike dynamics. Reviewers had to choose exactly one of the four potential bifurcations for each example.

**RESULTS:** For onsets, all three reviewers unanimously agreed in 80%, 2/3 agreed in 18.3%, and no agreement was found in 4/240 (1.7%). Compared to ground truth, reviewer 1, 2,

and 3 had 100%, 97.92%, and 80.42% accuracy, respectively. For offsets, there was majority agreement in all 240 seizures, 78.75% of which were unanimous. The Fleiss Kappa score for these results has a p-value that is lower than the smallest number possible to express in Matlab ( $p < 4.94e-324$ ). Compared to ground truth, reviewer 1 and 2 both had accuracies of 99.85% while reviewer 3 had 78.75%.

**CONCLUSION:** These results clearly show that the visual classification system can distinguish the four bifurcation types, and that human reviewers are accurate and consistent.

	Unanimous	2/3 agree	No consensus	P value
Onset (N=240)	192	44	4	$P < 4.9 e-324$
Offset (N=240)	189	51	0	$P < 4.9 e-324$

Table S2 – Reviewer agreement on simulated data. Reviewers were highly consistent with each other in the simulated data. The interrater reliability is extremely high, as the p-value (Fleiss Kappa, 3 reviewers) is negligible.

Step 3: Validation on clinical data:

**OBJECTIVE:** The strong results of Steps 1 and 2 validate the use of these methods in clinical data. The goal of the present step is to determine reliability of the three reviewers when labeling the human seizures, and to use these labels for the taxonomy in Fig. 2.

**METHODS:** We evaluated the 51 DC-coupled seizures and 69 non-DC-coupled seizures separately (see main paper). We used similar methods as in Step 2 to classify the human seizures. One important difference in this analysis is that SubH onsets were grouped with SN (-DC), and SNIC offsets with SH (-DC), as described. We calculated the Fleiss Kappa statistic between the three reviewers to assess inter-rater agreement.



RESULTS: As seen in Table S3, the three reviewers had high agreement, especially in the DC-coupled data. We also used the majority labels with the bootstrapped automated feature analysis as in step 1, to determine how well the given features captured the specific chosen bifurcation. These results showed that the DC onset and offset both had excellent GoF with the chosen features. Non-DC offset was also excellent, but the non-DC onset had less consistent results ( $p=0.0969$ ). This demonstrates the usefulness of DC-coupled recordings to identify the onset bifurcations.

CONCLUSION: These results show that the labels are highly consistent between different reviewers. Given the results from Steps 1 & 2, we conclude that it is highly likely that the bifurcations are present in the data and that these methods are correctly identifying them. Given these positive results, we used the majority-vote classification for the taxonomy seen in Fig. 2.

	DC (N=51)	Non-DC (N=69)
Onset	P = 1.78e- 15	P = 4.51e-12
Offset	P = 4.51e- 11	P = 9.72e-4

A. Reviewer agreement on human data

	DC	Non-DC
Onset	P < 1e-4	P = 0.0969
Offset	P = 7e-4	P < 1e-4

B. Automated features permutation test

Table S3 – Accuracy identifying bifurcations in clinical data. (A) Reviewers were highly consistent with each other scoring the bifurcations in the clinical data. (Fleiss Kappa, 3 reviewers). Each patient was stratified based upon whether their EEG had DC-coupled recordings, as the non-DC group could not disambiguate SN or SH with DC shifts. (B) The model fit of the automated features to each chosen bifurcation was performed versus human majority vote, then bootstrapped as in Step 1. The chosen model parameters were clearly highly descriptive of chosen bifurcations in DC onset and offset and non-DC offset. As expected, the lack of DC coupling makes it difficult to disambiguate the four onset bifurcations.

### ***1.6 Challenges with classification***

There were several conditions in the data that required rules for disambiguation between the different bifurcations:

1. Amplitude scaling. Amplitude was often arbitrary in our clinical data, showing considerable variability from spike to spike. This variability sometimes made it difficult to determine if there was scaling to zero (square-root). In those cases, we observed the

spikes closest to  $T=0$ : if the first 5-10 spikes appeared to arise from the baseline noise and consistently grow in later spikes, it was classified as square-root scaling (SupH). If the first 5-10 spikes were clearly  $> 3$  times higher than baseline noise, the seizure was classified as constant (i.e. arbitrary) amplitude even if later spikes increased in amplitude.

2. Late amplitude increase. In many seizures, after  $\sim 10$  seconds it was common for the spiking activity to increase in amplitude as the seizure spread to neighboring electrodes. This late increase was not part of the onset bifurcation, and only the initial trend during the first 10 seconds was used for classification, which was typically not SupH.
3. 'Arbitrary' scaling usually constant. Although the "non-zero" scaling listed in Fig. 1 theoretically includes many arbitrary patterns, we found that the vast majority of examples manifested as a constant value, similar to the analysis in (V. Jirsa et al. 2014). For instance, nearly all SN onsets had constant amplitude and ISI, and SH offsets had constant amplitude.
4. Mixed dynamics. In cases where features from more than one bifurcation were present in the data (e.g. DC shift and amplitude scaling), we used the following prioritization order: DC shift  $\rightarrow$  amplitude scaling  $\rightarrow$  frequency scaling. The highest priority was used as the final bifurcation, e.g. if DC shift and amplitude scaling were both present, it was classified as SN (onset) or SH (offset). Table S1 presents the bifurcations in this order.
5. Unusual dynamics. There were rare examples in which the dynamical behavior was highly unusual, all of which we present in this Appendix (Figs. S1E, S2, S9-11). Each of these patterns was classified as 'arbitrary'. See section I.8 for further details.

Despite these rules, there were examples in which the human reviewers were either incorrect in the simulated data or did not agree with each other in the clinical data. While these errors were

uncommon, we evaluated each case to determine the conditions responsible. The following are a list of the conditions that can make classification difficult. “a” and “b” were specific to the simulated data, as it is necessary to know the ground truth to identify these problems.

- a. Misclassifying arbitrary bifurcations (in simulated data). This occurred when an arbitrary bifurcation had parameters that produced trends very similar to scaling laws (either amplitude or ISI). This is expected, as the full range of “arbitrary” can encompass some of the other parameters.
- b. Distinguishing SN from SupH onsets (in simulated data). This was due to a technical aspect of the simulation. In order to produce the full range of SupH parameters, it was sometimes necessary to move the model to a region of the map near the SN bifurcation with a DC shift before the seizure could begin. This parameter correction was not part of the initial bifurcation, but did produce a DC shift close to seizure onset that sometimes confused the reviewers. However, this situation most likely is not pertinent to physiological seizures, as it is an artifact of the model construction.

The following phenomena are not described by the canonical features of the bifurcations, and were difficult for the reviewers to classify. The majority of disagreements between reviewers contained at least one of the following:

- c. Polyspikes or spike waves at seizure onset, especially prior to low voltage fast activity
- d. Preictal spikes

- e. Noisy data, especially ‘extraneous’ spikes that disrupt scaling laws and “Unusual dynamics” (#5 in preceding section)
- f. Ambiguous seizure onset/offset times
- g. Low voltage fast activity that speeds up at seizure onset

These patterns (a-g) are inherent challenges of seizure data, and such conditions have the potential for ambiguous classification. However, we do not consider this to be a failure of our method—rather, Epidynamics provides a method of identifying and quantifying these conditions. While these phenomena are not uncommon, they are not invariant features that define the bifurcation. In effect, the fact that they deviate from the basic Epidynamics not only allows us to identify them as atypical, but also to quantify *how and why* they are atypical.

We include these graphical fits and RMSE for constant and square root/logarithmic equations to demonstrate how this tool may be used to determine parameters for these equations, which can be used for quantitative analysis, comparison, and robust discussion of seizure dynamics in future work.

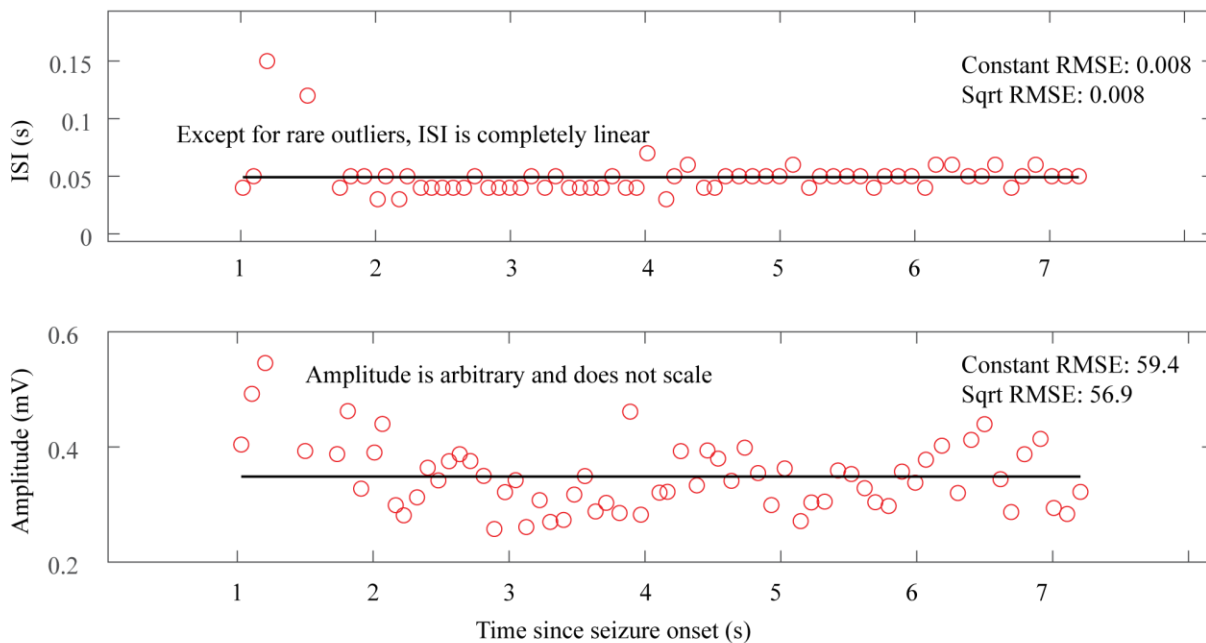
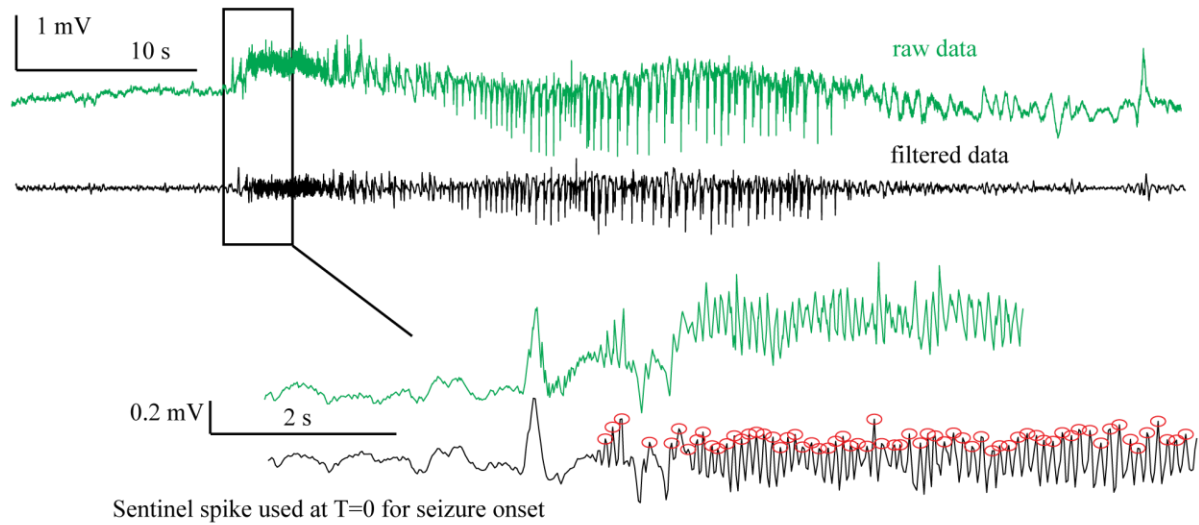


Fig. S1A – Saddle Node Onset. DC-coupled recordings (green, top) show DC shift that occurs immediately upon seizure onset. To determine spike amplitudes and ISI, data must be high-pass filtered (black). Those filtered data are then used to identify the spikes (red circles) for analysis. The interspike intervals (ISI, middle) and amplitude (bottom) of each spike are then plotted versus time since seizure onset for visual analysis and curve fitting. The seizure begins with fast

20 Hz firing at arbitrary amplitude for over 5 seconds. This is followed by changing amplitude, irregular firing, and then clonic bursting, but those are clearly after the initial onset. The combination of arbitrary amplitude, ISI, and DC shift is consistent with Saddle Node.

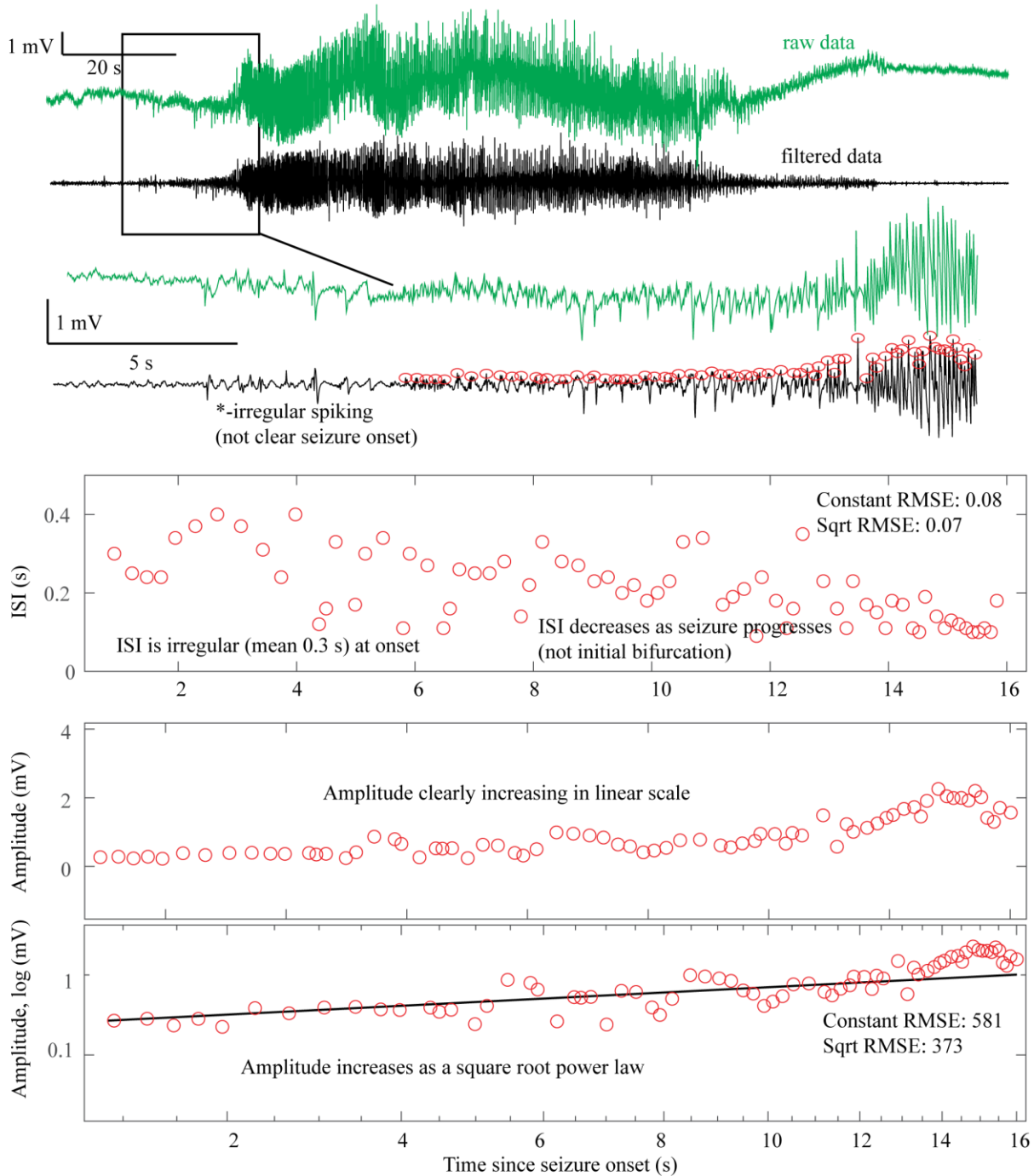


Fig. S1B – Supercritical Hopf Onset. DC-coupled recordings (green, top) do not have a DC shift at onset. The ISI is arbitrary at onset, then after 10 s starts to decrease (middle). This irregular spiking prior to the seizure (\*) is not part of a clear seizure onset, does not conform to any initial bifurcation, and thus was not chosen as the unequivocal seizure onset. The sustained spiking that



begins at 8 seconds, however, follows the SupH dynamics very well. Amplitude shows steady increase in linear scale, which appears as a straight line in loglog plots, consistent with a square root power law (loglog plot). This seizure is most consistent with SupH due to the amplitude scaling.

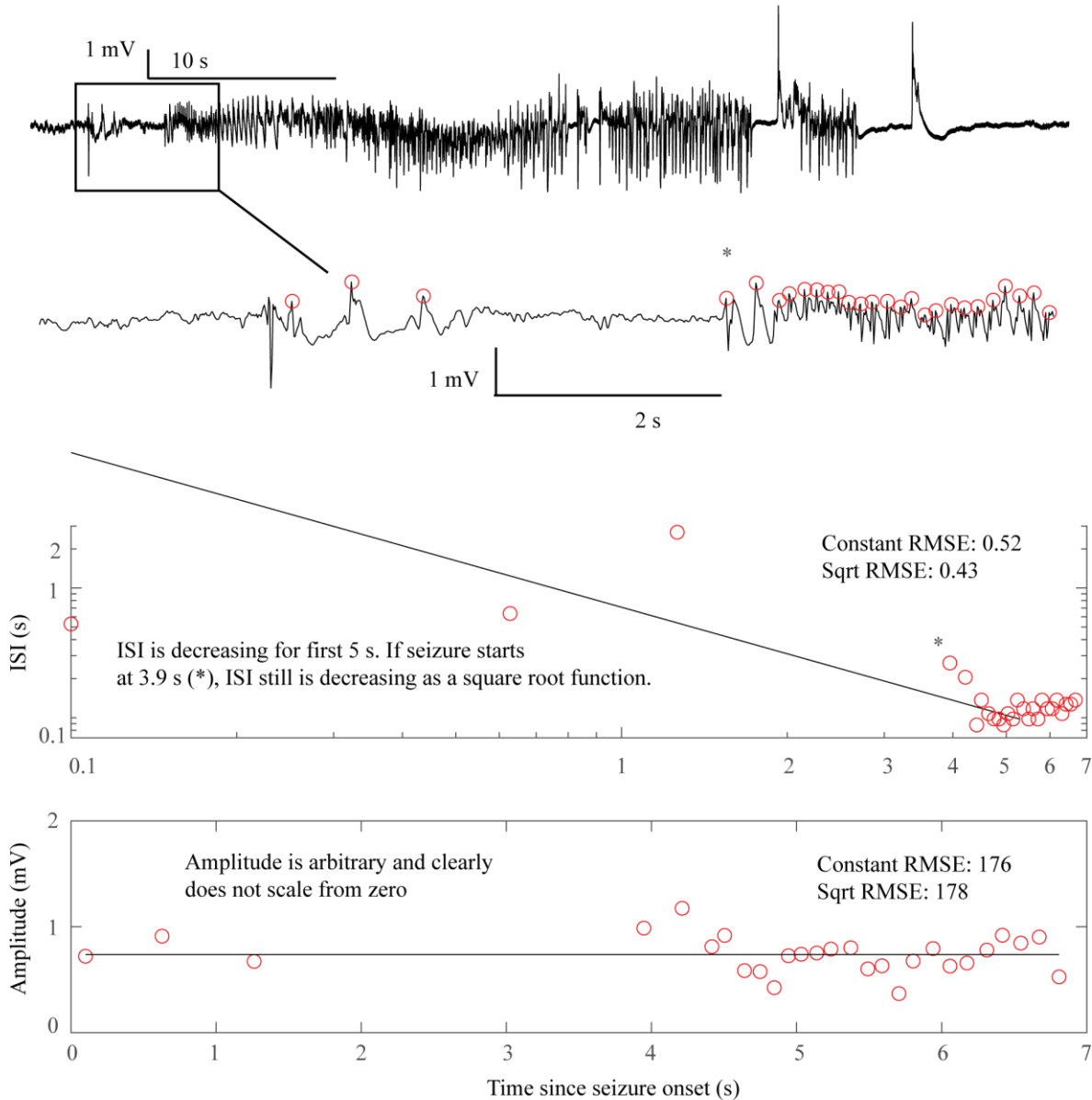


Fig. S1C – **SNIC Onset**. The seizure begins at some point after a sentinel spike. The true starting time of this seizure is debatable, as there are three spike-waves with large ISI and amplitude but they do not persist. At 3.9 s after the sentinel spike (\*) there is a fourth spike wave that leads into the unequivocal seizure onset, with accelerating frequency until 5 s. Whether one chooses  $T=0$  or  $T=3.9$  as the starting time, this seizure clearly starts with high amplitude spike waves that accelerate in frequency, characteristic of the SNIC. Spike wave discharges were present in both

patients that we classified as SNIC, but are not a requirement. In this case, visual inspection was more reliable than fitting equations to make the determination because seizure onset was irregular.

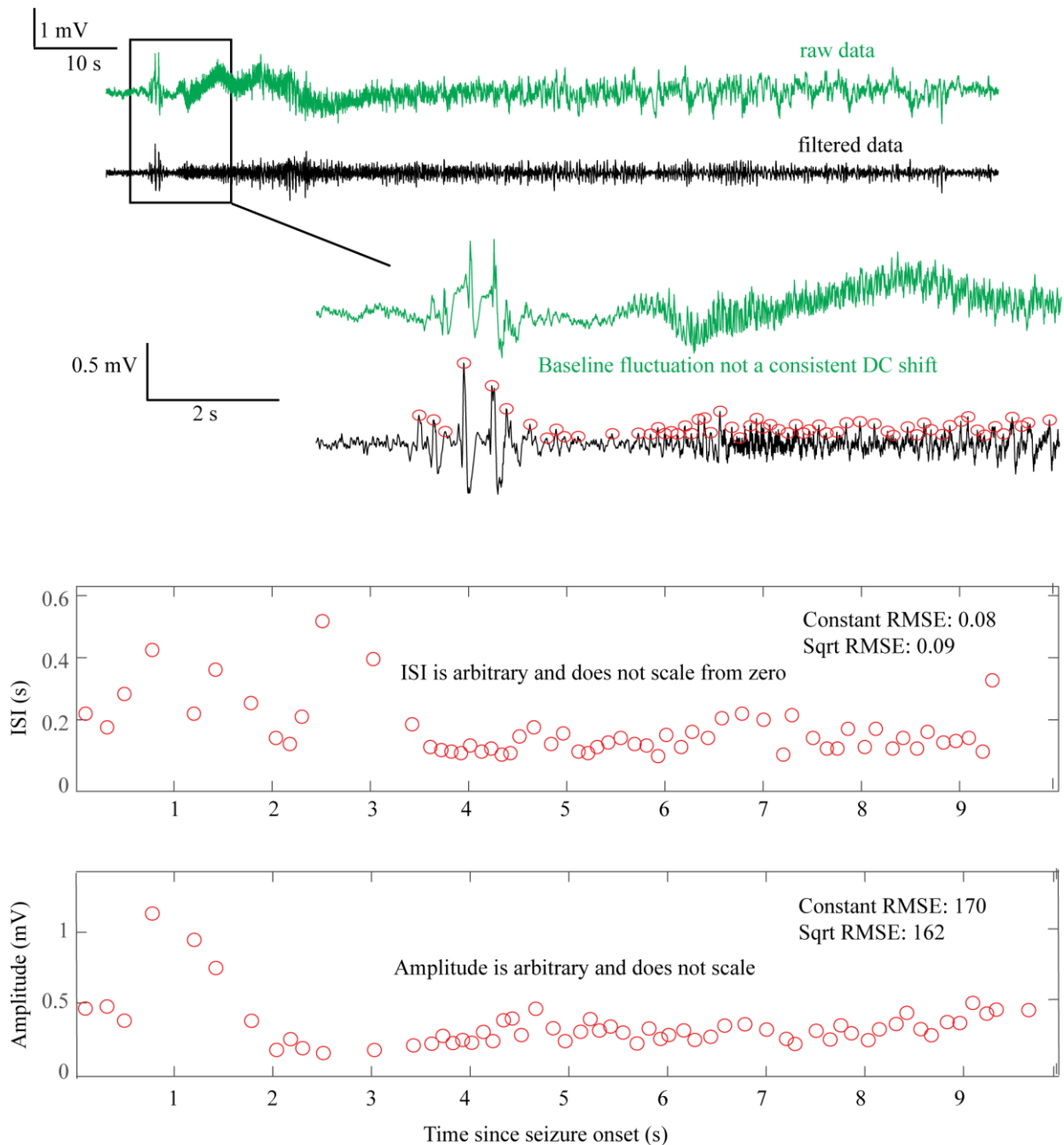


Fig. S1D – Saddle Node or Subcritical Hopf Onset. DC-coupled recordings (green, top) show some baseline fluctuations that are not consistent and too slow to be considered a DC shift. This recording was capable of showing DC, but this patient’s data did not have a clear DC onset. The ISI and amplitudes are both arbitrary and do not scale from zero. This seizure is consistent with either SN or SubH.

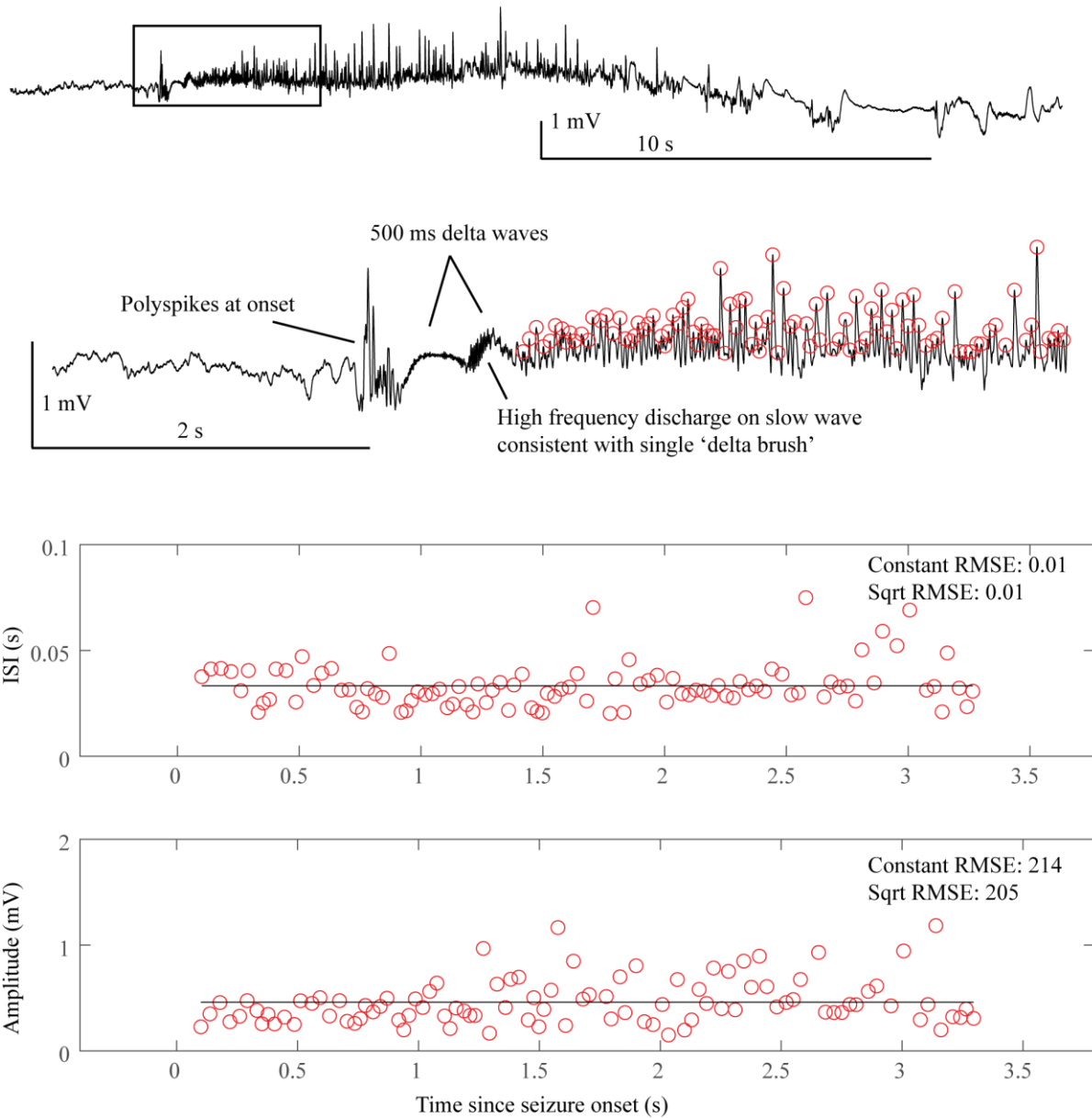


Fig. S1E – SN or SubH onset after delta brush. After a sentinel spike, there is a burst of fast spikes, followed by low voltage fast spikes that lead into an unusual slow wave similar to the “delta brush” pattern. The onset pattern is unusual: there are fast polyspikes with arbitrary amplitude after the sentinel spike, then the delta brush, and it is unclear whether there was a DC shift or a slow wave. These early patterns do not fit with any bifurcation. This seizure was

labeled as SN or SubH due to the arbitrary amplitude and constant ISI, but is an outlier due to unusual pattern. The delta brush pattern was consistent with Perucca type (vii), see Table S5.

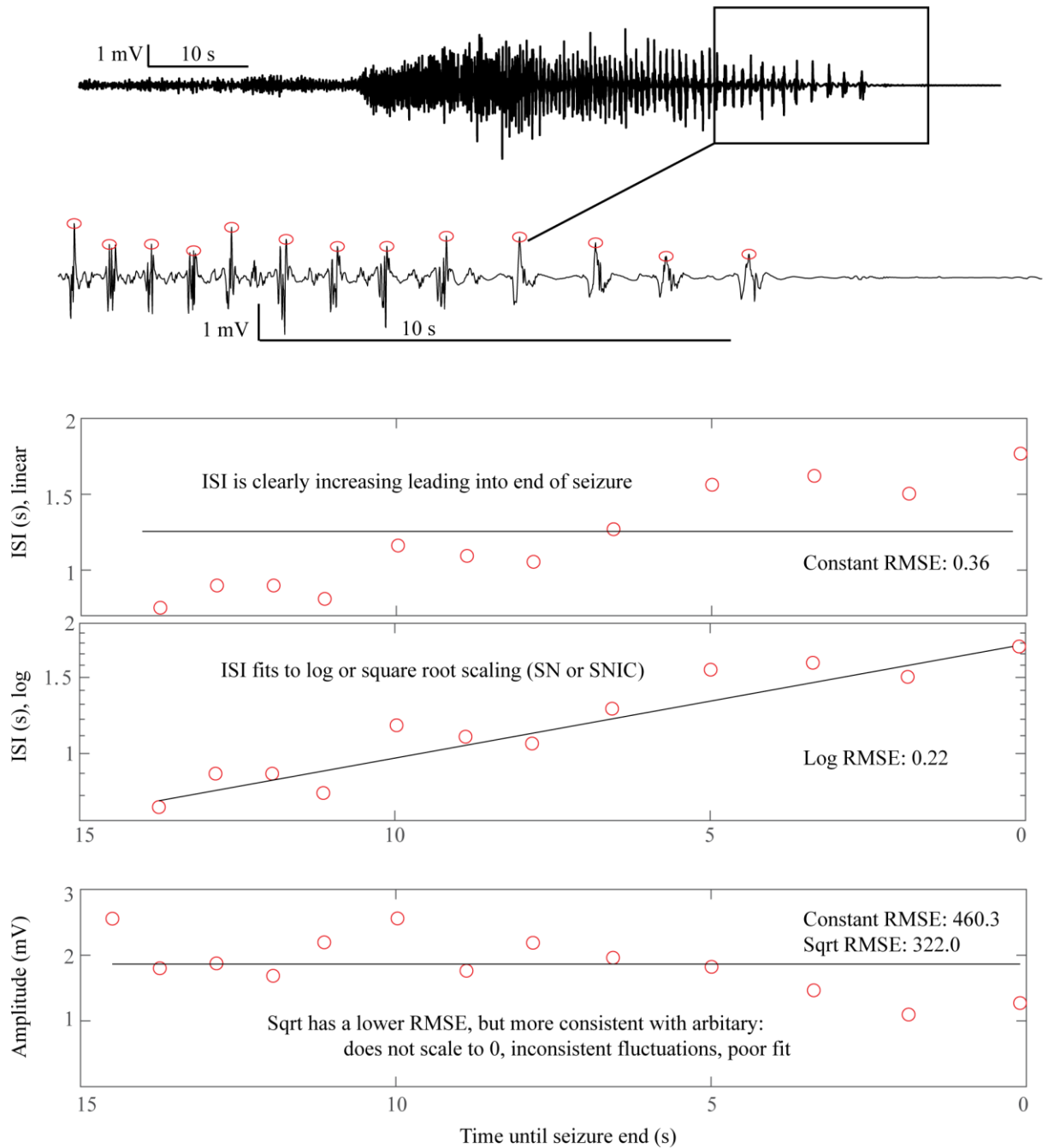


Fig. S1F – Saddle Homoclinic or SNIC offset. In this case the terminal ISI clearly increases as the end approaches and the amplitude of spikes does not scale all the way to zero (top). For visualization, we reverse the spike plots to coincide with the direction of the seizure, but to determine offset  $t = \text{'time until end of seizure'}$ , i.e. it is counting down. Hence the '0' is at the

right of the plots. ISI shows log scaling in 'semilogy' plots, which continues out to 25 s (not shown). The amplitude is somewhat variable but does not diminish to 0. This is consistent with a SH offset. This could also be a SNIC, as a square root function (loglog plot) is very similar at this scale for the ISI (not shown).



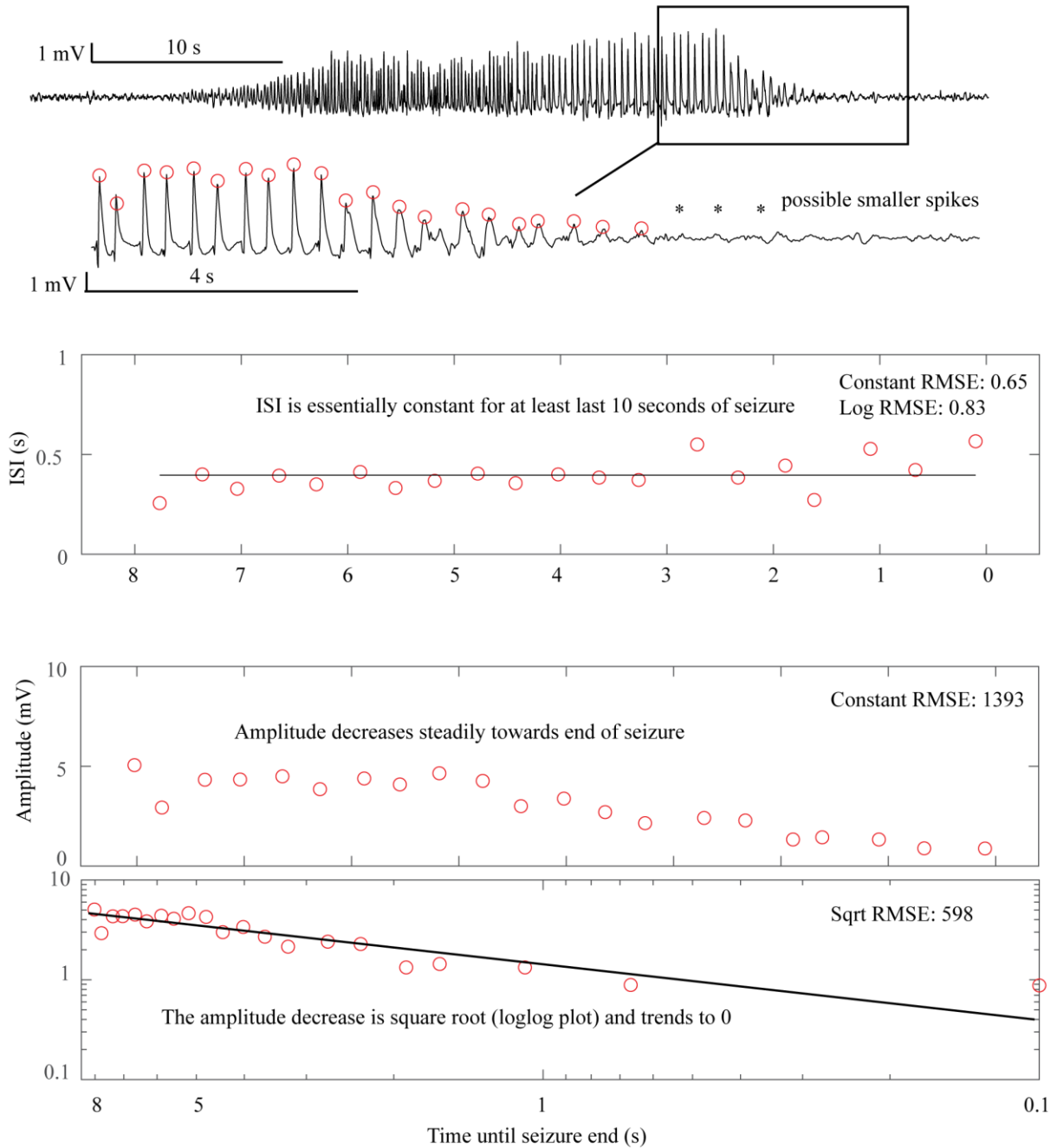


Fig. S1G – Supercritical Hopf offset. Here, the terminal ISI is nearly constant and does not have any “slowing down.” The amplitude, on the other hand, clearly diminishes and trends to zero as a square root power law by the end of the seizure. There are even some potential smaller spikes seen after the seizure (\*), as if the spikes have vanished into the background noise. In this case,

the seizure stops because the amplitude, rather than the frequency, has gone to zero. The constant ISI and diminishing amplitude are indicative of the SupH offset.

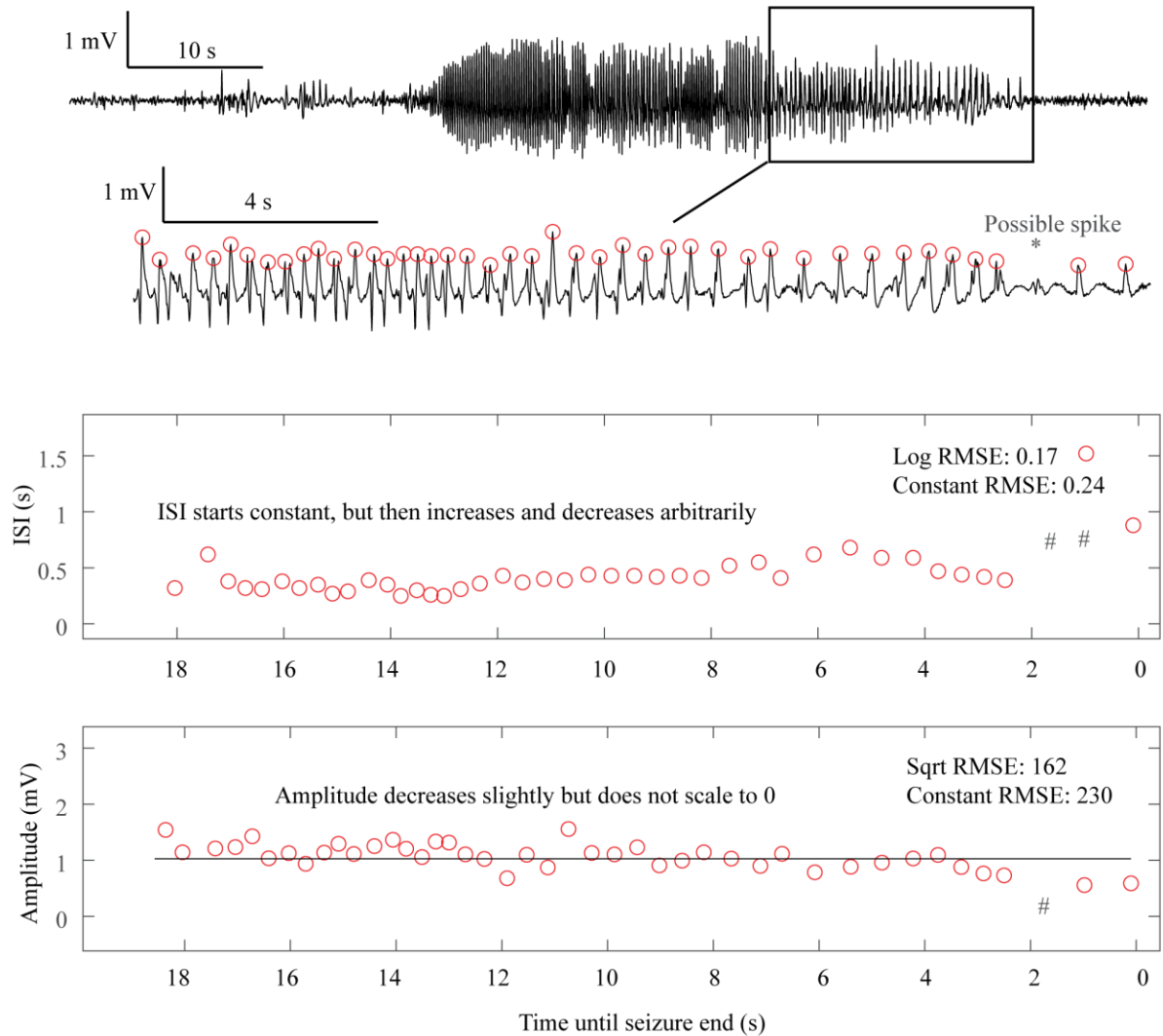


Fig. S1H – Fold Limit Cycle offset. The primary feature of the FLC is the lack of scaling laws. In this case, the ISI is constant until 8 sec prior to the termination, then begins to increase until 6.5 s, then decreases until 2 sec, then increases again. Even if including the one low-amplitude “failed” spike at the \*, the ISI is still arbitrary and does not follow log or square root scaling laws (#- location of ISI if the extra spike is included). The end of the seizure is abrupt. This arbitrary pattern is consistent with FLC offset. Other examples of FLC-terminal seizures are shown in Figs. S1D,E, S2, S9.

### *1.8 Unusual seizure dynamics*

There were rare seizures that contained some unusual dynamical phenomena in the amplitude and ISI. We labeled these as arbitrary, which led to classification as SN or SubH at onset or FLC at offset. However, it is important to reiterate that the vast majority of ‘non-zero scaling’ dynamics were constant values, rather than arbitrary patterns that appear clinically unusual. We have identified several examples of these unexpected patterns that we wish to highlight (1 onset, 4 offsets). For onset, there was a single example in which a delta brush pattern arises at seizure onset after several polyspikes, shown in Fig. S1E. The pattern lasted <1 s then progressed to arbitrary spiking. While this pattern is ‘arbitrary,’ it is very distinct from the other patterns seen with SN-SubH onset. For offset, there were four seizures encompassing a wide range of unusual dynamics. Fig. S2 shows three that were classified as FLC. Each of these tracings is highly irregular for a classical seizure offset, and some might question whether the electrode is truly in the seizure focus or if the seizure was correctly labeled; however, in each case a clinical epileptologist verified that this was indeed the focus and there was clear clinical correlation with these events, ending at seizure offset. These dynamics were not felt to be due to spatial undersampling, as the seizure onset in each case was clearly on the given electrode, and all neighboring electrodes had similar offset dynamics. The fourth offset example had an increasing frequency, and is analyzed in section V (Figs. S9-S11).

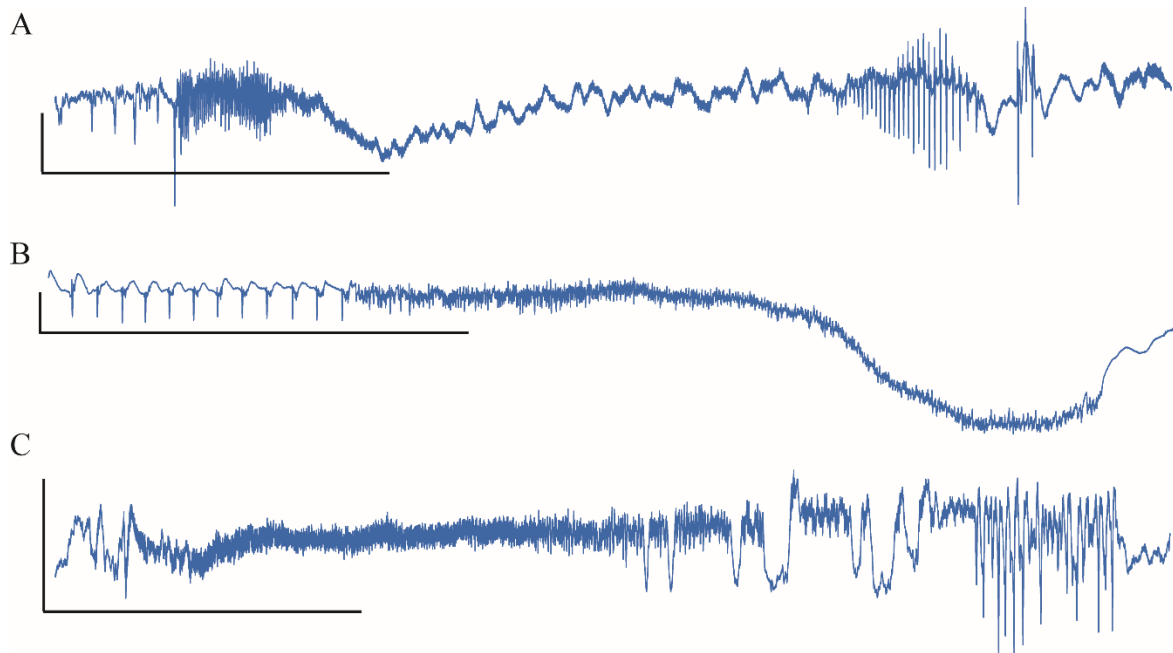


Fig. S2 - Unusual Fold Limit Cycle seizures. Each example is a single electrode from a separate patient, showing the voltage trace at the seizure focus. A: spike amplitude increases at end of seizure. B: abrupt start/stop of low voltage fast activity, without any change in frequency. (Note: the slow downward deflection was too slow to be labeled a DC shift). C: Seizure with low voltage fast that progresses into arbitrary spike waves. Scale bars: 1 mV by 10 sec.

### ***1.9 Patient metadata***

Full clinical metadata were available for 88 of the patients (Table S4). We stratified all patients by their onset and offset bifurcations and evaluated the prevalence of gender, age, pathology, and seizure localization in each case. Due to the vast heterogeneity of electrode locations, all electrodes were stratified into the four main lobes (frontal, occipital, parietal, temporal). Note that not all patients had onset bifurcations available, and some of the rows do not reconcile because some patients had portions of the metadata missing, most commonly the pathology. For simplification and to include all data, all SN and SH were treated as if there were

no DC coupling, and so were grouped with the SubH and SNIC bifurcations as shown. There was a correlation between patient age and onset bifurcation, with a higher proportion of SupH in ages 41-60 ( $p=0.0019$  after Bonferroni correction). There was no significant correlation between any of the bifurcations and pathology, or location (chi-square test). Note that some bifurcations were rare, so even with 88 patients they did not have sufficient numbers to make strong conclusions.

Onset	Sex		Age			Pathology				Location			
	M	F	1-20	21-40	41-60	CD	MTS	T	O	Te	F	Oc	P
SN-SubH	30	23	13	29	10	20	17	1	1	26	12	5	8
SNIC	3	3	4	2	0	2	2	1	1	2	0	0	0
SupH	10	4	2	3	9	2	5	2	0	9	4	2	2
<b>Offset</b>													
SH-SNIC	17	13	5	16	8	10	10	1	1	17	9	2	3
SupH	1	0	0	0	1	0	1	0	0	1	1	0	0
FLC	23	19	12	19	9	14	12	3	1	20	8	5	8

Table S4 – Comparison of bifurcations with metadata. All available patient metadata from all centers are included. CD: cortical dysplasia (including 2 heterotopias). MTS: mesial temporal sclerosis. T: tumor. O: other. F: frontal. Oc: Occipital. P: parietal. Te: temporal.

### *1.10 Comparison with previous classification method*

We also compared our results with a previous classification method (Table S5). The classifications from Perucca et al. (P. Perucca, Dubeau, and Gotman 2014) are as listed: (i) low-voltage fast, (ii) low-frequency high-amplitude periodic spikes, (iii) sharp activity, (iv) spike-and-wave activity, (v) burst of high-amplitude polyspikes, (vi) burst suppression, and (vii) delta brush. Additionally, we created the category (U) to indicate seizure onsets that were not explained by the Perucca classification. In our analysis, we did not find any seizure onsets that corresponded with (vi). There was no significant correlation between the onset types and any of

the patient metadata (chi-square). In addition, we compared these classifications with the onset and offset bifurcations. A chi-squared test was performed on all combinations of Jirsa onset (i.e. based upon bifurcations in (V. Jirsa et al. 2014) ), Jirsa offset, and Perucca onset. There was no significance between any of the pairings. Note that two patients had type (vii) (delta brush, see Fig. S1E), but did not have the expected anti-NMDA receptor encephalitis that was originally described with this pattern (Schmitt et al. 2012).



onset	Sex		Age			Pathology				Location			
	M	F	1-10	21-40	41-60	CD	MTS	T	O	Te	F	Oc	P
i.	15	15	7	10	12	9	10	1	1	18	5	1	5
ii.	9	8	5	8	4	6	6	2	0	7	5	4	3
iii.	13	10	6	14	3	7	8	0	1	13	7	0	4
iv.	3	2	2	3	0	2	2	0	0	3	1	0	1
v.	2	2	2	2	0	1	0	0	1	0	1	2	1
vii.	1	1	0	2	0	0	0	0	0	0	1	0	0
U	5	2	1	5	1	1	2	2	1	6	4	0	0
			Jirsa Onset			Jirsa Offset							
			SN/SubH	SNIC	SupH	SH/SNIC	SupH	FLC					
Perucca Onset	i.		21	2	8	12	0	17					
	ii.		14	2	6	10	0	13					
	iii.		22	1	4	12	1	14					
	iv.		4	1	0	3	0	3					
	v.		3	0	2	1	1	3					
	vii.		2	0	0	0	0	2					
	U		1	0	2	2	0	0					
Jirsa Offset	SH/SNIC		30	3	14								
	SupH		1	1	3								
	FLC		53	3	7								

Table S5 – Comparison of visual with dynamic classifications. Top: Metadata stratified by Perucca classification. There is no clear correlation between Perucca onset type and any of the clinical metadata. Bottom: Comparison of Perucca visual onset classification with our bifurcation analysis. There was no significant correlation between the two classifications. Note that numbers sometimes do not reconcile between different sections and between Tables S4 and S5 due to lack of metadata in some patients.

## II. Construction of the Dynamic Class model and the dynamic map

In this work we used the model in (M. Saggio et al. 2017) and we refer to that paper for details. It consists of three ordinary differential equations:

Equation S1:

$$\begin{aligned}\frac{dx}{dt} &= -y \\ \frac{dy}{dz} &= x^3 - \mu_2(z)x - \mu_1(z) - y(v(z) + x + x^2) \\ \frac{dz}{dt} &= -c(\sqrt{(x - x_S(z))^2 + y^2} - d^*)\end{aligned}$$

The first two of them are based on the normal form of the unfolding of the degenerate Takens-Bogdanov singularity (Dumortier et al. 1991). They depend upon three parameters  $(\mu_2, \mu_1, \nu)$ . We can consider a sphere, with radius  $R$ , centered at the origin in the three-dimensional parameter space. On the spherical surface there are curves of bifurcations that divide the surface into regions with different sets of attractors. It can be shown that, up to a certain value of the radius, the bifurcation diagrams on the spherical surface do not change (Dumortier et al. 1991). For this reason, the number of parameters relevant to describe the bifurcations in the system can be reduced, from the three Cartesian parameters  $(\mu_2, \mu_1, \nu)$  to the two spherical parameters  $(\theta, \varphi)$  keeping the radius fixed. In the present work we use a radius  $R=0.4$ . This reduction allows for easier analysis and visualization of the parameter space. A flat sketch of the spherical surface and its bifurcations can be found in the map in Fig. 4C. A flat projection of the

real map, as shown in Fig. 5, is obtained with Lambert equal area azimuthal projection. Details on how to reconstruct these maps can be found in (M. Saggio et al. 2017). Movement on the sphere is promoted by making the three Cartesian parameters (or the two spherical ones) depending on a third variable,  $z$ , acting on a slower timescale described by the parameter  $0 < c \ll 1$ . Movement is implemented so that, when the fast subsystem  $(x, y)$  is in the resting state  $(x_S, 0)$ , it moves towards the onset bifurcation, and when the distance from the resting state is bigger than  $d^*$  it moves towards the offset bifurcation. When  $d^* > 0$  this gives periodic bursting.

The shape of the path along which the fast subsystem moves is taken to be the arc of the great circle linking the offset point  $\mathbf{A}$  to the onset point  $\mathbf{B}$  on the sphere. It is described by the following parameterization:

Equation S2:

$$\boldsymbol{\mu} = \begin{pmatrix} \mu_2 \\ -\mu_1 \\ \nu \end{pmatrix}$$

$$\boldsymbol{\mu}(z) = R(\mathbf{e} \cos z + \mathbf{f} \sin z)$$

where  $\mathbf{e} = \mathbf{A}/R$  and  $\mathbf{f} = ((\mathbf{A} \times \mathbf{B}) \times \mathbf{A}) / \|(\mathbf{A} \times \mathbf{B}) \times \mathbf{A}\|$ . An example of path for each class is sketched in Fig. 4C with a black arrow.

In this model the dynamics of  $z$  exploit feedback from the fast subsystem. This is possible because the fast subsystem exhibits bistability and hysteresis along the bursting path ('hysteresis-loop bursting' in Izhikevich nomenclature (Izhikevich 2000)). This allows having bursting with one slow variable only. Other possibilities exist, in which the slow subsystem oscillates independently from the fast one ('slow-wave bursting' in Izhikevich nomenclature (Izhikevich

2000)). The hysteresis-loop mechanism is well suited to model the mechanisms leading to seizure termination, which are thought to be triggered by the presence of the seizure itself, as done in (V. Jirsa et al. 2014). For this reason in this work we focus on this type of mechanism for bursting. However, a slow-wave mechanism may be possible and we refer to (M. Saggio et al. 2017) for details on how to obtain slow-wave bursters for all the classes of the taxonomy using the same map.

### *II.1 Definition of onset*

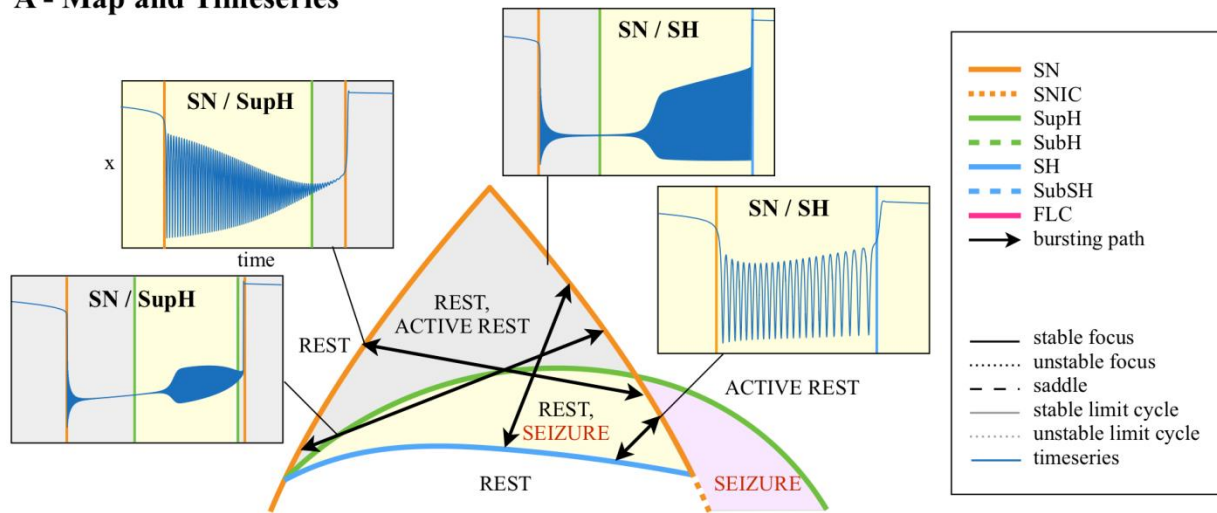
While previous works on the taxonomy define the onset bifurcation as the bifurcation that starts the oscillatory activity (M. Saggio et al. 2017; V. Jirsa et al. 2014; Izhikevich 2000), we here define the onset bifurcation as the first one that destabilizes the resting state (or healthy condition). This affects the classes in which transition to the ‘active rest’ (onset bifurcation with the present definition) precedes the transition to the limit cycle (onset bifurcation with the definition in the literature). This does not change the mechanism or dynamics of seizure initiation, merely the nomenclature. We chose this method because under clinical conditions the “seizure initiation” is defined as the first departure from resting state. We note that this definition, which we used for practical reasons, highlights that the mechanisms triggered by the seizure, such as the inversion in the direction of the slow variable, may be triggered before oscillations are evident. Examples of this effect are shown in the next paragraph, in which we use a different label for two of the classes in (M. Saggio et al. 2017) in which SupH (which started the oscillations) was preceded by SN (which destabilized the resting state): SupH/SH becomes a different realization of SN/SH, and SupH/SupH becomes a different realization of SN/SupH.

## *II.2 Examples of Dynamic Classes*

In Fig. S3 we show bifurcation diagrams for the classes in the bistability region in the upper portion of the map from Fig. 4C. Note that, for all Classes except SN / SH, additional bifurcations (aside from the first and last used in the Dynamic Class name) may be necessary for the Class to exist (to allow the presence of the hysteresis-loop). In particular, all the classes in this portion of the map show a baseline jump, due to the crossing of the SN bifurcation. By our definition, these would be classified as SN onsets. However, in two of the examples shown it is not until the trajectory then crosses the SupH bifurcation that the oscillation begins. These are the conditions which our previous work had classified as SupH onsets, and which we now classify as SN. We based this decision on the fact that our human data showed this precise combination several times, but clinicians always identified the SN as the start of the seizure. The ability to identify a seizure trajectory prior to crossing the oscillatory bifurcation has intriguing implications for future work.

In Fig. S4 we show bifurcation diagrams for the classes in the bistability region in the lower portion of the map. Here classes occur without baseline shifts, even when starting with a SN bifurcation. This makes it impossible to discern SN from SubH onsets based on Fig. 1.

### A - Map and Timeseries



### B - Bifurcation Diagrams

Modified from Saggio, Spiegel et al. 2017, Figure 6.

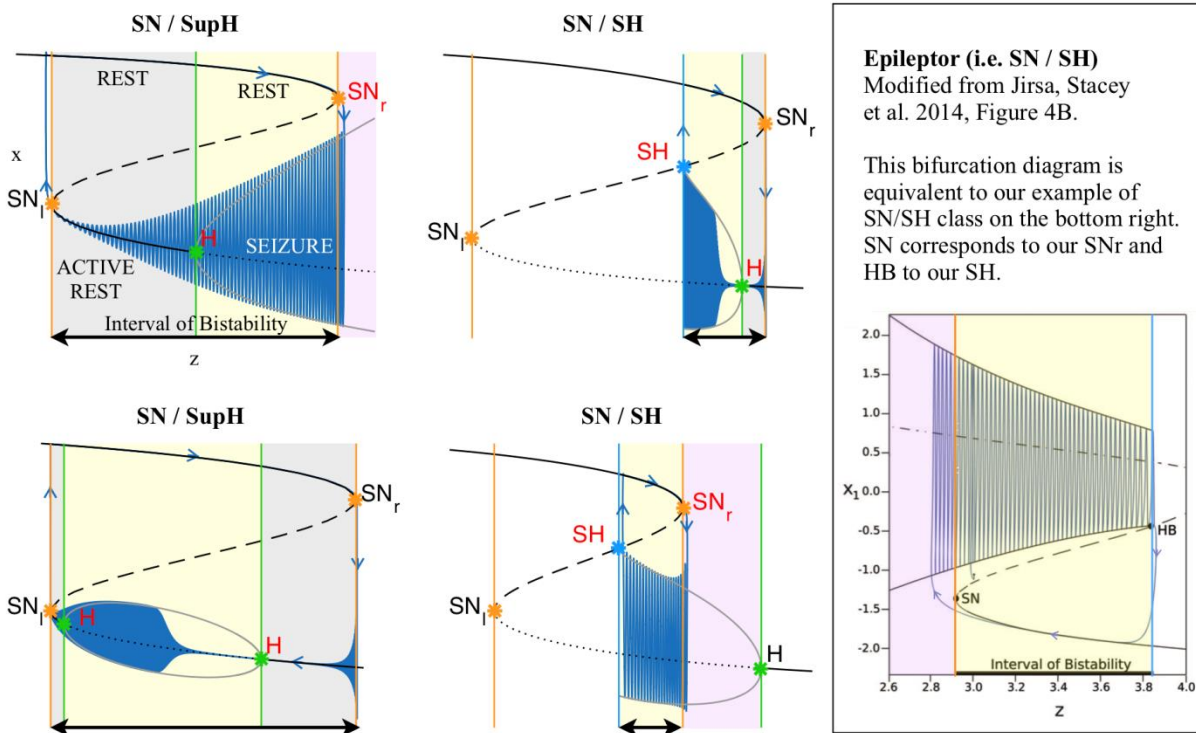
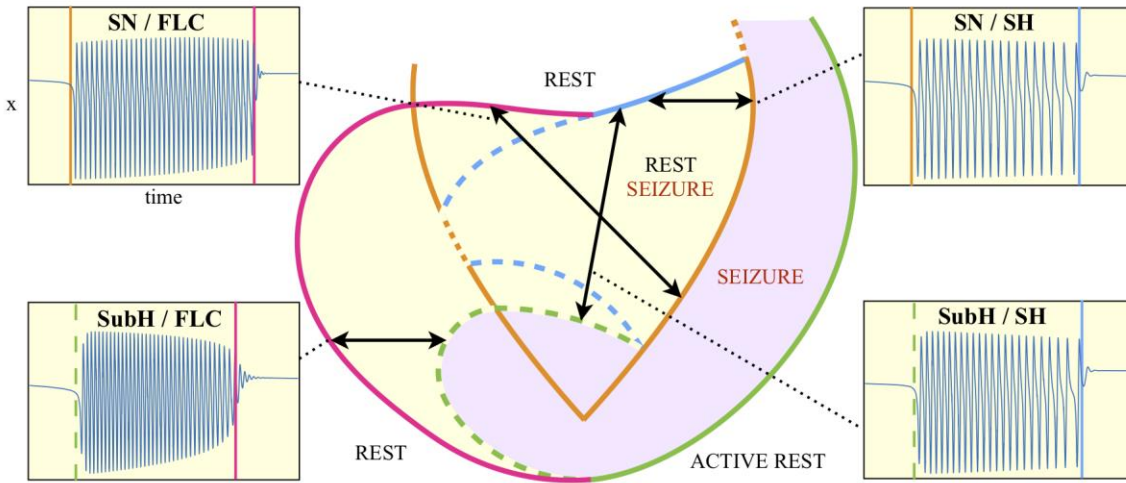


Fig. S3 – Dynamic classes with baseline shift. A: Zoom of the bistability region in the upper part of Figure 4C. In this region, the Dynamic Classes are combinations of SN, SupH, and SH. All begin with a SN bifurcation, which causes a baseline shift. The background of the timeseries is

shaded with the same color of the portion the map traversed. Vertical colored lines mark the value of  $z$  at which bifurcations on the map are crossed. Two of the trajectories (top right, bottom left) do not have sustained oscillations until after crossing the SupH bifurcation a short time after the SN onset. B: Bifurcation diagrams for the same classes. Onset and offset bifurcations for the oscillatory phase are marked with red letters. SNr refers to the SN curve on the right of the map, SNl to the SN at the left. Inset: comparison with the ‘Epileptor’ class from (V. Jirsa et al. 2014).

### A - Map and Timeseries



### B - Bifurcation Diagrams

Modified from Saggio, Spiegler et al. 2017, Figure 7.

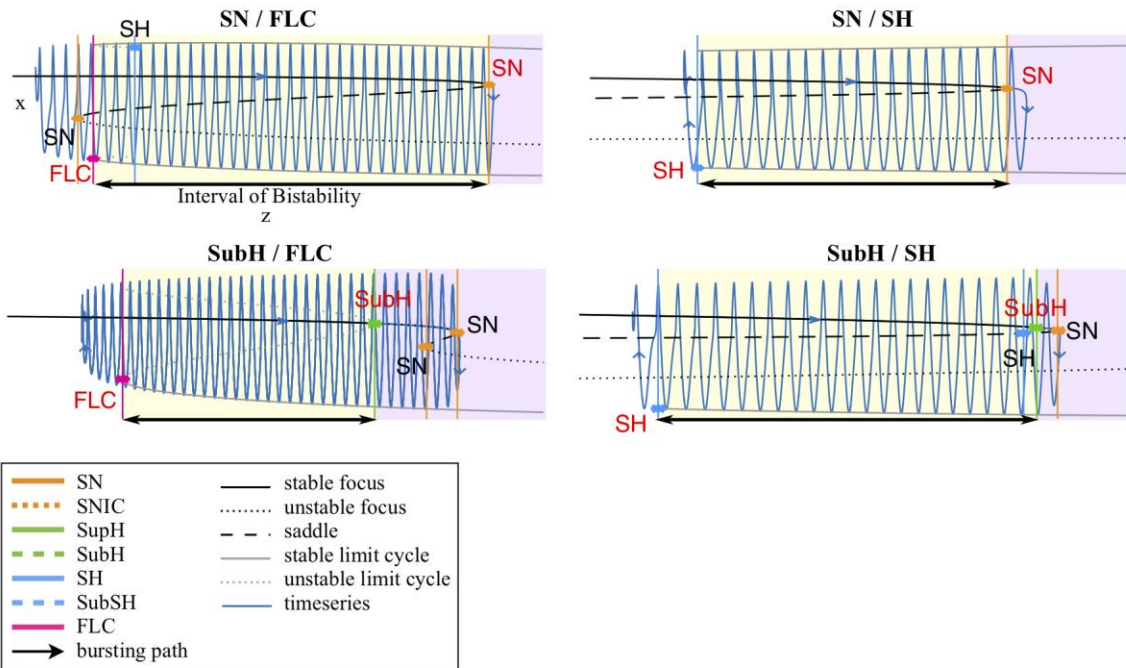


Fig. S4 – Dynamic classes without baseline shift. A: Zoom of the bistability region in the lower part of Figure 4C. For each class possible in this region we show an example of the timeseries. The background of the timeseries is shaded with the same color of the portion the map traversed. Vertical colored lines mark the value of  $z$  at which bifurcations on the map are crossed. B:



Bifurcation diagrams for the same classes. Onset and offset bifurcations are marked with red letters.

### ***II.3 Ranking the complexity of each Dynamic Class***

We can use mathematical arguments to rank the classes according to how complex they are, with more complex classes being more difficult to encounter in models, and potentially also in nature. The first criterion to define the complexity of a class is based on the minimum number of parameters (called ‘codimension’) necessary to describe a map in which a path for this class can be placed (see (Golubitsky, Josic, and Kaper 2001), in which this criterion is introduced, for a more mathematical definition). We base this analysis on the hysteresis loop classes proposed in (M. Saggio et al. 2017) , and which are illustrated in Fig. 4, S3, S4. The basis of the dynamic trajectory (or ‘bursting path’) of this seizure model is that, once the seizure begins, there is a feedback mechanism in which the slow permittivity variable tends to terminate the seizure. Using this seizure mechanism, the least complex class is SubH/FLC, which requires a codimension of two. Following that are SN/SH, SN/SupH, SN/FLC, SupH/SH, SupH/SupH and SubH/SH. These classes require a codimension three, which is the basis for our current model (M. Saggio et al. 2017). In Fig. 4C of the main paper we show a representation of this map that is two-dimensional for more readability, but the map is in fact lying on a spherical surface in a three-parameter space (Fig. 4B). The other classes of the taxonomy require higher codimensions (M. Saggio et al. 2017). We can further rank classes with the same codimension based on how many bifurcation curves their paths must cross on the map 5 . For example, Class SN/SH (two curves to cross) is less complex than the other codimension three classes (3 or more curves to cross).

In Figure S5 we show the classes' ranking superimposed with results from our classification of human seizures (adapted from Fig. 2F). In the clinical data (DC recordings only), the most common classes are SN/FLC, SN/SH and possibly SubH/FLC and SubH/SH, which have low complexity (complexity 2 and 3). However, it is worth recalling that classes with FLC offset may be overestimated due to noise. Thus, the clinical data are consistent with the predicted complexity. Interestingly, though not assessed in this work, absence seizures may be best described with the most common SubH/FLC, which can be found in the lower bistability region of the map (see Discussion). Note that the number of seizures in each class is based upon our method of identifying the first bifurcation, while the complexity is based upon the initiation of the limit cycle (M. Saggio et al. 2017). Reconciling these methods would likely result in some of the SN onset seizures being reclassified as SupH. Additionally, it should be noted that this complexity refers only to seizures that are produced by the hysteresis mechanism. Other plausible mechanisms are independent changes in the permittivity variable and fluctuations due to noise, both of which can produce seizures with different codimensions/complexity than those shown here.

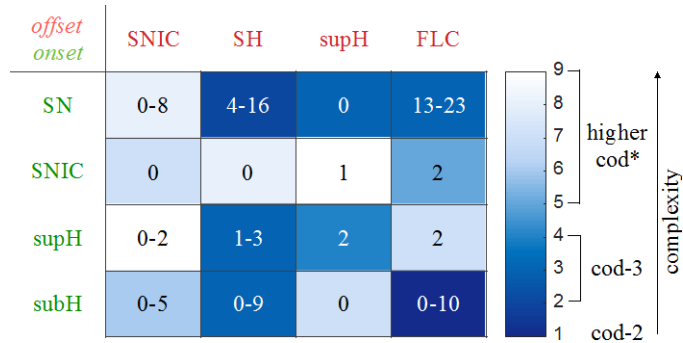


Fig. S5 – Complexity of classes and data classification results. The complexity of the 16 Dynamic Classes is shown, with darker colors being the least complex. Superimposed on that are the number of seizures from Fig. 2 E-F in each Class. Note that some of the seizures could not be distinguished between SH and SNIC offsets, or between SN (no DC shift) and SubH, so for these classes there is a range. \*-The codimension of some of these classes is presumed, see (M. Saggio et al. 2017) for details.

#### ***II.4 Modeling noise-driven or bifurcation-driven transitions***

When  $d^* > 0$  this model produces periodic bursting, while  $d^* = 0$  gives no bursting at all since the whole system would be in a fixed point. In the presence of noise, we have periodic bursting if the variance of the noise is smaller than  $d^* > 0$ . However, by setting a  $d^*$  value close to the noise variance, and initial conditions for  $z$  within the bistability region, we have a different scenario. In this case a seizure can be initiated if noise is strong enough to bring the system beyond the separatrix (i.e. outside the domain of attraction of the fixed point and within the domain of attraction of the limit cycle). Noise-induced transitions like this one have been

proposed as a mechanism to initiate a seizure (Fernando H. Lopes da Silva et al. 2003).

However, in our model, once the fast subsystem has left the fixed point of the fast variables, the whole system is no longer in a fixed point and the slow variable will activate to bring to seizure offset. Setting  $d^*$  close to the noise variance thus allows a mixed scenario in which the onset is noise-driven (with the transition to seizure being more likely the closer the system is to the bifurcation) and offset is determined by a deterministic slow variable. Noise-driven transitions require the presence of bistability. The probability of having such a transition increases when approaching the bifurcation point, which gives origin to this bistability, from within the bistability region, since the separatrix gets closer to the resting state. In the presence of noise this mechanism can contribute to seizure onset. Noise-driven transitions lack any scaling law.

However, the only two bifurcations here that allow for noise-driven transition in their proximity (because they feature bistability) are SN and SubH, which also lack any scaling law. This implies that, if noise-induced transitions rather than bifurcations are causing seizure onset in any seizure in our dataset, these seizures would be classified under the ‘SN or SubH’ label. As our analysis already classifies “noisy” events as being “arbitrary” and thus either SN or SubH, our classification system already accounts for this potential discrepancy.

### ***II.5 Biophysical meaning of the variables***

As discussed in the main text, we use a bursting model as a phenomenological model for seizure generation and termination. This implies that the variables of the model do not have any explicit biophysical meaning. While we can make considerations, based on the timescales at which they operate, on which class of biophysical processes are best candidates to be represented within a given variable (e.g. neuroelectric processes for the fast variables, neurochemical

substances for the slow ones), the biophysical meaning of the variables may depend on the specific type of epilepsy or even on the specific patient.

One strategy to identify the correlates of the model variables could be to rely on the comparison with more realistic biological models. Our phenomenological model is based on the unfolding of the degenerate Takens-Bogdanov singularity. This singularity appears to be quite common both in neural models (Kirst et al. 2015) and in neural population models, such as the Jansen-Rit or the Wendling-Chauvel models (Touboul et al. 2011). When this singularity exists, the bifurcation diagram in its surroundings is equivalent to the one shown in our model. This allows us to produce a mapping between the variables and parameters of the models in which this singularity can be found and those of the phenomenological model in (M. Saggio et al. 2017). Applications of this model, however, do not necessarily depend on the understanding of the biophysical correlates of its variables. This is true for the investigation of the synchronization and propagation patterns linked to each Dynamic Class—the dynamic phenomena are invariants and do not depend upon the specific physiological parameters.

However, there is clearly great utility in determining how specific physiological parameters can be related to this model, specifically for the application of designing methods to stop or prevent seizures by acting upon the slow and ultra-slow variables. In particular, it will be important in future work to model the effect of stimulation on specific Dynamic Classes. In this case, an external current applied to the fast subsystem will modify the additive term  $\mu_1$ .

## *II.6 Limitations of the model*

Planar bifurcations. One limitation of the present study is that it considers only planar (i.e. two variables) bifurcations as possible onset or offset mechanisms. When considering higher dimensional systems, additional offset bifurcations exist, while the possible onsets are unchanged (Dumortier et al. 1991). However, the exact number of additional bifurcations is unknown (Kuznetsov 2004).

Planar bifurcations are used to organize the bifurcation diagrams of many neural populations or field models for seizures, even high dimensional ones (Touboul et al. 2011; Breakspear et al. 2006; Marten et al. 2009; Meijer et al. 2015; Taylor et al. 2013). Phenomenological models in the literature are planar or have planar fast subsystems (V. Jirsa et al. 2014; Hutchings et al. 2015; Kalitzin, Velis, and Lopes 2010; Sinha et al. 2017; Terry, Benjamin, and Richardson 2012). The presence of additional variables, acting on a different timescale (still fast as compared to the slow permittivity variable  $z$  of the present paper), are used to create spike and wave discharges (V. Jirsa et al. 2014; Marten et al. 2009; Y. Wang et al. 2012). In these cases, non-planar bifurcations may appear in the model, such as period doubling of limit cycles (Marten et al. 2009), but they are not used to start or stop a seizure, but rather to change the number of spikes riding on the wave. This does not affect the present work, which instead focuses solely on the onset/offset dynamics. We cannot exclude the possibility of non-planar bifurcations playing a role in seizure offset, but with current knowledge and available data it may not be possible to distinguish them from planar bifurcations. Using a planar system also excludes the possible role of low dimensional chaos in seizure generation (Iasemidis et al. 1994).

Bursting with higher dimensional fast subsystems. Our model is built upon the minimum number of dimensions necessary to produce the bursting behavior. Obviously, more complex models could also generate similar activity with different bifurcations (Izhikevich 2000; Kuznetsov 2004). Among those known, some are characterized by non-zero frequency at the bifurcation point: the subcritical flip of limit cycles (or period doubling), subcritical Neimark-Sacker, FLC on a homoclinic torus and Blue-sky bifurcations. Other have zero-frequency at the bifurcation point: Saddle Focus Homoclinic and Focus Focus Homoclinic. The latter requires at least a four-dimensional fast subsystem. In addition, planar bifurcations may display additional features when they occur in higher dimensions, such as baseline jumps in a FLC.

Other mechanisms of dynamic trajectories. As stated previously, our model assumes a hysteresis in the seizure trajectory, in which the slow variable acts to pull the system out of a seizure once it starts. There are other methods of starting seizures, such as independent changes of the slow permittivity variable causing a crossing of the bifurcation, which will be the subject of future work.

### ***III. Switching between Dynamic Classes due to fluctuations and ultra-slow modulations***

In the model above, the path along which the fast subsystem slowly moves is a simple arc linking the offset and onset points. However, movements promoted by real changes of parameters can be more complex. As a proof of concept of the effects that this can have on the system, we considered modifications of the path due to (i) ultra-slow drifting of the offset and onset points **A** and **B** and (ii) fluctuations produced by noise.

The ultra-slow drift was obtained as in (M. Saggio et al. 2017). The offset point moves along an arc of great circle linking the initial offset  $\mathbf{A}_1$  to the final offset  $\mathbf{A}_2$  with velocity  $c_A \ll c$ . This movement is promoted by an ultra-slow variable  $u$ . Analogously for the onset point  $\mathbf{B}$ , from  $\mathbf{B}_1$  to  $\mathbf{B}_2$  with velocity  $c_A \ll c$ , movement is promoted by the ultra-slow variable  $w$ . The equations are:

$$\frac{du}{dt} = c_A$$

$$\frac{dw}{dt} = c_B$$

$$\mathbf{A} = \mathbf{A}(u) = R(\mathbf{g} \cos u + \mathbf{h} \sin u)$$

$$\mathbf{B} = \mathbf{B}(w) = R(\mathbf{l} \cos w + \mathbf{m} \sin w)$$

where  $\mathbf{g} = \mathbf{A}_1/R$ ,  $\mathbf{h} = ((\mathbf{A}_1 \times \mathbf{A}_2) \times \mathbf{A}_1)/\|(\mathbf{A}_1 \times \mathbf{A}_2) \times \mathbf{A}_1\|$ ,  $\mathbf{l} = \mathbf{B}_1/R$  and  $\mathbf{m} = ((\mathbf{B}_1 \times \mathbf{B}_2) \times \mathbf{B}_1)/\|(\mathbf{B}_1 \times \mathbf{B}_2) \times \mathbf{B}_1\|$ .

Depending on the location on the map of the points  $\mathbf{A}_1$ ,  $\mathbf{A}_2$ ,  $\mathbf{B}_1$  and  $\mathbf{B}_2$ , this type of drift can cause the system to produce seizures of different classes in different moments, which is consistent with the results of our longitudinal analysis. The addition of noise fluctuations can potentially alter the trajectory of the seizure while the seizure is ongoing, which might explain some of the unusual seizures identified in the data, such as in Fig. 5. For example, to obtain transitions between the SN / SupH class and a class with SH offset (Fig. 5A), we simulated a



seizure that began on a path for SN / SupH slowly drifting downwards towards a path for SN / SH. The two paths lie very close on the map. We then added normally distributed noise, which allowed the system to deflect off its normal trajectory. This noise then allowed to get close to different bifurcations within a single seizure. Transitions of the type observed in data (which is a subcase of class SN / SH) were observed in 10 of the 100 simulations we ran with the same settings. The other simulations produced mostly SN / SH seizures (43/100) and some SN / SupH (8/100), other forms of transitions within seizures and 12 examples of status epilepticus in which the system entered a long seizing state that did not resolve by the end of the simulation. When more than one seizure occurred in the same simulation we classified only the first unless otherwise stated. Seizures were classified by determining the onset and offset bifurcations crossed by the path, rather than by analyzing the frequency/amplitude profile of the time series.

Of course, these rates of occurrence of classes are not meant to reflect real rates in data, since parameters for the simulations were carefully chosen to obtain the specific transition within seizure observed in data. However, since simulation settings were the same for the 100 trials, these results show that fluctuations can easily cause different classes to occur when these classes are close on the map.

Integration settings for Fig. 5 B-C: Euler-Meruyama method; integration step 0.002 s; simulation length 10000 s; initial conditions were set to 0 for all variables; noise variance was 0.005 for fast variables, 0.0005 for the slow variable and 0.002 for ultra-slow variables. Model parameter settings:  $c = 0.002$ ;  $c_A = 0.00005$ ;  $c_B = 0.000005$ ;  $d^* = 0.3$ ;  $R = 0.4$ ;  $\mathbf{A}_1 = (0.2731, -0.05494, 0.287)$ ;  $\mathbf{B}_1 = (0.3331, 0.074, 0.2087)$ ;  $\mathbf{A}_2 = (0.3524, 0.05646, 0.1806)$ ;  $\mathbf{B}_2 =$

(0.3496,0.07955,0.1774). The procedure to compute the amplitude and frequency of the limit cycle across the map, as shown in Fig. 5 H-I, is the same as in (M. Saggio et al. 2017).

#### ***IV. Analysis and simulation of status epilepticus***

In 44 out of the 100 simulations we ran in the previous section, after generating one or more seizures the system escaped from the bistability region to be trapped in the ‘seizure only region’. Activity in this region of the map is analogous to status epilepticus. The dynamic map allows us to analyze how this transition occurred. In 11 cases this escape occurred when the imposed ultraslow drift caused the system to cross the SH curve at the lower border of the upper bistability region and then enter the ‘seizure only’ region through the SN bifurcation. In the remaining 33 cases, instead, the system escaped the bistability region directly through the SN curve, thus before the downward ultra-slow drift could play a role in the escape. Our simulations show an example of each scenario (Fig. S6). To assess the role of noise in this phenomenon, we ran five simulations for each of several levels of noise variance. Decreasing the noise variance scaling factor  $a$  from 0.0005 to 0.0002 diminished the number of times the system ended up in status epilepticus, from 3/5 to 1/5, then to 0/5 for  $a = 0.0001$  and below. One of the status epilepticus obtained with  $a = 0.0005$  is shown in Fig. 5. These results indicate that high levels of noise variance can contribute to the system being trapped in the seizure only regime.

Integration settings: Euler-Meruyama method; integration step 0.002 s; simulation length 10000 s; initial conditions were set to 0 for all variables; noise variance was  $a * (10$  for fast variables, 1 for the slow variable, 5 for ultra-slow variables). Tested values of  $a$  were: 0.0005, 0.0002, 0.0001, 0.00005. Model parameter settings:  $c = 0.0001$ ;  $c_A = c_B =$

0;  $d^* = 0.3$ ;  $R = 0.4$ ;  $\mathbf{A}_1 = (0.3483, 0.03698, 0.1931)$ ;  $\mathbf{B}_1 = (0.3331, 0.074, 0.2087)$ ;  $\mathbf{A}_2 = \mathbf{B}_2 = (0.279, 0.2187, 0.1854)$ .

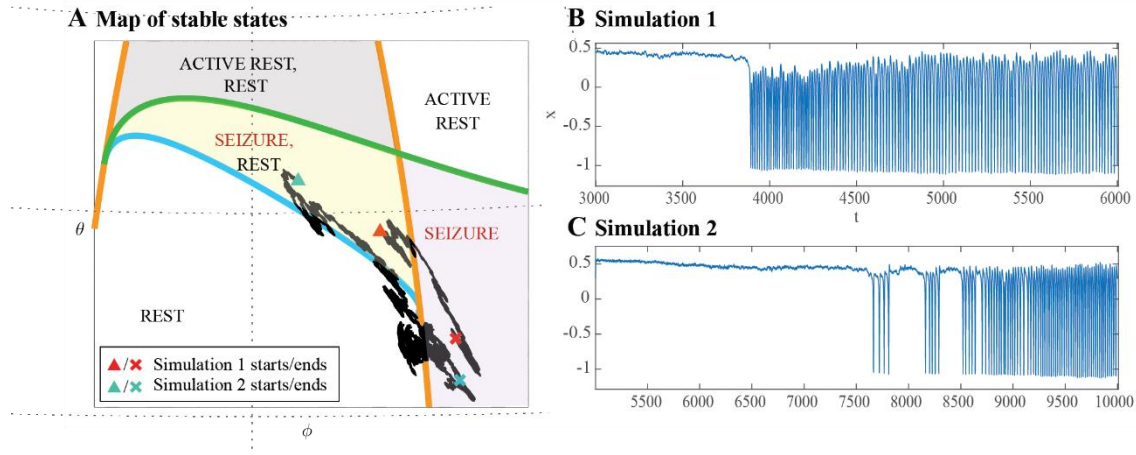


Fig. S6 – Escape from the bistability region into the seizure-only region. A: In some of the simulations performed with an ultra-slow downward drift and noise, the system escaped from the bistability region (yellow) into the seizure-only region (lavender). The escape could occur directly through SN (orange curve), as in Simulation 1, or passing below SH (blue curve) and then through SN, as in Simulation 2. B-C: Time series for Simulation 1 and 2. The clinical relevance of this is to illustrate how some episodes of status epilepticus might arise uniformly (B) while others have a stuttering onset (C).

These findings are very similar to examples from the clinical cohort. Two of the patients had unrecognized episodes of nonconvulsive status epilepticus lasting over 2 hours during sleep (see Fig. 5). We analyzed these seizures in the same manner as the others. One began with a brief seizure very similar to the most common SN/SH Class (though this was not DC-coupled, so the onset could potentially be SubH, and the offset SNIC). However, instead of terminating, it then transitioned through a SupH into irregular firing. The second example started with SupH

and went immediately into irregular firing. After each seizure started, there were numerous transition periods in which the seizure changed dynamics. The first patient had long periods of arbitrary amplitude and ISI, which occasionally organized into a brief SN-SubH/SH pattern before reverting to the disorganized firing (Fig. S7). In this patient, the seizure lasted over 24 hours, but the final offset could not be determined due to poor signal quality. In the second patient, there were prolonged periods of primarily constant ISI and amplitude, interspersed with brief periods of arbitrary firing, and the seizure finally ended with a SupH (Fig. S8). There were also several unusual periods in which the ISI became uniform for several seconds. During these periods there was nearly perfect  $\sim 7$  Hz spike wave discharges with constant amplitude, which were much more periodic than typical seizures. In both of these examples, the dynamical behavior is entirely consistent with the model: the seizure repeatedly approaches an offset bifurcation then returns to the seizure regime with disorganized (i.e. noisy) firing. This offset was SH in our simulations due to the chosen parameters, but can also be SupH under different conditions as it resides in the same bistability region, e.g. if the seizure started in the top of the region.

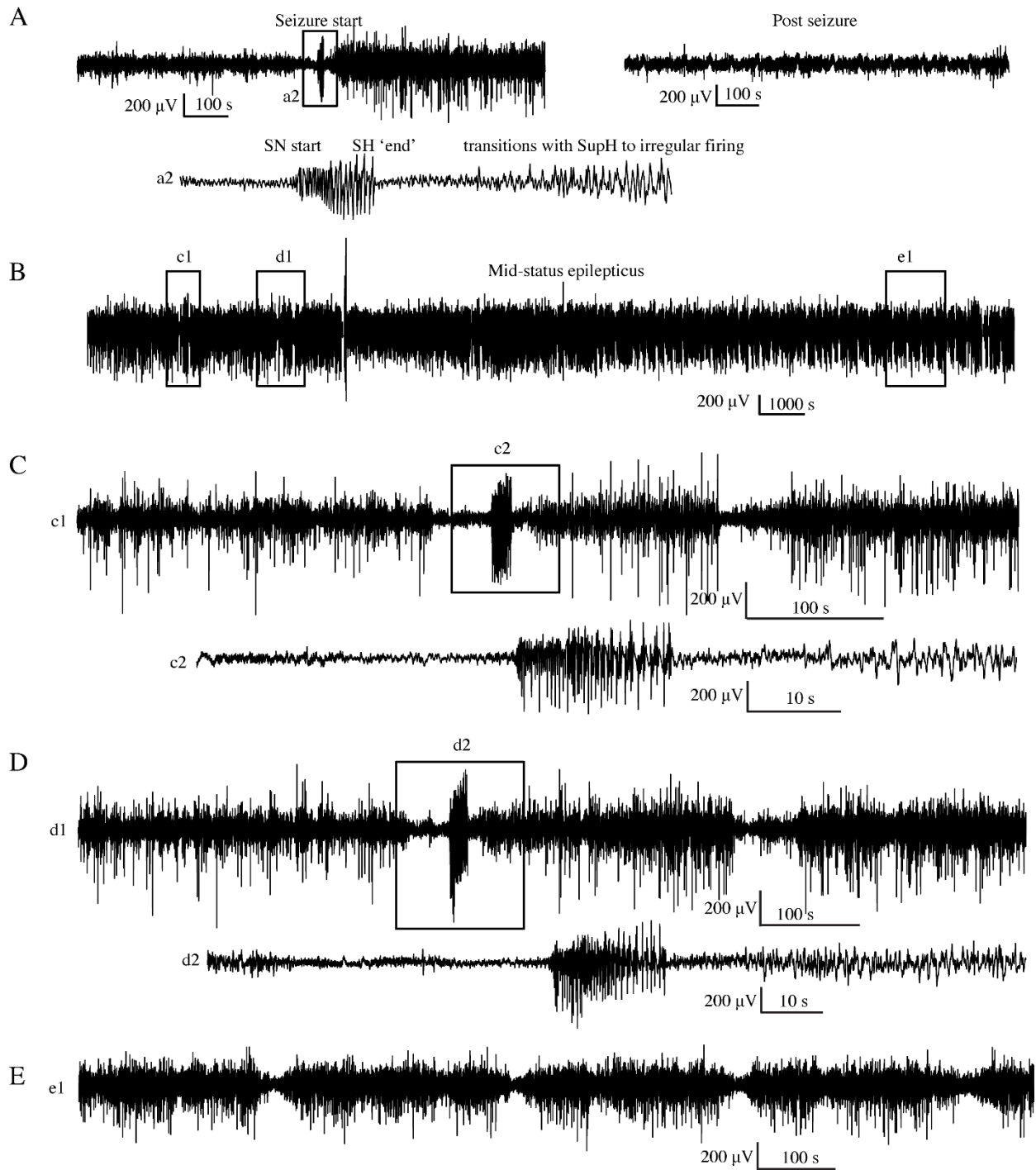


Fig. S7 – Status Epilepticus patient 1. A: Initiation (left) of seizure that begins to terminate with a SH/SNIC bifurcation, then transitions into a SupH onset. The post-seizure baseline (right) returns to prior levels. The seizure lasted > 24 hours, but due to signal dropout the exact time of termination was not recorded. Inset a2: expanded view of indicated portion of seizure start. B:

Subclinical status epilepticus was characterized by irregular firing interspersed with periods of organized, lower amplitude EEG. C, D: Expanded view of (c1, d1) from B, with further expansion of (c2, d2). The irregular firing organizes several times into discrete seizures that nearly terminate with SH dynamics, but revert to the previous pattern. E: Later in the seizure, there is waxing/waning of the firing pattern, similar to Fig. 5 D-F.

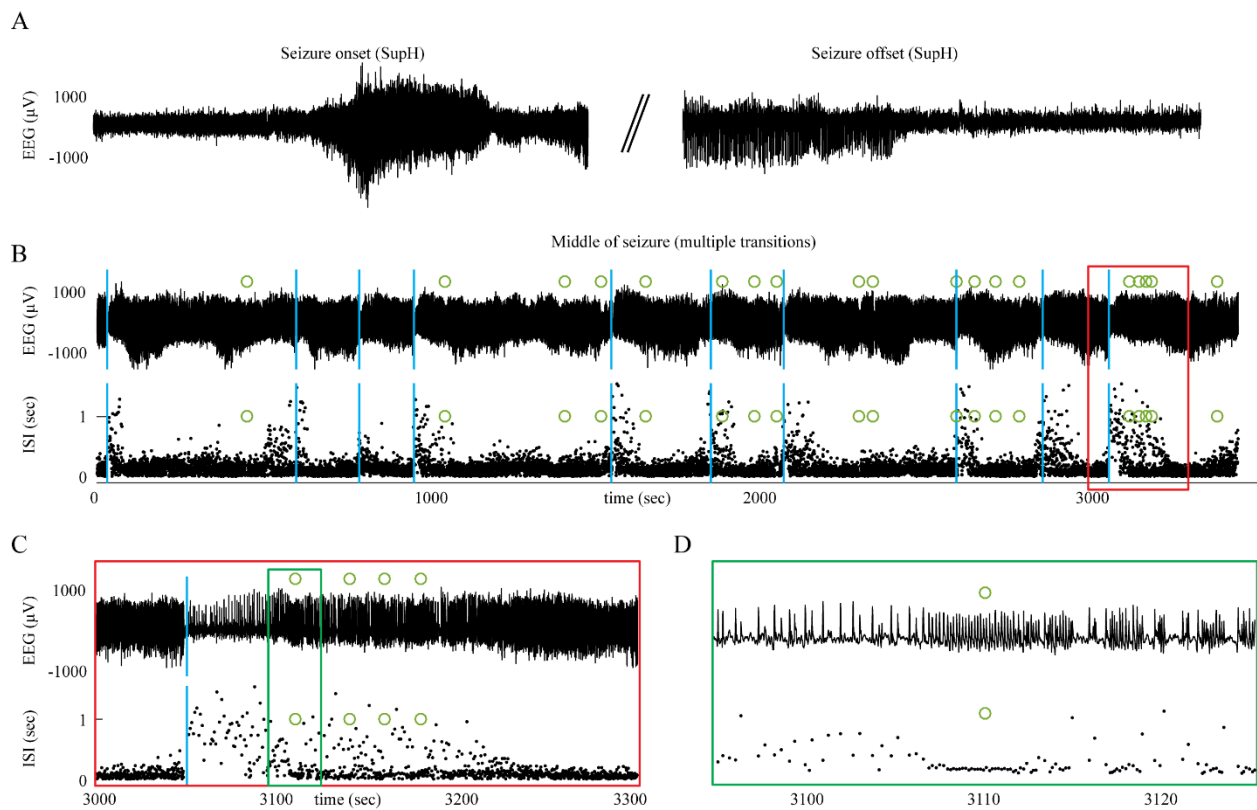


Fig. S8 – Status Epilepticus patient 2. A: Onset and offset of a seizure lasting 5 hours were both SupH bifurcations. B: During the seizure, there were many transitions in which the dynamics altered. Top: voltage trace. Bottom: interspike intervals (ISI) show multiple periods in which

nearly-constant ISI is interrupted by disorganized firing. Blue lines indicate these transition periods. C: expanded view of red box in B. D: Expanded view of green box in C. Green circles indicate runs of highly periodic, 7 Hz spike waves, which became more frequent later in seizure.

### ***V. Example of accelerating frequency at seizure offset***

One of the seizures we classified as FLC in figure 2E had increasing frequency towards the end, shown in Fig. S9. The best fit to the ISI for this seizure was a reversed power law scaling. While acceleration at the end of a seizure is peculiar from the clinical point of view, it fits with both FLC and SupH bifurcations, which do not have specific scaling laws for the behavior of the frequency. As the amplitude of this seizure was arbitrary (rather than decreasing with square root), it is most consistent with the FLC. We analyze it here to show how different frequency behaviors can be obtained in the model.

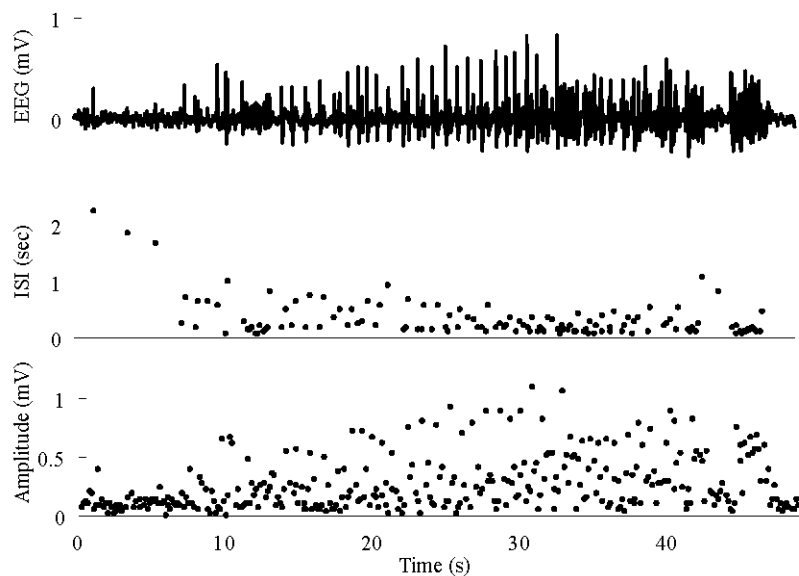


Fig. S9 – Seizure with acceleration of spike frequency at seizure terminus. In this case, the ISI progressively decreases and follows a reverse power law. The amplitude is arbitrary. This seizure was labeled as a FLC bifurcation for taxonomical purposes as it did not fit with any other single bifurcation.

Seizures with FLC offset occur when the system is in the bistability region in the lower part of the map, which is shown in Fig. S10A. This region has a wide range of frequency characteristics, depending on the specific path chosen. Figure S10 shows the simulated results for three different paths that link a SN onset with FLC offset: it is possible to have seizures that have increasing, decreasing, or constant frequency. These differences occur because this region of the map has a great diversity of scaling laws in a small region, and the frequency has to change smoothly between them. In this particular case, even though FLC occurs with non-zero frequency, it is close to a SH curve which requires oscillations to slow down to zero. The closer the path chosen to the SH curve the slower the oscillations towards FLC offset.



Integration settings (same for the three simulations): Euler-Meruyama method; integration step 0.5 s; simulation length 15000 s; initial conditions were set to 0 for all variables; simulations without noise. Model parameter settings:

Constant frequency:  $c = 0.001$ ;  $d^* = 0.3$ ;  $R = 0.4$ ;  $\mathbf{A}_1 = (0.1199, -0.0509, -0.3782)$ ;  $\mathbf{B}_1 = (0.2850, 0.0586, -0.2745)$ .

Increasing frequency:  $c = 0.002$ ;  $d^* = 0.3$ ;  $R = 0.4$ ;  $\mathbf{A}_1 = (-0.1031, -0.0996, -0.3734)$ ;  $\mathbf{B}_1 = (0.1436, 0.0331, -0.0622)$ .

Decreasing frequency:  $c = 0.003$ ;  $d^* = 0.3$ ;  $R = 0.4$ ;  $\mathbf{A}_1 = (0.2818, 0.0209, -0.2831)$ ;  $\mathbf{B}_1 = (0.2187, 0.0394, -0.3326)$ .

Seizures with SupH offset occur when the system is in the bistability region in the upper part of the map, as shown in Fig. S11A. Similar to the FLC case, the proximity of the SH curve, which has a frequency that goes to 0, affects the trajectories of SupH offsets (Fig. S11).

Integration settings (same for the three simulations): Euler-Meruyama method; integration step 0.5 s; simulation length 20000 s; initial conditions were set to 0 for all variables; simulations without noise. Model parameter settings:

Constant frequency:  $c = 0.00025$ ;  $d^* = 0.3$ ;  $R = 0.4$ ;  $\mathbf{A}_1 = (0.3101, -0.0217, 0.2517)$ ;  $\mathbf{B}_1 = (0.3426, 0.0772, 0.1915)$ .

Increasing frequency:  $c = 0.001$ ;  $d^* = 0.3$ ;  $R = 0.4$ ;  $\mathbf{A}_1 = (0.3216, 0.0625, 0.2294)$ ;  
 $\mathbf{B}_1 = (0.3479, 0.0790, -0.1810)$ .

Decreasing frequency:  $c = 0.0002$ ;  $d^* = 0.3$ ;  $R = 0.4$ ;  $\mathbf{A}_1 = (0.3102, -0.0437, 0.2488)$ ;  
 $\mathbf{B}_1 = (0.3249, 0.0713, 0.2221)$ .

These two examples show some of the complex characteristics that can occur when a seizure's dynamics are in a region of the map that is close to two different bifurcations. This can cause unusual phenomena such as accelerating spikes at seizure offset, but also seizures that combine features from different bifurcations, such as FLC (Fig. S10) or SupH (Fig. S11) that show slowing down. This slowing down is in principle different from that of SH or SNIC because it does not follow a scaling law down to zero. The slowing down becomes more similar to that of SH-SNIC the closer the path gets to these bifurcation curves. Some extreme examples are shown in Fig. S10 and S11, in which it would be ambiguous to classify based upon ISI of the timeseries. In such cases, only the presence of amplitude scaling (for SupH) would help disambiguate.

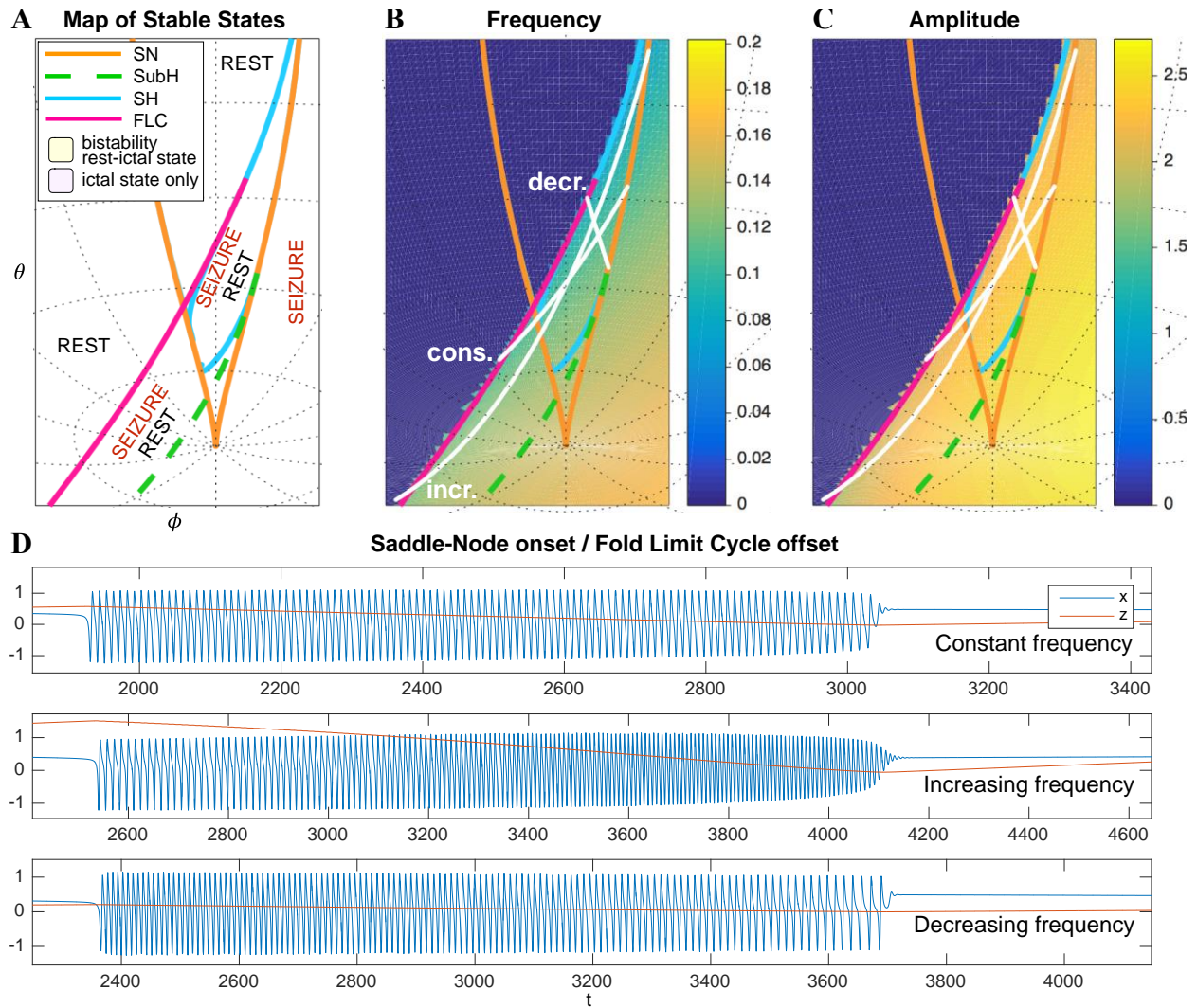


Fig. S10 – Varied frequency behavior of FLC offsets. Depending on how close the trajectory comes to the SH offset, an FLC offset can have a wide range of frequency behaviors. We show examples for three frequency trends for the FLC bifurcation. A) portion of the map in which the SubH / FLC class can be found. B-C) Frequency and amplitude trajectories of three different seizures showing constant, increasing, and decreasing frequency. D) simulations for the paths shown in B-C. Note the last few spikes drop in amplitude precipitously, characteristic of the FLC releasing from the limit cycle (which has a finite amplitude when it disappears) and settling on the fixed point. This is different from the square-root decreasing amplitude of the SupH

bifurcation, which is instead caused by a slow decrease in the amplitude of the limit cycle itself, in this latter case the limit cycle disappears when zero amplitude is reached.

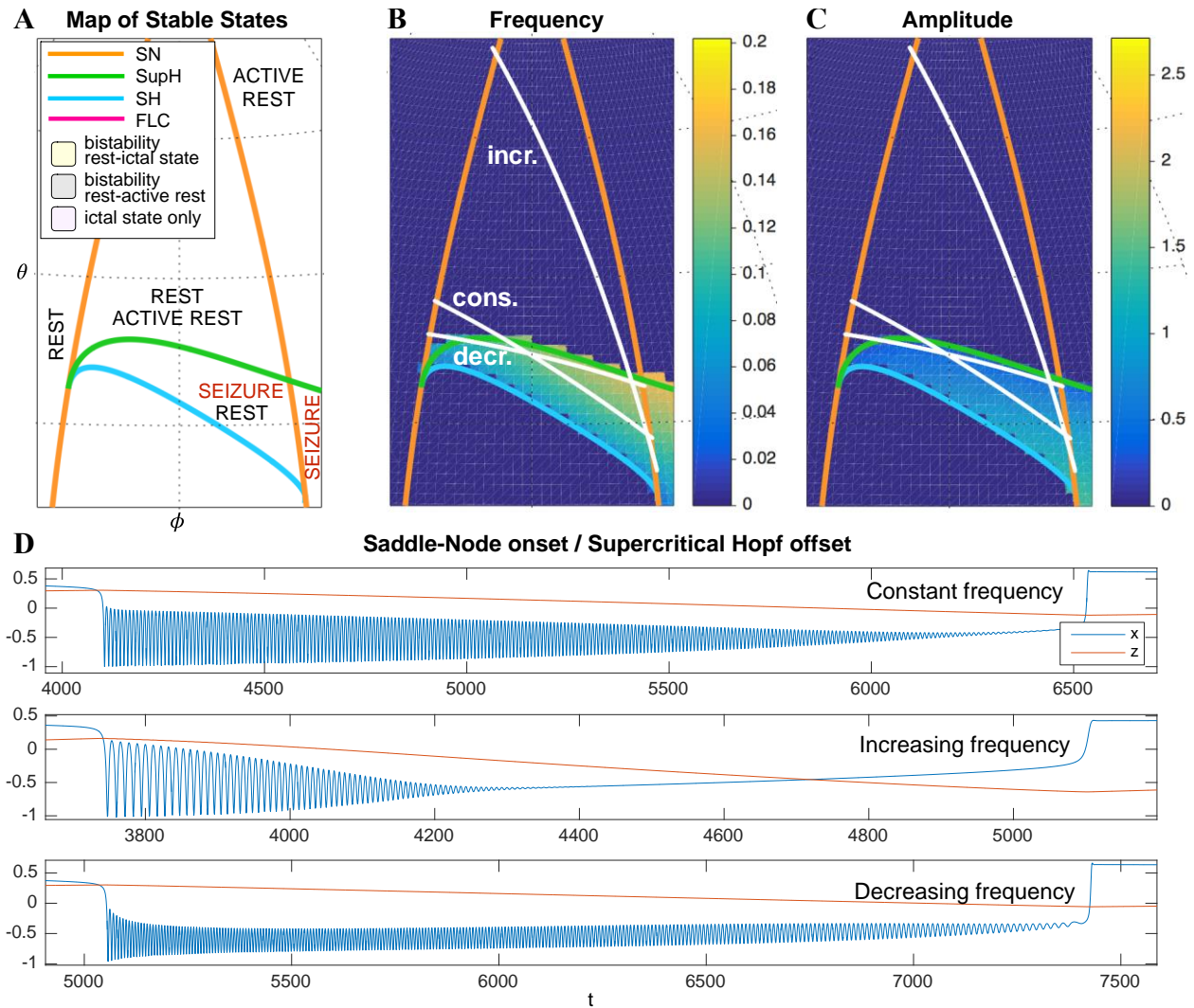


Fig. S11 – Frequency behavior of SupH offsets. The trajectory of seizure offset in SupH is influenced by the SH curve, allowing for constant, increasing and decreasing frequency trends. A) portion of the map in which the SN / SupH class can be found. B-C) Frequency and amplitude trajectories of three different seizures showing constant, increasing, and decreasing frequency. D) simulations for the paths shown in B-C. Note the amplitude in each case is very characteristic of the SupH, despite the different frequency behavior.

## ***VI. Projection of other epilepsy models onto the Epidynamics map***

The model in (M. Saggio et al. 2017) and Fig. 4 is capable of navigating the entire projection with first order trajectories and provides minimal models for many other bursting classes. For instance the Epileptor model maps to the region of the SN/SH Class. In addition to the Epileptor, the map contains the bifurcation diagrams of other seizure onset and/or offset models used in the literature. For instance, Sinha et al. (Sinha et al. 2017) used a model (only fast variables) with the same bifurcation diagram as the subH/FLC Dynamic Class. That class is also present in the lower portion of this map. The path of the SubH/FLC Class is equivalent to several bistable and physiologically-inspired seizure models (Marten et al. 2009; Benjamin et al. 2012; Hutchings et al. 2015; Terry, Benjamin, and Richardson 2012; Kalitzin et al. 2014, 2011; Suffczynski et al. 2005, 2006; Goodfellow, Schindler, and Baier 2012; Meisel and Kuehn 2012). Some of these models use noise induced transitions, others bifurcations (see Appendix III). Excitable models, such as those in Wendling et al (Wendling et al. 2002) and Goodfellow et al (Goodfellow et al. 2016), can be obtained in the map when the system is close to the SNIC curve. There are also models used in the context of epilepsy that contain bigger portions of the map, such as the Jansen-Rit and the Wendling-Chauvel (Touboul et al. 2011) models. This versatility led other authors to state that. the degenerate Bogdanov-Takens bifurcation (the basis of our map) is “a good candidate for a simple qualitative model of a cortical mass” (Touboul et al. 2011).

## BIBLIOGRAPHY

- Alarcon, G. 2005. "Electrical Stimulation in Epilepsy." *Clin Neurophysiol* 116 (3): 716–17.  
<https://doi.org/10.1016/j.clinph.2004.11.002>.
- Badawy, R A, G D Jackson, S F Berkovic, and R A Macdonell. 2013. "Cortical Excitability and Refractory Epilepsy: A Three-Year Longitudinal Transcranial Magnetic Stimulation Study." *Int J Neural Syst* 23 (1): 1250030. <https://doi.org/10.1142/S012906571250030X>.
- Badawy, R A, S J Vogrin, A Lai, and M J Cook. 2013. "Are Patterns of Cortical Hyperexcitability Altered in Catamenial Epilepsy?" *Ann Neurol* 74 (5): 743–57.  
<https://doi.org/10.1002/ana.23923>.
- Badawy, R, R Macdonell, G Jackson, and S Berkovic. 2009. "The Peri-Ictal State: Cortical Excitability Changes within 24 h of a Seizure." *Brain* 132 (Pt 4): 1013–21.  
<https://doi.org/awp017> [pii]10.1093/brain/awp017.
- Baer, S M, B W Kooi, Y A Kuznetsov, and H R Thieme. 2006. "Multiparametric Bifurcation Analysis of a Basic Two-Stage Population Model." *Siam Journal on Applied Mathematics* 66 (4): 1339–65. <https://doi.org/10.1137/050627757>.
- Baud, M O, A Ghestem, J J Benoliel, C Becker, and C Bernard. 2019. "Endogenous Multidien Rhythm of Epilepsy in Rats." *Exp Neurol* 315: 82–87.  
<https://doi.org/10.1016/j.expneurol.2019.02.006>.
- Baud, M O, J K Kleen, E A Mirro, J C Andrechak, D King-Stephens, E F Chang, and V R Rao. 2018. "Multi-Day Rhythms Modulate Seizure Risk in Epilepsy." *Nat Commun* 9 (1): 88.

<https://doi.org/10.1038/s41467-017-02577-y>[10.1038/s41467-017-02577-y](https://doi.org/10.1038/s41467-017-02577-y) [pii].

- Belykh, I, R Reimbayev, and K Zhao. 2015. “Synergistic Effect of Repulsive Inhibition in Synchronization of Excitatory Networks.” *Phys Rev E Stat Nonlin Soft Matter Phys* 91 (6): 62919. <https://doi.org/10.1103/PhysRevE.91.062919>.
- Benjamin, O, T H Fitzgerald, P Ashwin, K Tsaneva-Atanasova, F Chowdhury, M P Richardson, and J R Terry. 2012. “A Phenomenological Model of Seizure Initiation Suggests Network Structure May Explain Seizure Frequency in Idiopathic Generalised Epilepsy.” *J Math Neurosci* 2 (1): 1. <https://doi.org/10.1186/2190-8567-2-12190-8567-2-1> [pii].
- Berisha, V, A Wisler, A O Hero, and A Spanias. 2016. “Empirically Estimable Classification Bounds Based on a Nonparametric Divergence Measure.” *IEEE Trans Signal Process* 64 (3): 580–91. <https://doi.org/10.1109/TSP.2015.2477805>.
- Breakspear, M, J A Roberts, J R Terry, S Rodrigues, N Mahant, and P A Robinson. 2006. “A Unifying Explanation of Primary Generalized Seizures through Nonlinear Brain Modeling and Bifurcation Analysis.” *Cereb Cortex* 16 (9): 1296–1313. <https://doi.org/bhj072> [pii][10.1093/cercor/bhj072](https://doi.org/10.1093/cercor/bhj072).
- Bryant, P, and K Wiesenfeld. 1986. “Suppression of Period-Doubling and Nonlinear Parametric Effects in Periodically Perturbed Systems.” *Phys Rev A Gen Phys* 33 (4): 2525–43. <https://www.ncbi.nlm.nih.gov/pubmed/9896937>.
- Carter, B G, and W Butt. 2005. “Are Somatosensory Evoked Potentials the Best Predictor of Outcome after Severe Brain Injury? A Systematic Review.” *Intensive Care Med* 31 (6): 765–75. <https://doi.org/10.1007/s00134-005-2633-1>.
- Chang, W C, J Kudlacek, J Hlinka, J Chvojka, M Hadrava, V Kumpost, A D Powell, et al. 2018. “Loss of Neuronal Network Resilience Precedes Seizures and Determines the Ictogenic



- Nature of Interictal Synaptic Perturbations.” *Nat Neurosci* 21 (12): 1742–52.  
<https://doi.org/10.1038/s41593-018-0278-y>.
- Chen, Lingxuan, Takashi Saito, Takaomi C. Saïdo, and Istvan Mody. 2018. “Novel Quantitative Analyses of Spontaneous Synaptic Events in Cortical Pyramidal Cells Reveal Subtle Parvalbumin-Expressing Interneuron Dysfunction in a Knock-in Mouse Model of Alzheimer’s Disease.” *ENeuro* 5 (4). <https://doi.org/10.1523/ENEURO.0059-18.2018>.
- Chen, R., J. Classen, C. Gerloff, P. Celnik, E. Wassermann, M. Hallett, and L. Cohen. 1997. “Depression of Motor Cortex Excitability by Low-Frequency Transcranial Magnetic Stimulation.” *Neurology* 48 (5): 1398–1403. <https://doi.org/10.1212/WNL.48.5.1398>.
- Chow, J H, J R Winkelman, M A Pai, and P W Sauer. 1990. “Singular Perturbation Analysis of Large-Scale Power-Systems.” *International Journal of Electrical Power & Energy Systems* 12 (2): 117–26. [https://doi.org/Doi 10.1016/0142-0615\(90\)90007-X](https://doi.org/Doi 10.1016/0142-0615(90)90007-X).
- Cook, Mark J., Terence J. O’Brien, Samuel F. Berkovic, Michael Murphy, Andrew Morokoff, Gavin Fabinyi, Wendyl D’Souza, et al. 2013. “Prediction of Seizure Likelihood with a Long-Term, Implanted Seizure Advisory System in Patients with Drug-Resistant Epilepsy: A First-in-Man Study.” *The Lancet Neurology* 12 (6): 563–71.  
[https://doi.org/10.1016/S1474-4422\(13\)70075-9](https://doi.org/10.1016/S1474-4422(13)70075-9).
- Crisp, D N, M L Saggio, J Scott, W C Stacey, M Nakatani, S Gliske, and J Lin. 2019. “Epidynamics: Navigating the Map of Seizure Dynamics - Code and Data.”  
<https://doi.org/10.7302/Ejhy-5h41>. 2019. <https://doi.org/https://doi.org/10.7302/ejhy-5h41>.
- David, O, J Bastin, S Chabardes, L Minotti, and P Kahane. 2010. “Studying Network Mechanisms Using Intracranial Stimulation in Epileptic Patients.” *Front Syst Neurosci* 4: 148. <https://doi.org/10.3389/fnsys.2010.00148>.

- Dreier, J., C. Zhang, and U. Heinemann. 1998. “Phenytoin , Phenobarbital , and Midazolam Fail to Stop Status Epilepticus-like Activity Induced by Low Magnesium in Rat Entorhinal Slices , but Can Prevent Its Development.” *Acta Neurologica Scandinavica* 98: 154–60.
- Dudek, F E, and K J Staley. 2011. “The Time Course of Acquired Epilepsy: Implications for Therapeutic Intervention to Suppress Epileptogenesis.” *Neurosci Lett* 497 (3): 240–46. [https://doi.org/10.1016/j.neulet.2011.03.071S0304-3940\(11\)00385-5](https://doi.org/10.1016/j.neulet.2011.03.071S0304-3940(11)00385-5) [pii].
- Dumortier, F, R Roussarie, J Sotomayor, and H Zoladek. 1991. *Generic 3-Parameter Families of Vector Fields, Unfolding of Saddle, Focus, and Elliptic Singularities with Nilpotent Linear Part. Lecture Notes in Mathematics*. 2nd ed. Springer-Verlag.
- Ehrlén, Johan, and Jan Van Groenendael. 2008. “Direct Perturbation Analysis for Better Conservation.” *Conservation Biology* 12 (2): 470–74. <https://doi.org/10.1111/j.1523-1739.1998.96420.x>.
- Einevoll, G T, C Kayser, N K Logothetis, and S Panzeri. 2013. “Modelling and Analysis of Local Field Potentials for Studying the Function of Cortical Circuits.” *Nat Rev Neurosci* 14 (11): 770–85. <https://doi.org/10.1038/nrn3599>.
- Fisher, R., J. Cross, J. French, N. Higurashi, E. Hirsch, Floor E. Jansen, Lieven Lagae, et al. 2017. “Operational Classification of Seizure Types by the International League Against Epilepsy: Position Paper of the ILAE Commission for Classification and Terminology.” *Epilepsia* 58 (4): 522–30. <https://doi.org/10.1111/epi.13670>.
- Fisher, R., W. Van Emde Boas, W. Blume, C. Elger, P. Genton, P. Lee, and J. Engel. 2005. “Epileptic Seizures and Epilepsy: Definitions Proposed by the International League Against Epilepsy (ILAE) and the International Bureau for Epilepsy (IBE).” *Epilepsia* 46 (4): 470–72. <https://doi.org/10.1111/j.0013-9580.2005.66104.x>.

- Freestone, D., L. Kuhlmann, D. Grayden, A. Burkitt, A. Lai, T. Nelson, S. Vogrin, et al. 2011. “Electrical Probing of Cortical Excitability in Patients with Epilepsy.” *Epilepsy and Behavior* 22: S110–18. <https://doi.org/10.1016/j.yebeh.2011.09.005>.
- Golubitsky, M, K Josic, and T J Kaper. 2001. “An Unfolding Theory Approach to Bursting in Fast-Slow Systems.” *Global Analysis of Dynamical Systems*, 277–308. <https://doi.org/DOI.10.1887/0750308036/b1058c10>.
- Goodfellow, M, C Rummel, E Abela, M P Richardson, K Schindler, and J R Terry. 2016. “Estimation of Brain Network Ictogenicity Predicts Outcome from Epilepsy Surgery.” *Nature Scientific Reports*, 1–13. <https://doi.org/10.1038/srep29215>.
- Goodfellow, M, K Schindler, and G Baier. 2012. “Self-Organised Transients in a Neural Mass Model of Epileptogenic Tissue Dynamics.” *Neuroimage* 59 (3): 2644–60. [https://doi.org/10.1016/j.neuroimage.2011.08.060S1053-8119\(11\)00977-3](https://doi.org/10.1016/j.neuroimage.2011.08.060S1053-8119(11)00977-3) [pii].
- Haddad, S A, and E Marder. 2018. “Circuit Robustness to Temperature Perturbation Is Altered by Neuromodulators.” *Neuron* 100 (3): 609-623.e3. <https://doi.org/10.1016/j.neuron.2018.08.035>.
- Heppell, Selina S, Hal Caswell, and Larry B Crowder. 2000. “Life Histories and Elasticity Patterns: Perturbation Analysis for Species with Minimal Demographic Data.” *Ecology* 81 (3): 654–65. [https://doi.org/10.1890/0012-9658\(2000\)081\[0654:Lhaepp\]2.0.Co;2](https://doi.org/10.1890/0012-9658(2000)081[0654:Lhaepp]2.0.Co;2).
- Herman, S T. 2002. “Epilepsy after Brain Insult: Targeting Epileptogenesis.” *Neurology* 59 (9 Suppl 5): S21-6. <https://www.ncbi.nlm.nih.gov/pubmed/12428028>.
- . 2006. “Clinical Trials for Prevention of Epileptogenesis.” *Epilepsy Res* 68 (1): 35–38. <https://doi.org/10.1016/j.eplepsyres.2005.09.015>.
- Houssaini, K El, A I Ivanov, C Bernard, and V K Jirsa. 2015. “Seizures, Refractory Status

- Epilepticus, and Depolarization Block as Endogenous Brain Activities.” *Phys Rev E Stat Nonlin Soft Matter Phys* 91 (1): 10701. <https://doi.org/10.1103/PhysRevE.91.010701>.
- Hutchings, F, C E Han, S S Keller, B Weber, P N Taylor, and M Kaiser. 2015. “Predicting Surgery Targets in Temporal Lobe Epilepsy through Structural Connectome Based Simulations.” *PLoS Comput Biol* 11 (12): e1004642. <https://doi.org/10.1371/journal.pcbi.1004642>PCOMPBIOL-D-15-01015 [pii].
- Iasemidis, L D, L D Olson, R S Savit, and J C Sackellares. 1994. “Time Dependencies in the Occurrences of Epileptic Seizures.” *Epilepsy Res* 17 (1): 81–94. [https://doi.org/0920-1211\(94\)90081-7](https://doi.org/10.1016/0920-1211(94)90081-7) [pii].
- Ihle, M, H Feldwisch-Drentrup, C A Teixeira, A Witon, B Schelter, J Timmer, and A Schulze-Bonhage. 2010. “EPILEPSIAE - A European Epilepsy Database.” *Comput Methods Programs Biomed.* [https://doi.org/S0169-2607\(10\)00222-1](https://doi.org/10.1016/j.cmpb.2010.08.011) [pii]10.1016/j.cmpb.2010.08.011.
- Ikeda, A., K. Terada, N. Mikuni, R. Burgess, Y. Comair, W. Taki, T. Hamano, J. Kimura, H. Lüders, and H. Shibasaki. 1996. “Subdural Recording of Ictal DC Shifts in Neocortical Seizures in Humans.” *Epilepsia* 37 (7): 662–74. <https://doi.org/10.1111/j.1528-1157.1996.tb00631.x>.
- Ikeda, A, W Taki, T Kunieda, K Terada, N Mikuni, T Nagamine, S Yazawa, et al. 1999. “Focal Ictal Direct Current Shifts in Human Epilepsy as Studied by Subdural and Scalp Recording.” *Brain* 122 ( Pt 5): 827–38. [http://www.ncbi.nlm.nih.gov/entrez/query.fcgi?cmd=Retrieve&db=PubMed&dopt=Citation&list\\_uids=10355669](http://www.ncbi.nlm.nih.gov/entrez/query.fcgi?cmd=Retrieve&db=PubMed&dopt=Citation&list_uids=10355669).
- Izhikevich, Eugene M. 2000. “Neural Excitability, Spiking and Bursting.” *International Journal*

- of Bifurcation and Chaos* 10 (6): 1171–1266. <https://doi.org/10.1142/S0218127400000840>.
- Jefferys, J, and M Walker. 2006. “Tetanus Toxin Model of Focal Epilepsy.” In *Models of Seizures and Epilepsy*, edited by A Pitkanen, P A Schwartzkroin, and S L Moshe, 407–14. London: Elsevier Academic Press. <https://doi.org/https://doi.org/10.1016/B978-012088554-1/50035-9>.
- Jiménez-Jiménez, D., R. Nekkare, L. Flores, K. Chatzidimou, I. Bodi, M. Honavar, N. Mullatti, et al. 2015. “Prognostic Value of Intracranial Seizure Onset Patterns for Surgical Outcome of the Treatment of Epilepsy.” *Clinical Neurophysiology* 126 (2): 257–67. <https://doi.org/10.1016/j.clinph.2014.06.005>.
- Jirsa, V., W. Stacey, P. Quilichini, A. Ivanov, and C. Bernard. 2014. “On the Nature of Seizure Dynamics.” *Brain* 137 (8): 2210–30. <https://doi.org/10.1093/brain/awu133>.
- Jirsa, V K, T Proix, D Perdakis, M M Woodman, H Wang, J Gonzalez-Martinez, C Bernard, et al. 2017. “The Virtual Epileptic Patient: Individualized Whole-Brain Models of Epilepsy Spread.” *Neuroimage* 145 (Pt B): 377–88. [https://doi.org/S1053-8119\(16\)30089-1](https://doi.org/S1053-8119(16)30089-1) [pii]10.1016/j.neuroimage.2016.04.049.
- Jirsa, V K, W C Stacey, P P Quilichini, A I Ivanov, and C Bernard. 2014. “On the Nature of Seizure Dynamics.” *Brain* 137 (Pt 8): 2210–30. <https://doi.org/10.1093/brain/awu133>.
- Kadam, S D, A M White, K J Staley, and F E Dudek. 2010. “Continuous Electroencephalographic Monitoring with Radio-Telemetry in a Rat Model of Perinatal Hypoxia-Ischemia Reveals Progressive Post-Stroke Epilepsy.” *J Neurosci* 30 (1): 404–15. <https://doi.org/30/1/404> [pii]10.1523/JNEUROSCI.4093-09.2010.
- Kalitzin, S., J. Parra, D. Velis, and F. Lopes Da Silva. 2002. “Enhancement of Phase Clustering in the EEG/MEG Gamma Frequency Band Anticipates Transitions to Paroxysmal

- Epileptiform Activity in Epileptic Patients with Known Visual Sensitivity.” *IEEE Transactions on Biomedical Engineering* 49 (11): 1279–86.  
<https://doi.org/10.1109/TBME.2002.804593>.
- Kalitzin, S., D. Velis, and F. Lopes. 2010. “Stimulation-Based Anticipation and Control of State Transitions in the Epileptic Brain.” *Epilepsy and Behavior* 17 (3): 310–23.  
<https://doi.org/10.1016/j.yebeh.2009.12.023>.
- Kalitzin, S, M Koppert, G Petkov, and F L da Silva. 2014. “Multiple Oscillatory States in Models of Collective Neuronal Dynamics.” *Int J Neural Syst* 24 (6): 1450020.  
<https://doi.org/10.1142/S0129065714500208>.
- Kalitzin, S, M Koppert, G Petkov, D Velis, and F L da Silva. 2011. “Computational Model Prospective on the Observation of Proictal States in Epileptic Neuronal Systems.” *Epilepsy Behav* 22 Suppl 1: S102-9. <https://doi.org/10.1016/j.yebeh.2011.08.017>S1525-5050(11)00481-1 [pii].
- Kalitzin, S, D Velis, P Suffczynski, J Parra, and F L da Silva. 2005. “Electrical Brain-Stimulation Paradigm for Estimating the Seizure Onset Site and the Time to Ictal Transition in Temporal Lobe Epilepsy.” *Clin Neurophysiol* 116 (3): 718–28. [https://doi.org/S1388-2457\(04\)00417-1](https://doi.org/S1388-2457(04)00417-1) [pii]10.1016/j.clinph.2004.08.021.
- Kanazawa, K, R Matsumoto, H Imamura, M Matsubishi, T Kikuchi, T Kunieda, N Mikuni, S Miyamoto, R Takahashi, and A Ikeda. 2015. “Intracranially Recorded Ictal Direct Current Shifts May Precede High Frequency Oscillations in Human Epilepsy.” *Clin Neurophysiol* 126 (1): 47–59. <https://doi.org/10.1016/j.clinph.2014.05.028>S1388-2457(14)00303-4 [pii].
- Karoly, P J, H Ung, D B Grayden, L Kuhlmann, K Leyde, M J Cook, and D R Freestone. 2017. “The Circadian Profile of Epilepsy Improves Seizure Forecasting.” *Brain* 140 (8): 2169–82.

<https://doi.org/10.1093/brain/awx1734032453> [pii].

Karoly, Philippa J., Daniel M. Goldenholz, Dean R. Freestone, Robert E. Moss, David B.

Grayden, William H. Theodore, and Mark J. Cook. 2018. "Circadian and Circaseptan Rhythms in Human Epilepsy: A Retrospective Cohort Study." *The Lancet Neurology* 17 (11): 977–85. [https://doi.org/10.1016/S1474-4422\(18\)30274-6](https://doi.org/10.1016/S1474-4422(18)30274-6).

Kikani, J, and Jr. Pedrosa O. A. 1991. "Perturbation Analysis of Stress-Sensitive Reservoirs (Includes Associated Papers 25281 and 25292 )." Society of Petroleum Engineers.

<https://doi.org/https://doi.org/10.2118/20053-PA>.

Kirst, C, J Ammer, F Felmy, A Herz, and M Stemmler. 2015. "Fundamental Structure and Modulation of Neuronal Excitability: Synaptic Control of Coding, Resonance, and Network Synchronization." *BioRxiv*. <https://doi.org/doi:https://doi.org/10.1101/022475>.

Kramer, M A, W Truccolo, U T Eden, K Q Lepage, L R Hochberg, E N Eskandar, J R Madsen, et al. 2012. "Human Seizures Self-Terminate across Spatial Scales via a Critical Transition." *Proc Natl Acad Sci U S A* 109 (51): 21116–21.

<https://doi.org/10.1073/pnas.1210047110> [pii].

Kramer, Mark a., Wilson Truccolo, Uri T. Eden, Kyle Q. Lepage, Leigh R. Hochberg, Emad N.

Eskandar, Joseph R. Madsen, et al. 2012. "Human Seizures Self-Terminate across Spatial Scales via a Critical Transition." *Proceedings of the National Academy of Sciences* 109 (51): 21116–21. <https://doi.org/10.1073/pnas.1210047110>.

Kuznetsov, Y. 2004. *Elements of Applied Bifurcation Theory*. Vol. 3. Springer.

Kwan, P., A. Arzimanoglou, A. Berg, M. Brodie, E. Perucca, S. Wiebe, W. Hauser, G. Mathern, S. Moshe, and J. French. 2010. "Definition of Drug Resistant Epilepsy : Consensus Proposal by the Ad Hoc Task Force of the ILAE Commission on Therapeutic Strategies."

*Epilepsia* 51 (6): 1069–77. <https://doi.org/10.1111/j.1528-1167.2009.02397.x>.

Lagarde, S, F Bonini, A McGonigal, P Chauvel, M Gavaret, D Scavarda, R Carron, et al. 2016.

“Seizure-Onset Patterns in Focal Cortical Dysplasia and Neurodevelopmental Tumors: Relationship with Surgical Prognosis and Neuropathologic Subtypes.” *Epilepsia* 57 (9): 1426–35. <https://doi.org/10.1111/epi.13464>.

Lagarde, S, S Buzori, A Trebuchon, R Carron, D Scavarda, M Milh, A McGonigal, and F

Bartolomei. 2019a. “The Repertoire of Seizure Onset Patterns in Human Focal Epilepsies: Determinants and Prognostic Values.” *Epilepsia* 60 (1): 85–95.

<https://doi.org/10.1111/epi.14604>.

———. 2019b. “The Repertoire of Seizure Onset Patterns in Human Focal Epilepsies:

Determinants and Prognostic Values.” *Epilepsia* 60 (1): 85–95.

<https://doi.org/10.1111/epi.14604>.

Long, C, B Fureman, and R Dingledine. 2016. “2014 Epilepsy Benchmarks: Progress and

Opportunities.” *Epilepsy Curr* 16 (3): 179–81. <https://doi.org/10.5698/1535-7511-16.3.179>.

Lopes da Silva, F, W Blanes, S N Kalitzin, J Parra, P Suffczynski, and D N Velis. 2003.

“Epilepsies as Dynamical Diseases of Brain Systems: Basic Models of the Transition between Normal and Epileptic Activity.” *Epilepsia* 44 Suppl 1: 72–83. <https://doi.org/12005> [pii].

Lopes da Silva, F H, W Blanes, S N Kalitzin, J Parra, P Suffczynski, and D N Velis. 2003.

“Dynamical Diseases of Brain Systems: Different Routes to Epileptic Seizures.” *IEEE Trans Biomed Eng* 50 (5): 540–48. <https://doi.org/10.1109/TBME.2003.810703>.

Lopes da Silva, Fernando H., Wouter Blanes, Jaime Parra, Demetrios N. Velis, Stiliyan N.

Kalitzin, and Piotr Suffczynski. 2003. “Dynamical Diseases of Brain Systems: Different



- Routes to Epileptic Seizures.” *IEEE Transactions on Biomedical Engineering* 50 (5): 540–48. <https://doi.org/10.1109/TBME.2003.810703>.
- Louis, Erik K St., and Lauren C Frey. 2016. “EEG: An Introductory Text and Atlas of Normal and Abnormal Findings in Adults, Children, and Infants.” Edited by Erik K St. Louis and Lauren C Frey. Chicago: American Epilepsy Society.  
<https://doi.org/http://dx.doi.org/10.5698/978-0-9979756-0-4>.
- Lukasiuk, K, and A J Becker. 2014. “Molecular Biomarkers of Epileptogenesis.” *Neurotherapeutics* 11 (2): 319–23. <https://doi.org/10.1007/s13311-014-0261-6>.
- Luna-Munguia, H, A G Zestos, S V Gliske, R T Kennedy, and W C Stacey. 2019. “Chemical Biomarkers of Epileptogenesis and Ictogenesis in Experimental Epilepsy.” *Neurobiol Dis* 121: 177–86. <https://doi.org/10.1016/j.nbd.2018.10.005>.
- Luttjohann, A, S Zhang, R de Peijper, and G van Luijtelaar. 2011. “Electrical Stimulation of the Epileptic Focus in Absence Epileptic WAG/Rij Rats: Assessment of Local and Network Excitability.” *Neuroscience* 188: 125–34.  
<https://doi.org/10.1016/j.neuroscience.2011.04.038>.
- Ma, Jing, Xue Wang, and Xinbin Lan. 2012. “Small-Signal Stability Analysis of Microgrid Based on Perturbation Theory.” *2012 Asia-Pacific Power and Energy Engineering Conference*. IEEE. <https://doi.org/10.1109/appeec.2012.6306946>.
- Marten, F, S Rodrigues, P Suffczynski, M P Richardson, and J R Terry. 2009. “Derivation and Analysis of an Ordinary Differential Equation Mean-Field Model for Studying Clinically Recorded Epilepsy Dynamics.” *Phys Rev E Stat Nonlin Soft Matter Phys* 79 (2 Pt 1): 21911. <https://doi.org/10.1103/PhysRevE.79.021911>.
- Martinez, I, A R Messina, and E Barocio. 2004. “Perturbation Analysis of Power Systems:

- Effects of Second- and Third-Order Nonlinear Terms on System Dynamic Behavior.” *Electric Power Systems Research* 71 (2): 159–67. [https://doi.org/Doi.10.1016/S0378-7796\(04\)00029-X](https://doi.org/Doi.10.1016/S0378-7796(04)00029-X).
- Medeiros, D C, L B Oliveira, F A Mourao, C P Bastos, N G Cairasco, G S Pereira, E M Mendes, and M F Moraes. 2014. “Temporal Rearrangement of Pre-Ictal PTZ Induced Spike Discharges by Low Frequency Electrical Stimulation to the Amygdaloid Complex.” *Brain Stimul* 7 (2): 170–78. <https://doi.org/10.1016/j.brs.2013.11.005>.
- Meijer, H G, T L Eissa, B Kiewiet, J F Neuman, C A Schevon, R G Emerson, R R Goodman, et al. 2015. “Modeling Focal Epileptic Activity in the Wilson-Cowan Model with Depolarization Block.” *J Math Neurosci* 5: 7. <https://doi.org/10.1186/s13408-015-0019-419> [pii].
- Meisel, C, and C Kuehn. 2012. “Scaling Effects and Spatio-Temporal Multilevel Dynamics in Epileptic Seizures.” *PLoS ONE* 7 (2): e30371. <https://doi.org/10.1371/journal.pone.0030371> PONE-D-11-23603 [pii].
- Meisel, C, A Schulze-Bonhage, D Freestone, M J Cook, P Achermann, and D Plenz. 2015. “Intrinsic Excitability Measures Track Antiepileptic Drug Action and Uncover Increasing/Decreasing Excitability over the Wake/Sleep Cycle.” *Proc Natl Acad Sci U S A*. <https://doi.org/201513716> [pii]1513716112 [pii]10.1073/pnas.1513716112.
- Milton, J G. 2012. “Neuronal Avalanches, Epileptic Quakes and Other Transient Forms of Neurodynamics.” *Eur J Neurosci* 36 (2): 2156–63. <https://doi.org/10.1111/j.1460-9568.2012.08102.x>.
- Moore, S., B. Throesch, and G. Murphy. 2011. “Of Mice and Intrinsic Excitability: Genetic Background Affects the Size of the Postburst Afterhyperpolarization in CA1 Pyramidal

- Neurons.” *Journal of Neurophysiology* 106 (3): 1570–80.  
<https://doi.org/10.1152/jn.00257.2011>.
- Morrell, M J. 2011. “Responsive Cortical Stimulation for the Treatment of Medically Intractable Partial Epilepsy.” *Neurology* 77 (13): 1295–1304. <https://doi.org/WNL.0b013e3182302056> [pii]10.1212/WNL.0b013e3182302056.
- Narayan, R K, R P Greenberg, J D Miller, G G Enas, S C Choi, P R Kishore, J B Selhorst, H A Lutz 3rd, and D P Becker. 1981. “Improved Confidence of Outcome Prediction in Severe Head Injury. A Comparative Analysis of the Clinical Examination, Multimodality Evoked Potentials, CT Scanning, and Intracranial Pressure.” *J Neurosurg* 54 (6): 751–62.  
<https://doi.org/10.3171/jns.1981.54.6.0751>.
- Perucca, P., F. Dubeau, and J. Gotman. 2014. “Intracranial Electroencephalographic Seizure-Onset Patterns: Effect of Underlying Pathology.” *Brain* 137 (iv): 183–96.  
<https://doi.org/10.1093/brain/awt299>.
- Perucca, Piero, François Dubeau, and Jean Gotman. 2014. “Intracranial Electroencephalographic Seizure-Onset Patterns: Effect of Underlying Pathology.” *Brain* 137 (1): 183–96.  
<https://doi.org/10.1093/brain/awt299>.
- Pigorini, A, S Sarasso, P Proserpio, C Szymanski, G Arnulfo, S Casarotto, M Fecchio, et al. 2015. “Bistability Breaks-off Deterministic Responses to Intracortical Stimulation during Non-REM Sleep.” *Neuroimage* 112: 105–13.  
<https://doi.org/10.1016/j.neuroimage.2015.02.056>.
- Pitkanen, A, K Lukasiuk, F E Dudek, and K J Staley. 2015. “Epileptogenesis.” *Cold Spring Harb Perspect Med* 5 (10). <https://doi.org/10.1101/cshperspect.a022822>.
- Proix, T, F Bartolomei, M Guye, and V K Jirsa. 2017. “Individual Brain Structure and Modelling

Predict Seizure Propagation.” *Brain* 140 (3): 641–54.

<https://doi.org/10.1093/brain/awx0042996325> [pii].

Rajakulendran, Sanjeev, and Lina Nashef. 2015. “Postictal Generalized EEG Suppression and SUDEP: A Review.” *Journal of Clinical Neurophysiology: Official Publication of the American Electroencephalographic Society* 32 (1): 14–20.

<https://doi.org/10.1097/WNP.0000000000000147>.

Ranjan, P, and E H Abed. 2000. “Enhancing Detectability of Bifurcations in DC-DC Converters by Stochastic Resonance.” *Proceedings of the 39th Ieee Conference on Decision and Control, Vols 1-5*, 1608–12. <https://doi.org/10.1109/CDC.2000.912091>.

Reimann, M W, C A Anastassiou, R Perin, S L Hill, H Markram, and C Koch. 2013. “A Biophysically Detailed Model of Neocortical Local Field Potentials Predicts the Critical Role of Active Membrane Currents.” *Neuron* 79 (2): 375–90.

[https://doi.org/10.1016/j.neuron.2013.05.023S0896-6273\(13\)00443-1](https://doi.org/10.1016/j.neuron.2013.05.023S0896-6273(13)00443-1) [pii].

Reimbayev, R, and I Belykh. 2014. “When Transitions Between Bursting Modes Induce Neural Synchrony.” *International Journal of Bifurcation and Chaos* 24 (8). <https://doi.org/Artn144001310.1142/S0218127414400136>.

Rinzel, J. 1987. “A Formal Classification of Bursting Mechanisms in Excitable Systems.” In *Mathematical Topics in Population Biology, Morphogenesis and Neurosciences: Proceedings of an International Symposium Held in Kyoto, November 10–15, 1985*, edited by Ei Teramoto and Masaya Yumaguti, 267–81. Berlin, Heidelberg: Springer Berlin Heidelberg. [https://doi.org/10.1007/978-3-642-93360-8\\_26](https://doi.org/10.1007/978-3-642-93360-8_26).

Saggio, M., A. Spiegler, C. Bernard, and V. Jirsa. 2017. “Fast-Slow Bursters in the Unfolding of a High Codimension Singularity and the Ultra-Slow Transitions of Classes .” *Mathematical*

*Neuroscience* 7.

Saggio, M L, A Spiegler, C Bernard, and V K Jirsa. 2017a. “Fast-Slow Bursters in the Unfolding of a High Codimension Singularity and the Ultra-Slow Transitions of Classes.” *Journal of Mathematical Neuroscience* 7. [https://doi.org/UNSP 710.1186/s13408-017-0050-8](https://doi.org/UNSP%20710.1186/s13408-017-0050-8).

———. 2017b. “Fast-Slow Bursters in the Unfolding of a High Codimension Singularity and the Ultra-Slow Transitions of Classes.” *Journal of Mathematical Neuroscience* 7. [https://doi.org/UNSP 710.1186/s13408-017-0050-8](https://doi.org/UNSP%20710.1186/s13408-017-0050-8).

Salami, P., M. Lévesque, J. Gotman, and M. Avoli. 2015. “Distinct EEG Seizure Patterns Reflect Different Seizure Generation Mechanisms.” *J Neurophysiol* 113: 2840–44. <https://doi.org/10.1152/jn.00031.2015>.

Salami, P, M Levesque, J Gotman, and M Avoli. 2015. “Distinct EEG Seizure Patterns Reflect Different Seizure Generation Mechanisms.” *J Neurophysiol* 113 (7): 2840–44. <https://doi.org/10.1152/jn.00031.2015jn.00031.2015> [pii].

Schmitt, S E, K Pargeon, E S Frechette, L J Hirsch, J Dalmau, and D Friedman. 2012. “Extreme Delta Brush: A Unique EEG Pattern in Adults with Anti-NMDA Receptor Encephalitis.” *Neurology* 79 (11): 1094–1100. <https://doi.org/10.1212/WNL.0b013e3182698cd8WNL.0b013e3182698cd8> [pii].

Seydel, Rudiger. 2010. *Practical Bifurcation and Stability Analysis*. Edited by S. Antman, J. Marsden, and L. Sirovich. Third. Springer.

Sinha, N, J Dauwels, M Kaiser, S S Cash, M Brandon Westover, Y Wang, and P N Taylor. 2017. “Predicting Neurosurgical Outcomes in Focal Epilepsy Patients Using Computational Modelling.” *Brain* 140 (2): 319–32. <https://doi.org/10.1093/brain/aww299aww299> [pii].

Slaght, S J, T Paz, M Chavez, J M Deniau, S Mahon, and S Charpier. 2004. “On the Activity of

- the Corticostriatal Networks during Spike-and-Wave Discharges in a Genetic Model of Absence Epilepsy.” *J Neurosci* 24 (30): 6816–25. <https://doi.org/10.1523/jneurosci.1449-04.2004>.
- Slater, K D, N C Sinclair, T S Nelson, P J Blamey, H J McDermott, and Consortium Bionic Vision Australia. 2015. “NeuroBi: A Highly Configurable Neurostimulator for a Retinal Prosthesis and Other Applications.” *IEEE J Transl Eng Health Med* 3: 3800111. <https://doi.org/10.1109/JTEHM.2015.2455507>.
- Stoop, R., and E. Pralong. 2000. “Functional Connections and Epileptic Spread between Hippocampus, Entorhinal Cortex and Amygdala in a Modified Horizontal Slice Preparation of the Rat Brain.” *European Journal of Neurology* 12: 3651–63. <https://doi.org/10.1046/j.1460-9568.2000.00253.x>.
- Strogatz, Steven H. 2015. *Nonlinear Dynamics and Chaos : With Applications to Physics, Biology, Chemistry, and Engineering*. Second edi. Boulder, CO: Westview Press, a member of the Perseus Books Group.
- Suffczynski, P, F H Lopes da Silva, J Parra, D N Velis, B M Bouwman, C M van Rijn, P van Hese, et al. 2006. “Dynamics of Epileptic Phenomena Determined from Statistics of Ictal Transitions.” *IEEE Trans Biomed Eng* 53 (3): 524–32. <https://doi.org/10.1109/TBME.2005.869800>.
- Suffczynski, P, F Lopes da Silva, J Parra, D Velis, and S Kalitzin. 2005. “Epileptic Transitions: Model Predictions and Experimental Validation.” *J Clin Neurophysiol* 22 (5): 288–99. <https://doi.org/00004691-200510000-00002> [pii].
- Taylor, P N, G Baier, S Cash, J Dauwels, J Slotine, and Y Wang. 2013. “A Model of Stimulus Induced Epileptic Spike-Wave Discharges.” *2013 Symposium on Computational*

*Intelligence, Cognitive Algorithms, Mind, and Brain (CCMB).*

- Taylor, P N, Y Wang, and M Kaiser. 2017. “Within Brain Area Tractography Suggests Local Modularity Using High Resolution Connectomics.” *Sci Rep* 7: 39859.  
<https://doi.org/10.1038/srep39859> [pii].
- Terry, J R, O Benjamin, and M P Richardson. 2012. “Seizure Generation: The Role of Nodes and Networks.” *Epilepsia* 53 (9): e166-9. <https://doi.org/10.1111/j.1528-1167.2012.03560.x>.
- Touboul, J, F Wendling, P Chauvel, and O Faugeras. 2011. “Neural Mass Activity, Bifurcations, and Epilepsy.” *Neural Comput* 23 (12): 3232–86. [https://doi.org/10.1162/NECO\\_a\\_00206](https://doi.org/10.1162/NECO_a_00206).
- Vohra, S T, L Fabiny, and K Wiesenfeld. 1994. “Observation of Induced Subcritical Bifurcation by Near-Resonant Perturbations.” *Phys Rev Lett* 72 (9): 1333–36.  
<https://doi.org/10.1103/PhysRevLett.72.1333>.
- Wagenaar, J B, G A Worrell, Z Ives, D Matthias, B Litt, and A Schulze-Bonhage. 2015. “Collaborating and Sharing Data in Epilepsy Research.” *J Clin Neurophysiol* 32 (3): 235–39. <https://doi.org/10.1097/WNP.00000000000015900004691-201506000-00007> [pii].
- Wang, H X, Q Y Wang, and Q S Lu. 2011. “Bursting Oscillations, Bifurcation and Synchronization in Neuronal Systems.” *Chaos Solitons & Fractals* 44 (8): 667–75.  
<https://doi.org/10.1016/j.chaos.2011.06.003>.
- Wang, Y, M Goodfellow, P N Taylor, and G Baier. 2012. “Phase Space Approach for Modeling of Epileptic Dynamics.” *Phys Rev E Stat Nonlin Soft Matter Phys* 85 (6 Pt 1): 61918.  
[http://www.ncbi.nlm.nih.gov/entrez/query.fcgi?cmd=Retrieve&db=PubMed&dopt=Citation&list\\_uids=23005138](http://www.ncbi.nlm.nih.gov/entrez/query.fcgi?cmd=Retrieve&db=PubMed&dopt=Citation&list_uids=23005138).
- Wendling, F, F Bartolomei, J J Bellanger, and P Chauvel. 2002. “Epileptic Fast Activity Can Be

- Explained by a Model of Impaired GABAergic Dendritic Inhibition.” *Eur J Neurosci* 15 (9): 1499–1508. <https://www.ncbi.nlm.nih.gov/pubmed/12028360>.
- Wendling, F, P Benquet, F Bartolomei, and V Jirsa. 2015. “Computational Models of Epileptiform Activity.” *J Neurosci Methods*. [https://doi.org/S0165-0270\(15\)00122-3](https://doi.org/S0165-0270(15)00122-3) [pii]10.1016/j.jneumeth.2015.03.027.
- Wendling, F, U Gerber, D Cosandier-Rimele, A Nica, J De Montigny, O Raineteau, S Kalitzin, F Lopes da Silva, and P Benquet. 2016. “Brain (Hyper)Excitability Revealed by Optimal Electrical Stimulation of GABAergic Interneurons.” *Brain Stimul* 9 (6): 919–32. <https://doi.org/10.1016/j.brs.2016.07.001>.
- Wetjen, N M, W R Marsh, F B Meyer, G D Cascino, E So, J W Britton, S M Stead, and G A Worrell. 2009. “Intracranial Electroencephalography Seizure Onset Patterns and Surgical Outcomes in Nonlesional Extratemporal Epilepsy.” *J Neurosurg* 110 (6): 1147–52. <https://doi.org/10.3171/2008.8.JNS17643>.
- White, A, P A Williams, J L Hellier, S Clark, F E Dudek, and K J Staley. 2010. “EEG Spike Activity Precedes Epilepsy after Kainate-Induced Status Epilepticus.” *Epilepsia* 51 (3): 371–83. <https://doi.org/10.1111/j.1528-1167.2009.02339.x>.
- Williamson, Adam, Jonathan Rivnay, Loïg Kergoat, Amanda Jonsson, Sahika Inal, Ilke Uguz, Marc Ferro, et al. 2015. “Controlling Epileptiform Activity with Organic Electronic Ion Pumps.” *Advanced Materials* 27 (20): 3138–44. <https://doi.org/10.1002/adma.201500482>.
- World Health Organization, (WHO). 2017. “Epilepsy.” [www.who.int/mediacentre/factsheets/fs999](http://www.who.int/mediacentre/factsheets/fs999).
- Yaghoobi, H., M. Hassouneh, and E. Abed. 2001. “Detection of Impending Bifurcation Using a Near-Resonant Probe Signal.” *Proceedings of the American Control Conference*, 2285–91.



Yamamoto, J., A. Ikeda, T. Satow, K. Takeshita, M. Takayama, M. Matsuhashi, R. Matsumoto, et al. 2002. "Low-Frequency Electric Cortical Stimulation Has an Inhibitory Effect on Epileptic Focus in Mesial Temporal Lobe Epilepsy." *Epilepsia* 43 (5): 491–95.  
<https://doi.org/10.1046/j.1528-1157.2002.29001.x>.